MAGNETIC RESONANCE AND OPTICAL INVESTIGATIONS OF $KMgF_3$ AND $KTiOPO_4$

By

MICHAEL PAUL SCRIPSICK

Bachelor of Science in Arts and Sciences

Oklahoma State University

Stillwater, Oklahoma

1985

Submitted to the faculty of the
Graduate College of the
Oklahoma State University
in partial fulfillment of
the requirements for
the Degree of
DOCTOR OF PHILOSOPHY
December, 1990

MAGNETIC RESONANCE AND OPTICAL

INVESTIGATIONS OF $KMgF_3$

AND $KTiOPO_4$

Thesis Approved:

Larry E. Halliburton

Thesis Advisor

Stephen McKeever

Joel J. Martin

J. Paul Devlin

Jinjun Song

Norman N. Durham

Dean of Graduate College

ACKNOWLEDGEMENTS

This dissertation would not be possible without the support and guidance of many friends, colleagues and others. I wish to especially thank Dr. Larry Halliburton for serving as my patient advisor, generous employer, and primary educator. From him I have learned more about being a scientist than is written in any physics book.

I am grateful to the faculty of the Physics Department at Oklahoma State University for their time and effort in providing me with the education required to carry out such an endeavor. I would particularly like to express my appreciation to Dr. S. W. S. McKeever, Dr J. J. Martin, Dr. J. J. Song and Dr. J. P. Devlin (OSU Chemistry) for serving on my committee. I would like to acknowledge Dr. M. J. Jani, Dr. C. Y. Chen, Dr. M. H. Rezza, Mr. B. M. Zappta and Dr. G. J. Edwards without whose aid in the lab the data for this work would never have been completed.

Financial support during the last year has been partially provided through the Department of Education by way of a Lasers and Optical Materials Fellowship administered by Dr. G. E. Dixon and is greatly appreciated. Many thanks go to the staffs of the Physics Department office and the Physics-Chemistry Machine Shop, particularly Mr. Mike Lucas, for their help through the years.

I would like to thank those whose friendship over the years has provided the pleasant memories of graduate school specifically, Mr. K. Kraft, Dr. M. Kliewer, Mr. J. Allen, Mr. R. Cross, Dr. R. Reeves, and Mr. and Mrs. M. Isch.

I am most indebted to my family. My parents, John and Lottie Scripsick, have provided unending financial and moral support which can never be equally returned. I would like to thank my brother Vince Scripsick who has doubled as a roommate and occasionally a source of spirited conflict.

TABLE OF CONTENTS

LIST OF TABLES

LIST OF FIGURES

CHAPTER I

INTRODUCTION

Electron paramagnetic resonance, EPR, and electron-nuclear double resonance, ENDOR, have proven to be valuable techniques in the investigation of defects in crystals.[1] If a center in a crystal is paramagnetic then these magnetic resonance studies can yield information about the electronic structure, the extent of the wave function, and the surrounding environment. Magnetic resonance investigations at another level are used to identify the nature of centers which give rise to macroscopic material properties. This is usually accomplished by correlating known magnetic resonance spectra with other spectroscopic techniques such as optical absorption and luminescence. In this way magnetic resonance can often quickly identify or reduce the number of possibilities in determining the origin of these optical phenomena and suggest the source of such defects, i.e., impurities from growth, color centers produced by irradiation, oxygen vacancies from partial reduction, etc.

The two studies described in this dissertation will be examples of these different levels of magnetic resonance investigations. The first to be presented is an ENDOR study of the self-trapped hole, or V_k center, in $KMgF_3$. V_k centers have been studied since the early days of EPR beginning with the alkali halides and eventually in more complicated structures.[2-9] The V_k center in $KMgF_3$ was first studied using EPR as early as 1966[10] and the work contained herein builds upon these earlier studies in an effort to answer

some yet unresolved questions. The second study to be presented involves using EPR to give insight into the nature of defects encountered in potassium titanyl phosphate ($KTiOPO_4$ or KTP). Very few magnetic resonance studies have been done in KTP; however the preliminary indications show EPR as being a promising tool in the identification and characterization of defects arising from growth, laser damage, and hostile environments. At this point it should be helpful and for the sake of completeness to present a brief overview of EPR and ENDOR.

EPR

An unpaired electron which has spin vector $\vec{S}$ has spin angular momentum $\hbar S$. The magnetic moment of the electron is then proportional to $\hbar S$ and is given by

$$\vec{\mu}_e = -\gamma\hbar\vec{S} = -g_e\beta\,\vec{S} \qquad (I.1)$$

where γ is the gyromagnetic ratio, g is the electron g factor and β is the Bohr electron magneton. Since there is a magnetic moment there will be an interaction with a magnetic field and the energy of interaction (the spin-Hamiltonian) is given by

$$\mathcal{H} = -\vec{\mu}_e \cdot \vec{H} = g_e\,\beta\,\vec{S}\cdot\vec{H} \quad . \qquad (I.2)$$

If the magnetic field direction is defined to be the z direction then $\vec{H} = H_z$ and the energy levels are defined by

$$E = g_e \beta H m_s \quad . \tag{I.3}$$

Thus, for electrons with S = 1/2 and $m_s = \pm$ 1/2, there are two energy levels which separate linearly as the magnetic field strength is increased. The separation between the two levels is given by

$$\Delta E = g_e \beta H \quad . \tag{I.4}$$

If an electromagnetic field with photon energy equal to the energy of separation is introduced, then transitions can be induced between the two levels. The electromagnetic field induces transitions in both directions with transitions up absorbing photons and transitions down emitting photons. The rate at which these transitions occur depends on the incident photon density and the number of spins in each level. The population ratio of the two levels (at thermal equilibrium) is given by the Boltzmann factor. That is to say there are more spins in the lower energy level (m_s = - 1/2) than in the upper energy level (m_s = + 1/2). Since there are more spins in the lower level than the upper level, there will be a net absorption of photons. This absorption of photons is the EPR signal.

The system will continue to absorb the incident photons until the populations of the two levels become equal. At this point the number of transitions down equals the number of transitions up and there is no net absorption and no EPR signal. However, the system is subject to other interactions that are nonradiative which work to bring the system back into thermal equilibrium. These interactions are collectively called spin-lattice interactions and are a result of the thermal motion of the lattice.

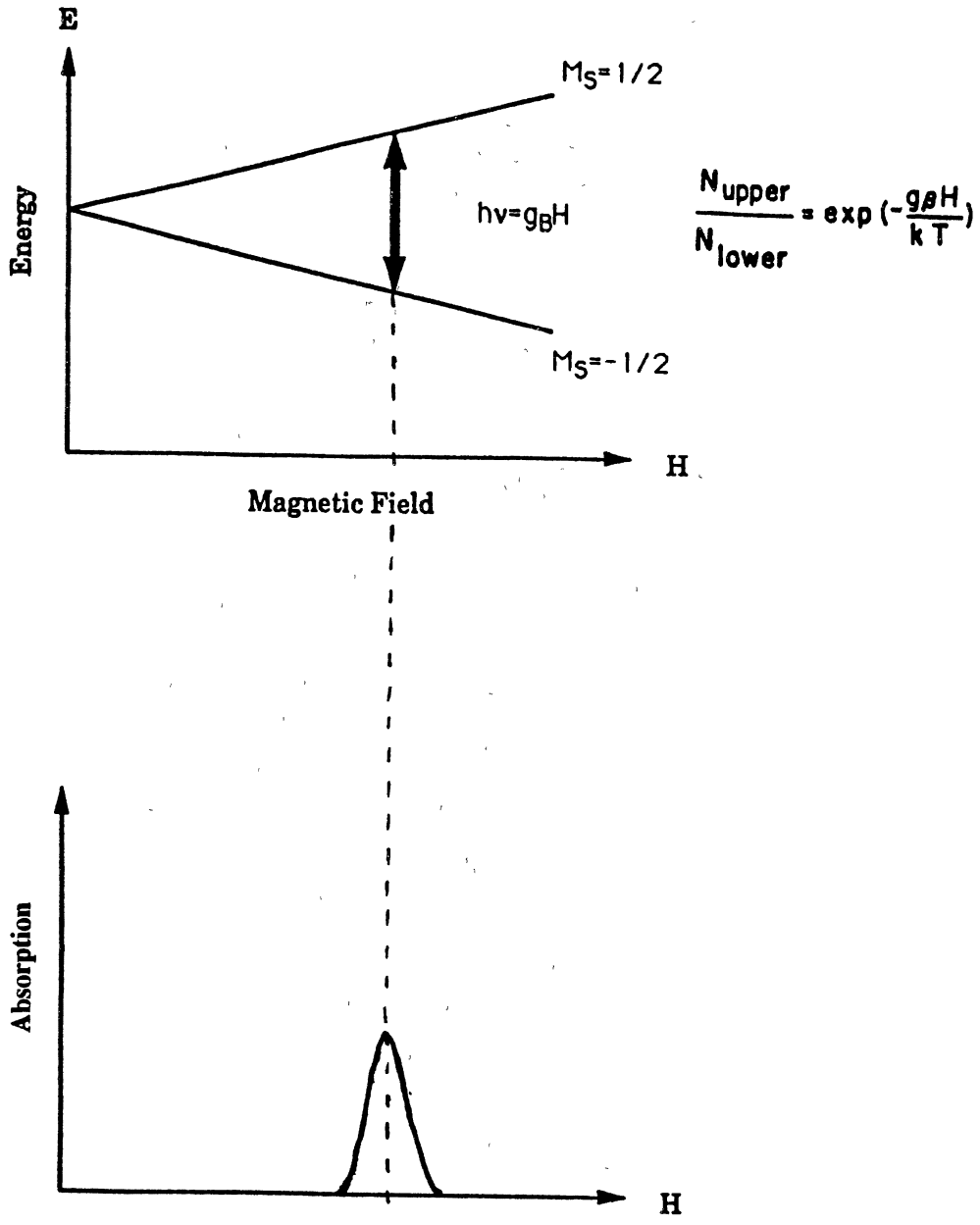

Figure 1. Zeemann Splitting and Microwave Absorption for S = 1/2 System

Experimentally the magnetic resonance phenomenon is detected by directing microwaves of a single frequency on to the sample and then increasing the magnetic field until the separation of the two energy levels is equal to the microwave energy. Figure 1[11] shows the energy levels and absorption of microwaves as a function of magnetic field for an S = 1/2 system. The EPR signal is enhanced by the appropriate choice of temperature and microwave power so as to balance the spin-lattice relaxation and microwave absorption to produce the maximum net absorption of microwaves.

If another spin I = 1/2 is added to the system then the spin-Hamiltonian has three terms

$$\mathcal{H} = \beta \vec{S} \cdot \overleftrightarrow{g} \cdot \vec{H} + \vec{S} \cdot \overleftrightarrow{A} \cdot \vec{I} - g_n \beta_n \vec{I} \cdot \vec{H} \quad . \tag{I.5}$$

The first term in this equation is the electron Zeeman term previously described. In the case of spin systems in environments of symmetry lower than cubic the g-factor discussed earlier is anisotropic and must be considered as a tensor. The second term is the hyperfine term which gives the energy of interaction of the electron spin with the nuclear spin. It also is generally anisotropic and is denoted by a tensor. The third term is the nuclear Zeeman term and is analogous to the electron Zeeman term and is generally considered to have an isotropic g factor. For isotropy, or fixed orientation, the above equation reduces to

$$\mathcal{H} = g \beta \vec{S} \cdot \vec{H} + A \vec{S} \cdot \vec{I} - g_n \beta_n \vec{I} \cdot \vec{H} \quad . \tag{I.6}$$

The first order energy levels are then given by

$$E_{1/2,1/2} = g \beta H/2 + hA/4 - g_n \beta_n H/2 \quad \text{(I.7.a)}$$

$$E_{1/2,-1/2} = g \beta H/2 - hA/4 + g_n \beta_n H/2 \quad \text{(I.7.b)}$$

$$E_{-1/2,-1/2} = g \beta H/2 + hA/4 + g_n \beta_n H/2 \quad \text{(I.7.c)}$$

$$E_{-1/2,1/2} = g\ b\ H/2 - hA/4 - g_n \beta_n H/2 \quad \text{(I.7.d)}$$

where the first subscript denotes the m_s value and the second subscript denotes the m_I value. If the assumption is made that the electron Zeeman term is larger than the hyperfine term which in turn is much larger than the nuclear Zeeman term, as is often the case, then the energy level spectrum would be represented as in Fig. 2 where broken lines correspond to EPR transitions in the absence of hyperfine interaction.

The EPR transitions are subject to the selection rules $\Delta m_s = \pm 1/2$ and $\Delta m_I = 0$. EPR transitions then occur between levels 1 - 4 and between levels 2 - 3. The separation between successive line positions will then give the magnitude of the hyperfine interaction A. The accuracy with which this hyperfine parameter can be determined is then limited by the consideration of linewidth. If the spacing of a set of lines does not exceed their linewidth then the splitting of electron levels due to the nuclear interaction cannot be detected except perhaps for a broadening of the EPR line. The accuracy of such hyperfine measurements would be greatly enhanced if nuclear transitions could be observed directly.

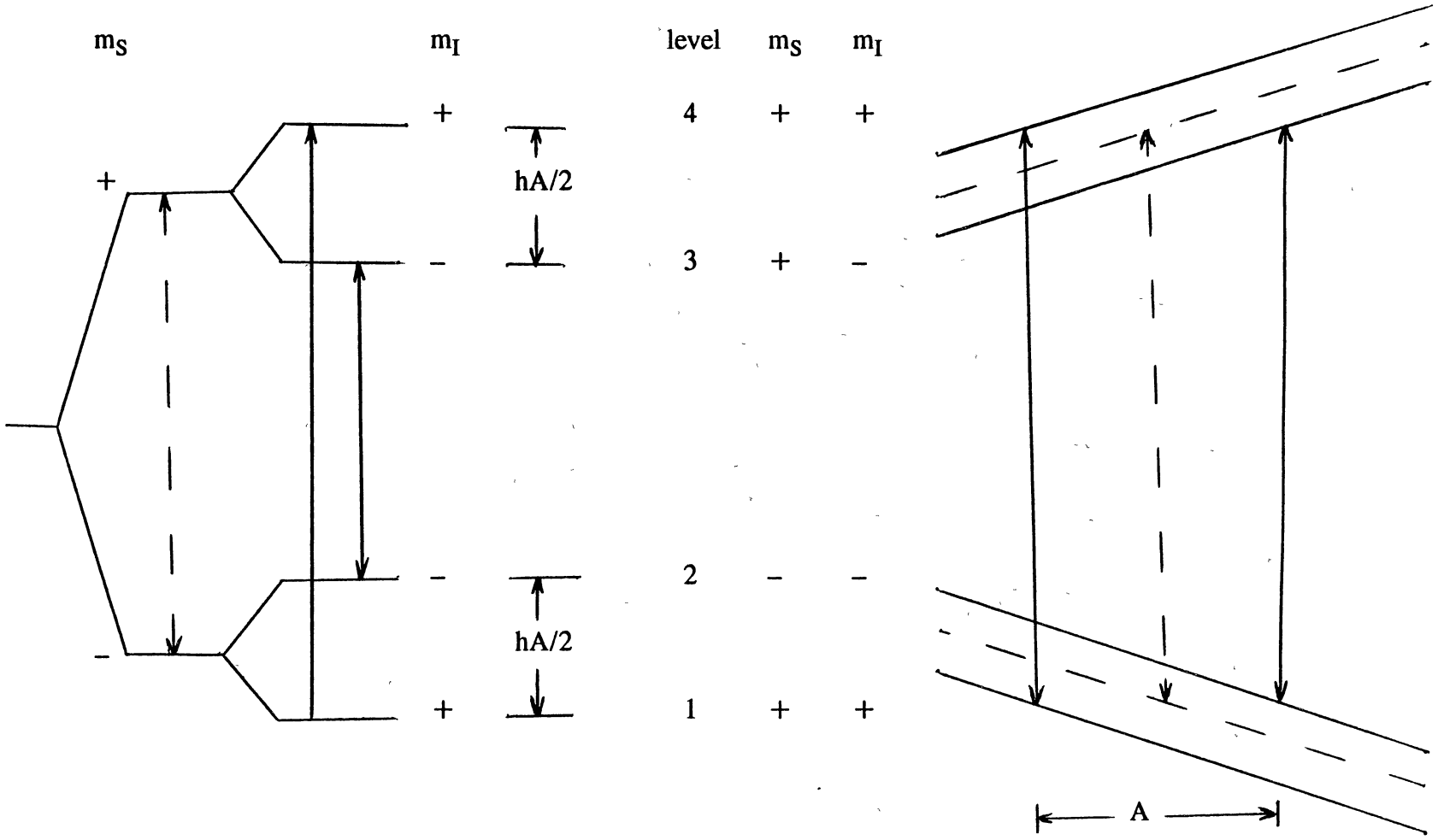

Figure 2. Zeemann and Hyperfine Energy Levels For S = 1/2, I = 1/2 System

ENDOR

In Fig. 2, the intensity of the EPR signal for transitions from 1 to 4 is dependent on the microwave power and on the population difference between the two levels. If the microwave power is high enough and the spin-lattice relaxation is slow enough then the populations of the two levels will approach each other. As the populations become more nearly equal, the net absorption of microwaves decreases and the EPR signal decreases. This is called power saturation. If a nuclear transition frequency is applied to the system which corresponds to the energy difference between levels 1 and 2 or the energy difference between 3 and 4, then nuclear transitions will be induced between these levels. Transitions driven between these nuclear energy levels will in turn change the populations of levels 1 and 4. As the population difference between levels 1 and 4 changes, the net microwave absorption changes and the intensity of the EPR signal will change accordingly. This change in EPR signal intensity is called the ENDOR response. It is therefore a necessary but not sufficient condition that the EPR signal be saturated in order to obtain an ENDOR spectrum. In order to saturate the EPR signal, the spin-lattice relaxation must be slowed so as to allow microwaves of some reasonable power to begin to equalize the populations of the two EPR levels. As a result, most ENDOR experiments must be conducted at very low temperatures (liquid helium).

Nuclear spin transitions are subject to the selection rules $\Delta m_S = 0$ and $\Delta m_I = \pm 1$. Applying these selection rules to the first order energy levels given in (I.7), the first order nuclear transition frequency for transitions between levels 3 and 4 is given by the relation

$$| E_{1/2,1/2} - E_{1/2,-1/2} | = h\nu_{n1} = | hA/2 - g_n \beta_n H | \quad . \tag{I.8}$$

Defining $g_n \beta_n H/h$ as the nuclear free spin frequency, ν_o, gives:

$$\nu_{n1} = | A/2 - \nu_o | \quad . \tag{I.9}$$

In a similar fashion

$$\nu_{n2} = | A/2 + \nu_o | \tag{I.10}$$

where ν_{n2} corresponds to transitions between levels 1 and 2 of Fig. 2. The nuclear free spin frequencies, ν_o, of common isotopes are known and can be looked up in regularly available tables.

These transition frequencies given above may manifest themselves as one of two possible spectra depending on which of the two terms in the absolute value is the largest. The case where $\nu_o > A/2$ (hereafter denoted as a type 1 ENDOR spectrum) is characterized by the two ENDOR lines centered on ν_o and separated by A. The type 1 ENDOR spectrum and its energy levels are shown in Fig. 3.[11] The second case, that where $A/2 > \nu_o$, is characterized by a pair of ENDOR lines centered on A/2 and separated by $2\ \nu_o$. This spectrum is denoted as a type 2 ENDOR spectrum and its energy levels and spectrum are shown in Fig. 4.[11] When one obtains an ENDOR spectrum the first task is to determine which of these two types of spectra is being observed. Once the type of spectrum has been determined, the nuclei responsible for the hyperfine can be identified directly (to first order) from the spectrum by

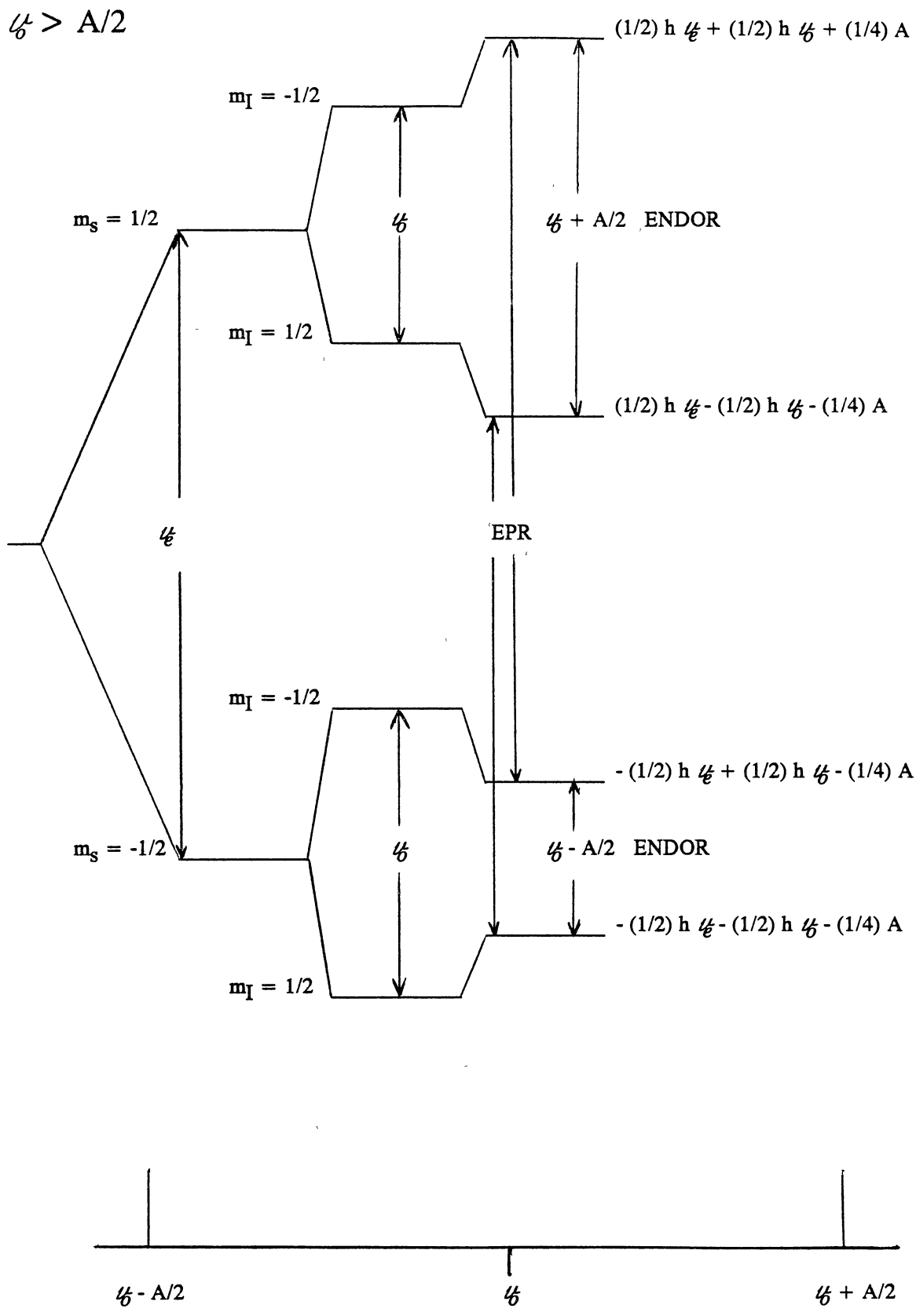

Figure 3. Type 1 ENDOR Energy Levels and Spectrum

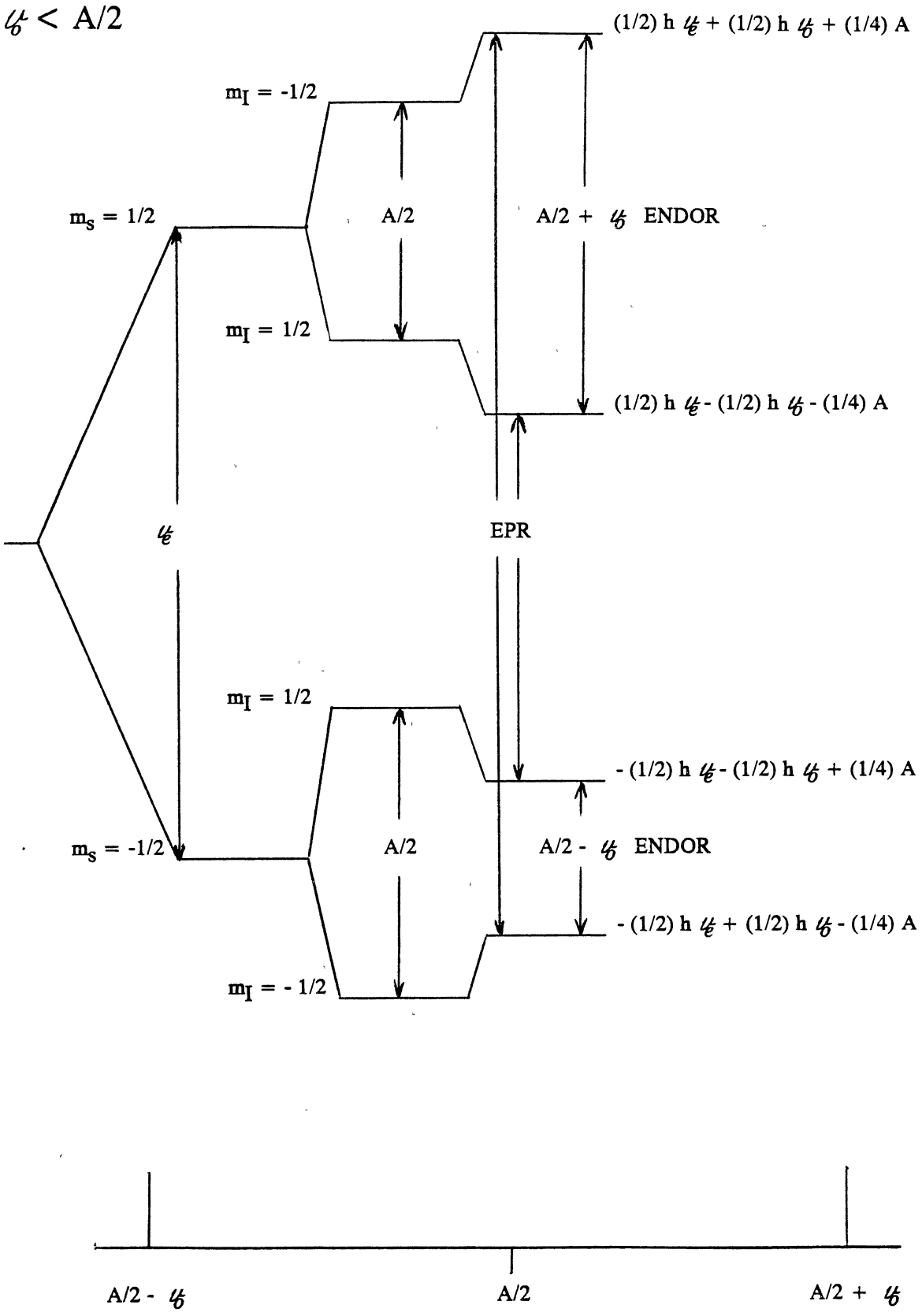

Figure 4. Type 2 ENDOR Energy Levels and Spectrum

measuring the frequency corresponding to the center of the spectrum for a type 1 spectrum or by measuring the separation between lines and dividing by two for a type 2 spectrum. Similarly, the magnitude of interaction can be read from the line separation in a type 1 spectrum or by measuring the frequency corresponding to the center of the spectrum and multiplying by two for a type 2 spectrum.

It should be noted at this point that the energy levels given in (I.7) were the first order energy levels and higher order terms may not be negligible. These higher order terms may produce ENDOR spectra which deviate somewhat from those shown in Fig. 3 and Fig. 4; however, the general features of these spectra are often a good approximation. ENDOR spectra may get much more complicated as spin values greater than I = 1/2 are encountered and as other terms in the spin-Hamiltonian become more important (nuclear quadrupole, crystal field, etc.). In addition, the discussion thus far has primarily dealt with isotropic Hamiltonians. In most single crystal studies, the electron g-factor and the hyperfine A parameter are not isotropic and are only truly specified by tensors. These are 3 x 3 hermitian tensors and are thus specified by 6 independent parameters. These six parameters are usually determined in one of two ways: (1) the six elements making up the upper right triangle of the tensor or (2) the three principal values of the diagonalized tensor and three angles (Euler angles) which rotate the tensor into its diagonalized form. In order to determine these parameters, the line positions are monitored as the orientation of the crystal relative to the external magnetic field is changed. A block diagram of an EPR/ENDOR spectrometer is given in Fig. 5.[11] The ENDOR components are outlined in bold.

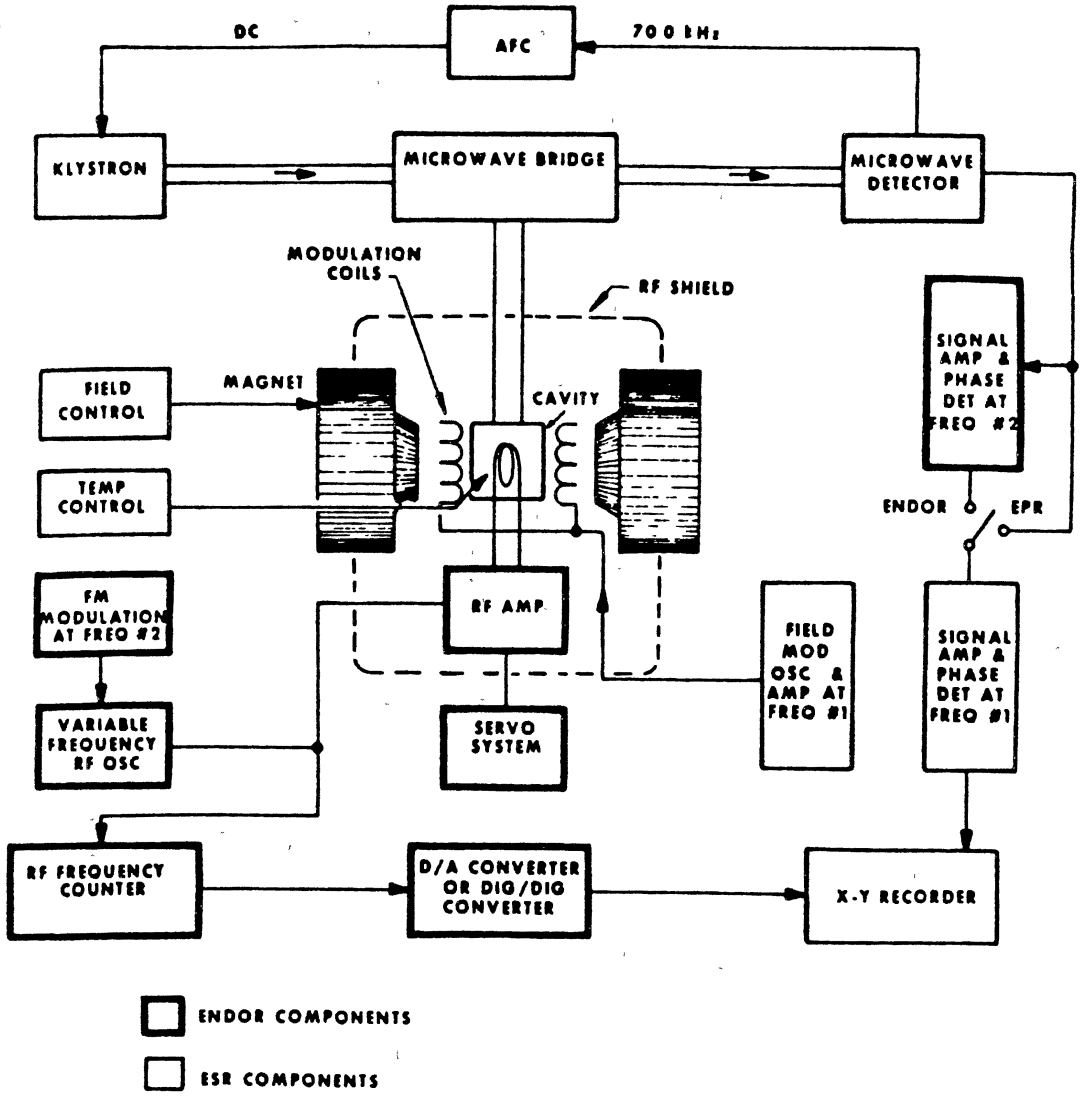

Figure 5. EPR/ENDOR Spectrometer

CHAPTER II

THE V_k IN $KMgF_3$

Introduction

Self-trapped holes, otherwise known as V_k centers, were first studied in alkali halide materials.[2-9,12] The commonaly accepted mechanism of production is the Pooley-Hersh mechanism.[13] Ionizing radiation produces excitons (electron-hole pairs) which subsequently dissociate and the hole becomes localized on a pair of adjacent halide ions. The halide ions move toward each other to form a molecular ion with a single negative charge [X_2^-]. As long as the hole is present there will be a local lattice distortion to stabilize the hole. Thus the hole is said to be self trapped. Figure 6[14] shows the [Cl_2^-] V_k center in KCl. The molecular ion may be oriented along any one of the [110]-type directions.

The V_k centers in alkali halides have a simple structure because of the cubic symmetry exhibited by these materials. On the other hand, $KMgF_3$ has the lower cubic perovskite symmetry. The $KMgF_3$ structure may be visualized as being made up of cubes in which the cube center is occupied by a Mg^{2+} ion, the cube corners are occupied by K^+ ions and the cube faces occupied by F^- ions as shown in Fig. 7(a)[14] The first report of the V_k center in $KMgF_3$ was made by T. P. P. Hall[10] and its configuration was determined by EPR. Figure 7(b) shows the configuration of the self-trapped hole as determined by Hall. By comparison with the V_k center in the alkali halides of

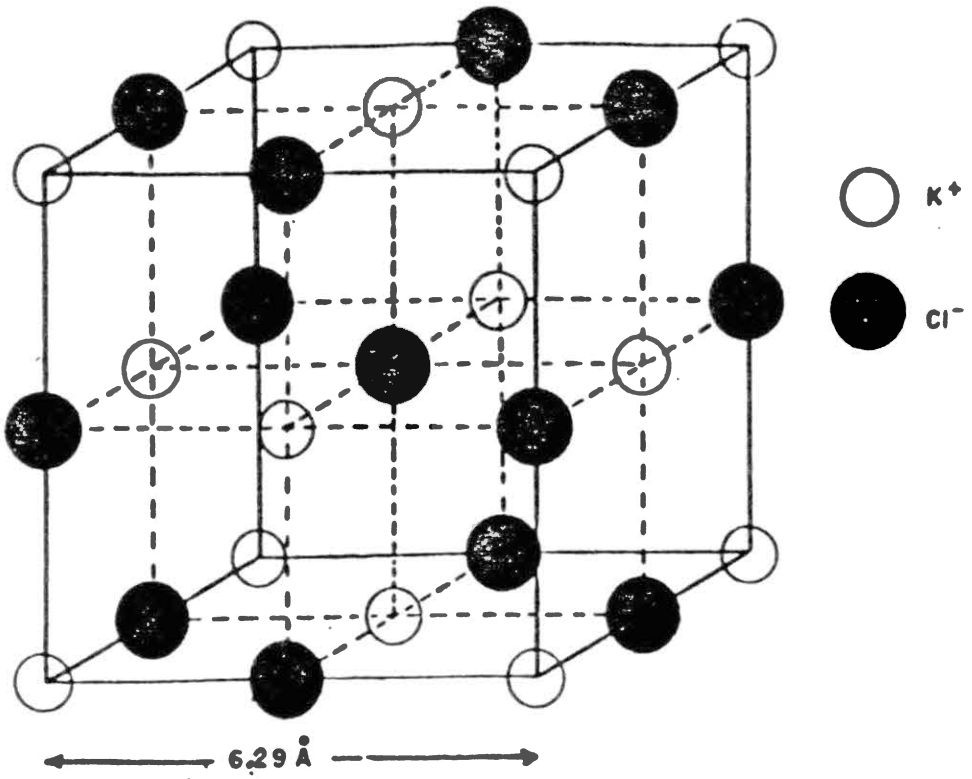

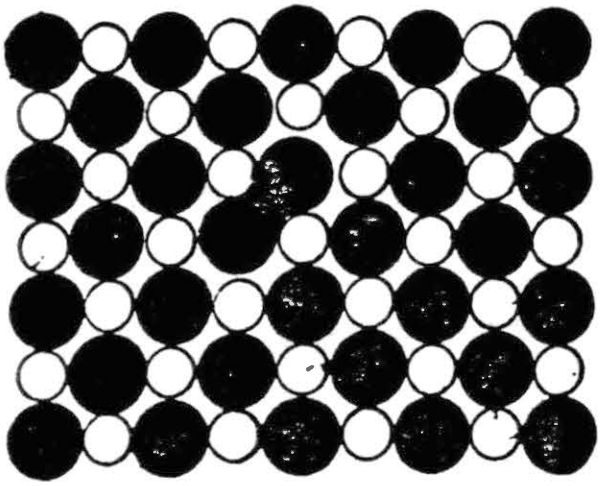

Figure 6. KCl Structure and [Cl_2^-] V_k Center

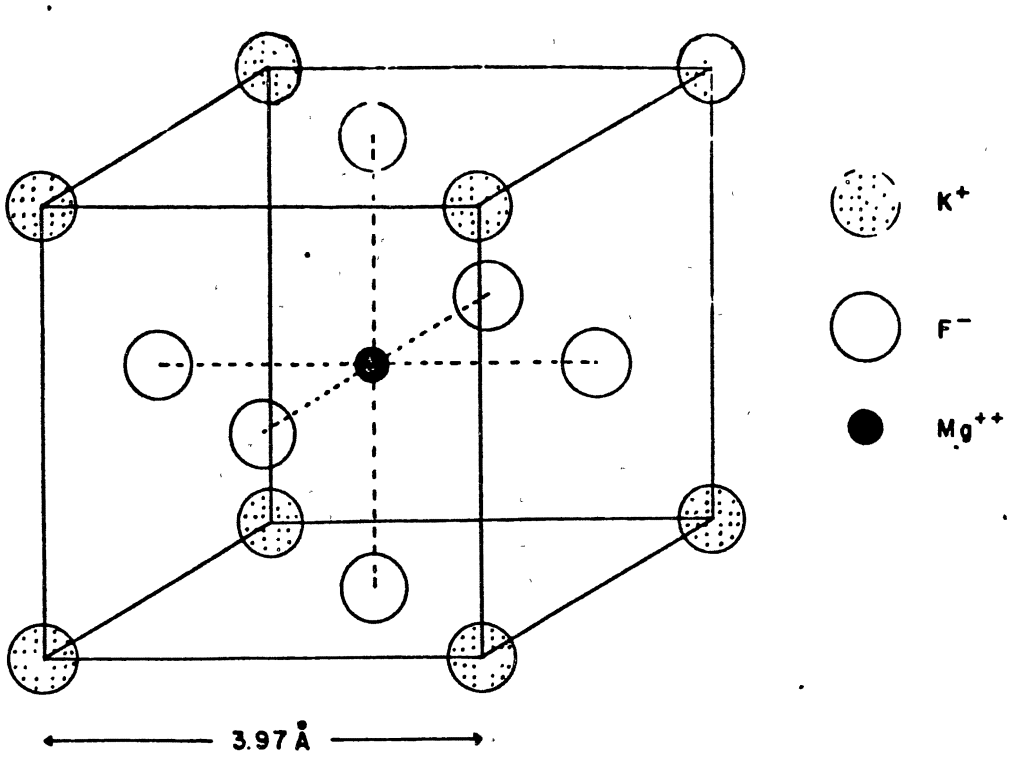

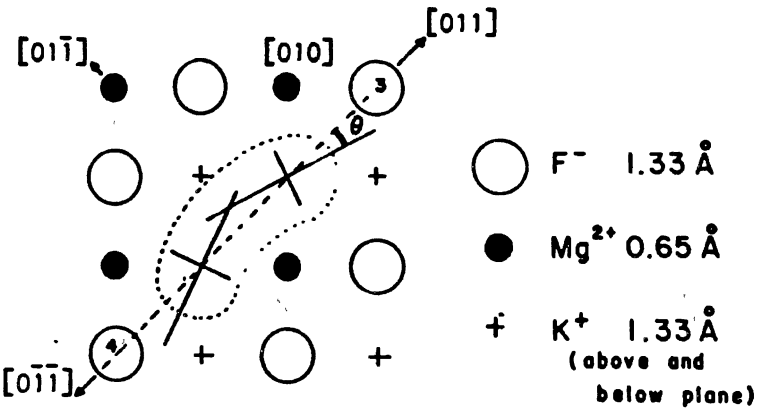

Figure 7. $KMgF_3$ Structure and $[F_2^-]$ V_k Center

Fig. 6, it should be immediately noted that the [F_2^-] molecular bond in the cubic perovskite is "bent " from that of the [011]-type bond observed in alkali halides. The origin of this bending can be thought of as due to a repulsion of the hole away from the doubly positive ionized Mg ion. This bent bond is detected experimentally through the angular dependence of the EPR spectra which shows that the principal axes of the two fluorine ions which constitute the [F_2^-] molecule are not colinear with each other or the [011] direction. The angle of deviation from [011] shown in Fig. 7 was found to be 7^o. Hall showed that an approximation to the molecular bond could be constructed from p-orbitals which lie nearly along the [011] direction and are centered on the two constituent fluorine ions.

The EPR spectra of the V_k center for H along the two high symmetry directions are shown in Fig. 8.[14] From Fig. 7 it can be seen that there are twelve possible crystallographic orientations of the [F_2^-] molecular ion in the unit cube. With H || [001] the twelve different orientations will fall into two magnetic orientations relative to the magnetic field direction. The four crystallographic orientations which lie in the (001) plane will have a molecular axis oriented 90^o to the magnetic field while the other eight crystallographic orientations which lie in the (100) and (010) planes will be oriented 45^o to the magnetic field. Thus the EPR spectra shown in Fig. 8 for H || [001] is composed of a superposition of two sets of lines, i.e., eight molecules oriented 45^o and four molecules oriented 90^o to the magnetic field. As the magnetic field is rotated about the [100] away from the [001] toward the [011], many of these degeneracies will be lifted. Of the four molecules which lie in the (100) plane and are oriented 45^o to the magnetic field with H || [001], two will rotate into a 0^o orientation with the magnetic field with H || [011] and two will rotate into a 90^o orientation. All of the four molecules which lie in the

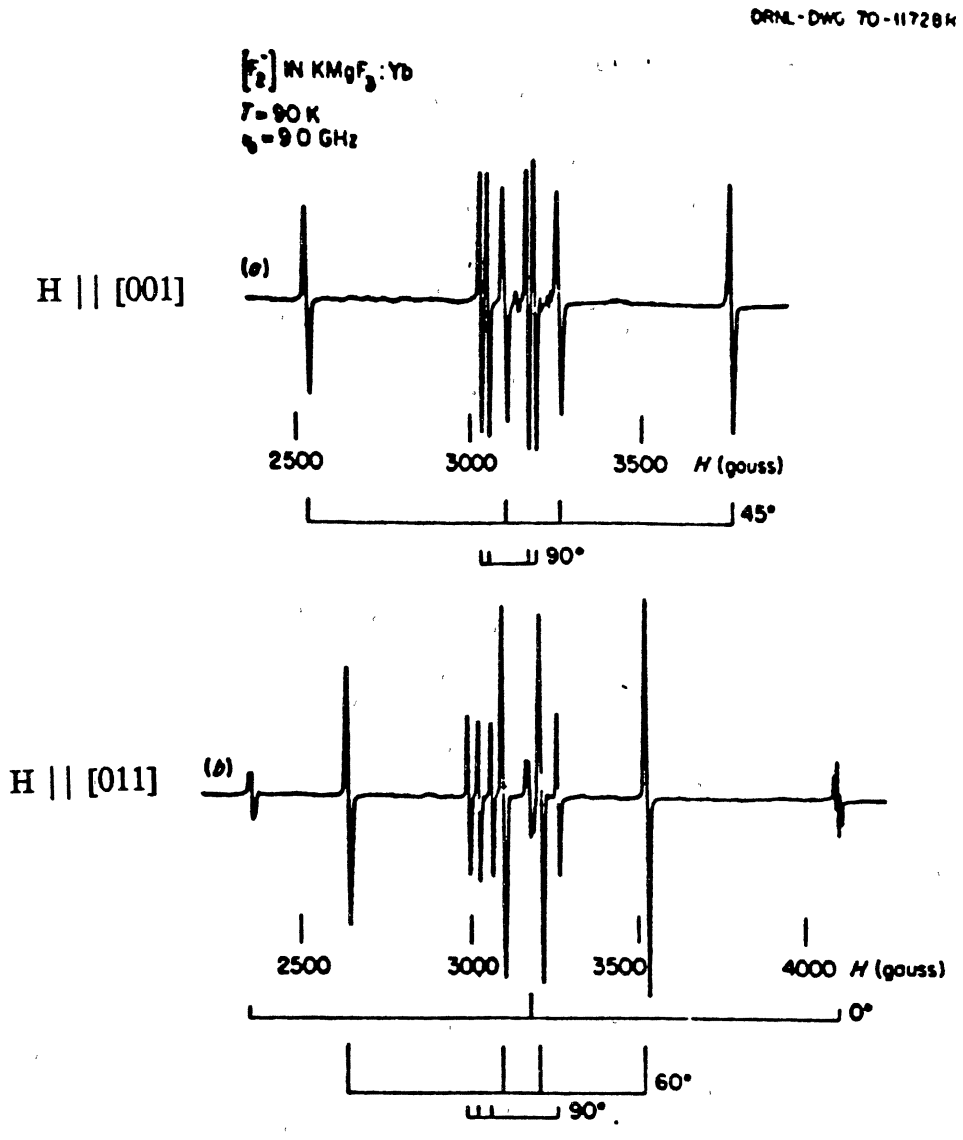

Figure 8. EPR of V_k Center with (a) H || [001] and (b) H || [011]

(010) plane and have a 45° orientation with H ∥ [001] will be rotated to a 60° orientation with H ∥ [011]. Thus the 45° orientation EPR lines when H ∥ [001] will split into three lines in a 1:2:1 ratio with the lines rotating into 90°, 60° and 0° orientation respectively when H ∥ [011]. The four molecules which lie in the (001) plane and are oriented 90° to the magnetic field with H ∥ [001] will all rotate into a 60° orientation with the magnetic field when H ∥ [011]. Therefore, the H ∥ [011] spectrum is a superposition of three spectra having molecular axes oriented 0°, 90°, and 60° with the magnetic field.

All of the EPR lines of Fig. 8 are inhomogeneously broadened due to unresolved hyperfine with neighboring nuclei, whereas the 0° EPR lines of the [011] spectrum show some resolved hyperfine. Except for the unresolved hyperfine, the EPR spectra can adequately be fit to a spin-Hamiltonian of the form

$$\mathcal{H} = \vec{S} \cdot \overleftrightarrow{g} \cdot \vec{H} + \vec{S} \cdot \overleftrightarrow{A}_1 \cdot \vec{I}_1 + \vec{S} \cdot \overleftrightarrow{A}_2 \cdot \vec{I}_2 - g_n \beta_n \vec{H} \cdot (\vec{I}_1 + \vec{I}_2) \qquad \text{(II.1)}$$

Where $\overleftrightarrow{g}$ is the g-tensor of the hole and $\overleftrightarrow{A}_1$ and $\overleftrightarrow{A}_2$ are the hyperfine tensors of the two fluorine nuclei of the [F_2^-] molecule.

It is the subject of this work to determine the nature of the unresolved hyperfine using ENDOR. In order to accomplish this, an additional term must be added to the spin-Hamiltonian to account for the interaction with other surrounding nuclei. Thus the spin-Hamiltonian takes the form

$$\mathcal{H} = \vec{S} \cdot \overleftrightarrow{g} \cdot \vec{H} + \vec{S} \cdot \overleftrightarrow{A}_1 \cdot \vec{I}_1 + \vec{S} \cdot \overleftrightarrow{A}_2 \cdot \vec{I}_2 + \vec{S} \cdot \overleftrightarrow{A}_3 \cdot \vec{I}_3$$

$$- g_n \beta_n \vec{H} \cdot (\vec{I}_1 + \vec{I}_2 + \vec{I}_3) \qquad \text{(II.2)}$$

The end result of this work is then to determine the principal values and principal axes of the $\overleftrightarrow{A}_3$ tensor in the above Hamiltonian for each of the neighboring nuclei contributing appreciably to the unresolved hyperfine interaction.

Experimental Procedure

The V_k center in $KMgF_3$ is produced by ionizing radiation and is unstable above 110 K. In the experiments described here a sample of $KMgF_3$ was irradiated for 3 minutes in liquid nitrogen with 1.5 MeV electrons produced by a Van de Graaff accelerator operating at 10 μA. The sample was then kept cold as it was quickly transferred into an Oxford Instruments ESR900 continuous flow liquid helium cryostat inside of the microwave cavity and the temperature stabilized at 20 K. The coil that delivered the rf field was mounted directly on the glassware of the cryostat as shown in Fig. 9.[15] All data was taken on an ER 200 Bruker EPR spectrometer with ENDOR attachment.

The cavity was critically tuned at 9.31 GHz and the magnetic field was swept to produce the EPR spectrum. The sample was carefully aligned to produce the EPR spectra shown in Fig. 8. Once the alignment was completed and the EPR spectrum obtained, the magnetic field was set to the field value corresponding to the peak of the microwave absorption and then recorded using a Varian E-500 NMR gaussmeter. The microwave power was then increased to cause partial saturation of the EPR signal. The EPR signal began to saturate at 0.67 mW and the microwave power required to optimize the ENDOR signal was determined to be 3.36 mW.

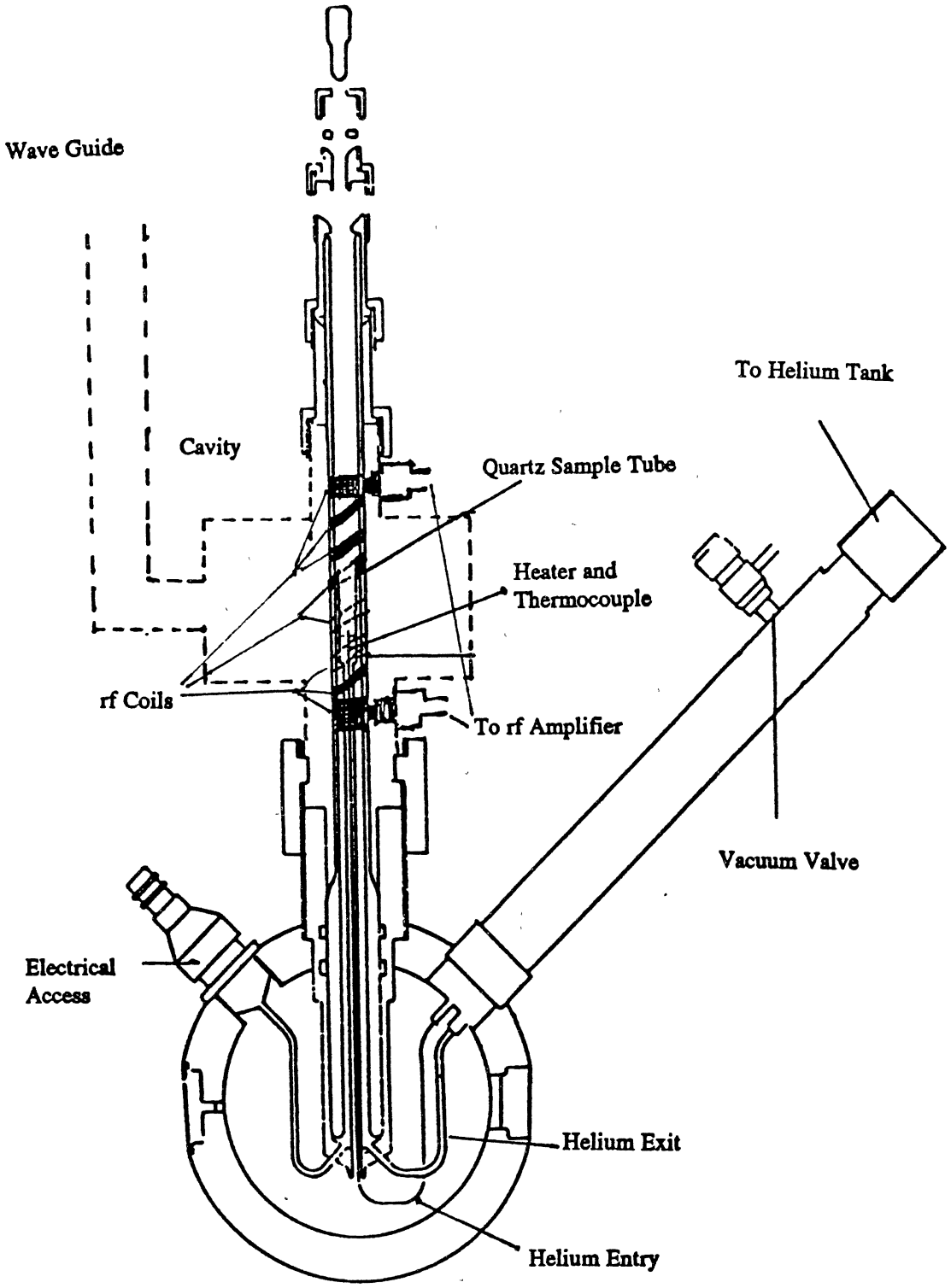

Figure 9. Oxford Instruments ESR900 Cryostat in ENDOR Cavity

With magnetic field set to the peak of the microwave absorption the spectrometer was switched to the ENDOR mode and the rf frequency was swept from 5 to 30 MHz. The rf amplifier was capable of delivering 200 W of peak power; however, power was not constant over the sweep range. The rf attenuation was set to 0 dB to deliver maximum available power. The rf field was frequency modulated at 12.5 kHz and the modulation depth varied from 10 to 50 kHz. Several rf scans were taken and added together in order to improve the signal-to-noise ratio of the ENDOR signals. The ENDOR spectra which were recorded into a computer were stored as first derivative spectra. The spectra were later integrated to give the absorption curves so that peak positions could be determined.

After recording the ENDOR spectrum, the magnet was rotated about one of the crystallographic axes by an angle as small as 1^{o} and no greater than 5^{o}. As described earlier, this rotation will split the EPR lines and they will move to new magnetic field values. The spectrometer was then returned to the EPR mode and the magnetic field was swept to generate the new EPR spectrum. The magnetic field was then moved to the new field value of the EPR line of interest and recorded via the NMR probe. Next, the ENDOR spectrum was taken. This processes was repeated for the 45^{o} of rotation that takes the magnetic field from H || [001] to H || [011], recording the magnetic field, the angle, and the ENDOR spectrum.

ENDOR spectra were recorded primarily while monitoring two EPR lines. One being the line that corresponds to a 45^{o} orientation of the molecular ion when H || [001] and which rotates into a 0^{o} orientation when H || [011]. It is hereafter denoted as the 0-45 line. The second is the line which correspond to a 45^{o} orientation of the molecular ion when H || [001] and rotates into a 60^{o} orientation when H || [011]. It is hereafter denoted as the

45-60 line. This is equivalent to following a single V_k center through two 45° rotations in perpendicular planes as shown in Fig 10. One rotation being H || [001] → H || [011] and the other being H || [010] → H || [101]. After integration of the ENDOR spectra, the frequencies corresponding to nuclear spin transitions were determined and each data point was recorded as three numbers: angle, magnetic field, and rf frequency.

Results and Analysis

The simplest of the ENDOR spectra is that taken while monitoring the 0° orientation EPR line with H || [110] shown in Fig. 11. The first task is to determine which of the two possible types of ENDOR spectra mentioned earlier is being observed. This was accomplished by comparing the ENDOR spectra obtained from monitoring the high field and low field 0° EPR lines.

The high field 0° line and the low field 0° line should contain the same information. As stated earlier there are two terms in the first order ENDOR transition frequencies, the hyperfine and the nuclear free spin. Recall that the nuclear free spin frequency, defined as $g_N\beta_N H/h$, is dependent on the magnetic field while the hyperfine parameter, A, is not. Therefore, although the ENDOR spectra obtained by monitoring the high and low field 0° EPR lines should contain the same information, they will not be identical since the magnetic fields of the two lines are vastly different. If the ENDOR spectrum of the high field 0° EPR line is type 1 then the ENDOR lines are centered on the free spin frequency which is magnetic field dependent. By moving to the low field 0° EPR to produce the ENDOR spectrum the free spin frequency shifts to lower frequency. Thus, the low field spectrum should be identical to

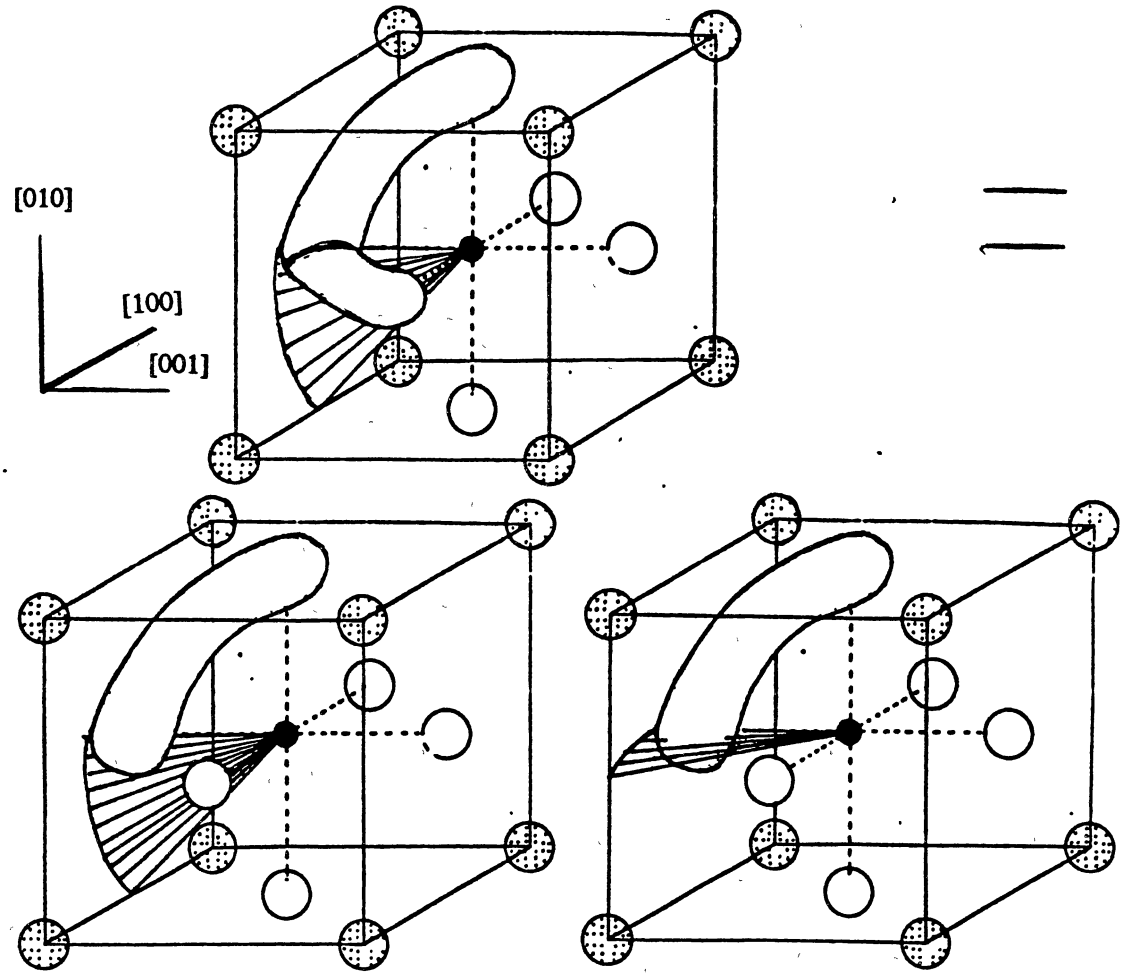

Figure 10. Equivalence of Two Molecules and One Rotation with One Molecule and Two Rotations

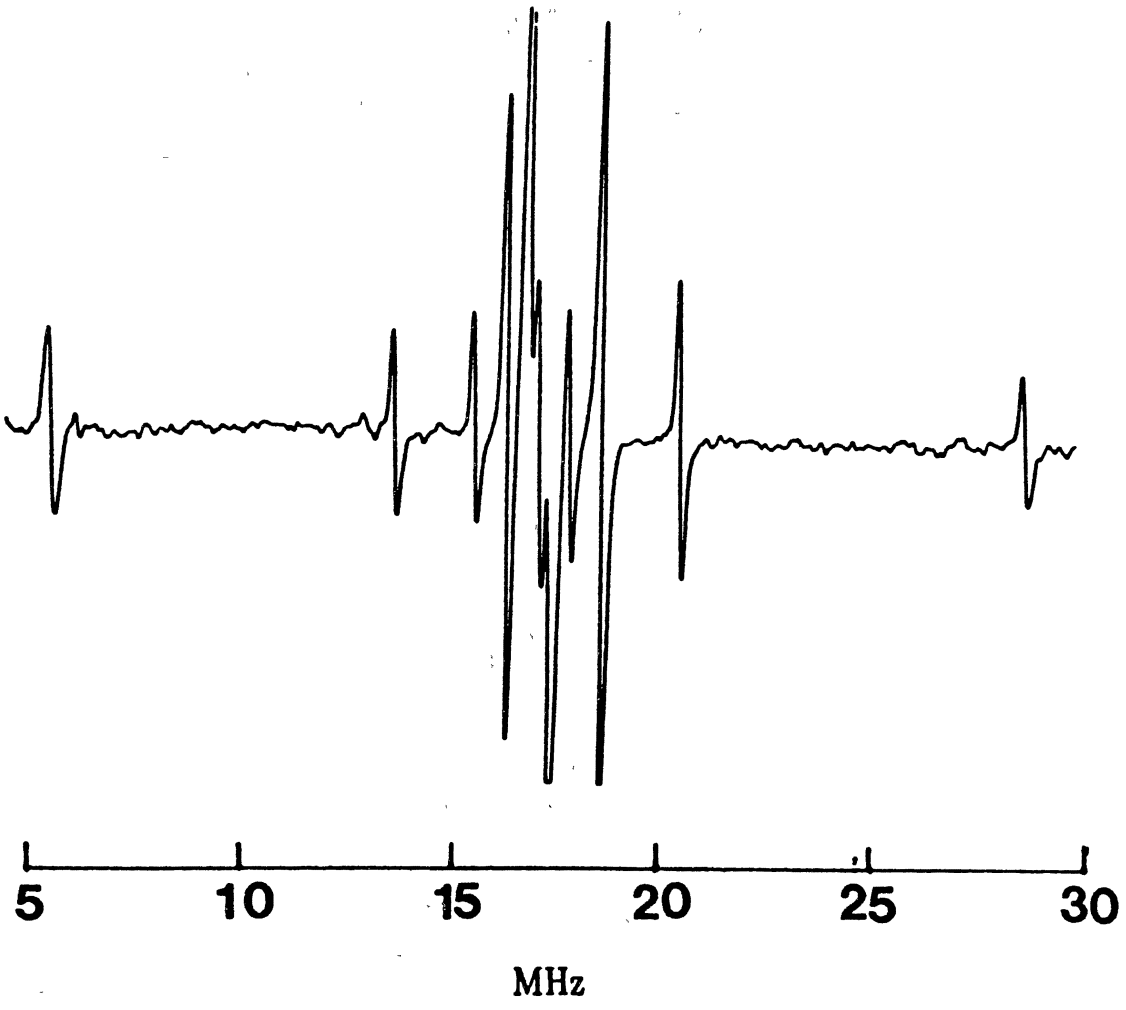

Figure 11. ENDOR Spectrum Obtained While Monitoring the High Field 0^{o} EPR Line When H || [110]

the high field spectrum only shifted to lower frequency. If the ENDOR spectrum were a type 2 spectrum then the center of the spectrum, which is given by A/2, should remain the same but the line separation should change since it is the separation that is determined by the field dependent nuclear free spin term in a type 2 spectrum. Fig. 12 shows conclusively that the spectra from the V_k center are indeed type 1.

Once the type of spectrum is known one must determine which neighboring nucleus is responsible for a particular pair of ENDOR lines. Figure 11 shows five pairs of lines all approximately centered on 17 MHz. Table 1 shows the possible origins of the lines and their respective free spin values. Nuclear free spin values are typically referenced at a magnetic field of 3500 G and their value at some other field can be easily calculated from the relation

$$\nu_0(H) = \nu_0(3500G) \times H / 3500G \ . \qquad (II.3)$$

The spectrum of Fig. 11 was taken at 4201 G. Using (II.3), the fluorine free spin frequency at 4201 G is 16.8367 MHz. Comparing with Fig. 11 it can easily been seen that all of the ENDOR lines are due to fluorine nuclei since all of the other free spin frequencies of Table 1 are much lower than that corresponding to the center of the spectrum. Having determined the origin of the ENDOR lines as being fluorine it is helpful to eliminate the dependence on the magnetic field by plotting the ENDOR line positions as measured from the calculated fluorine free spin frequency for each respective measured magnetic field. In this way the angular dependence of the ENDOR line positions appear as in Fig. 13.

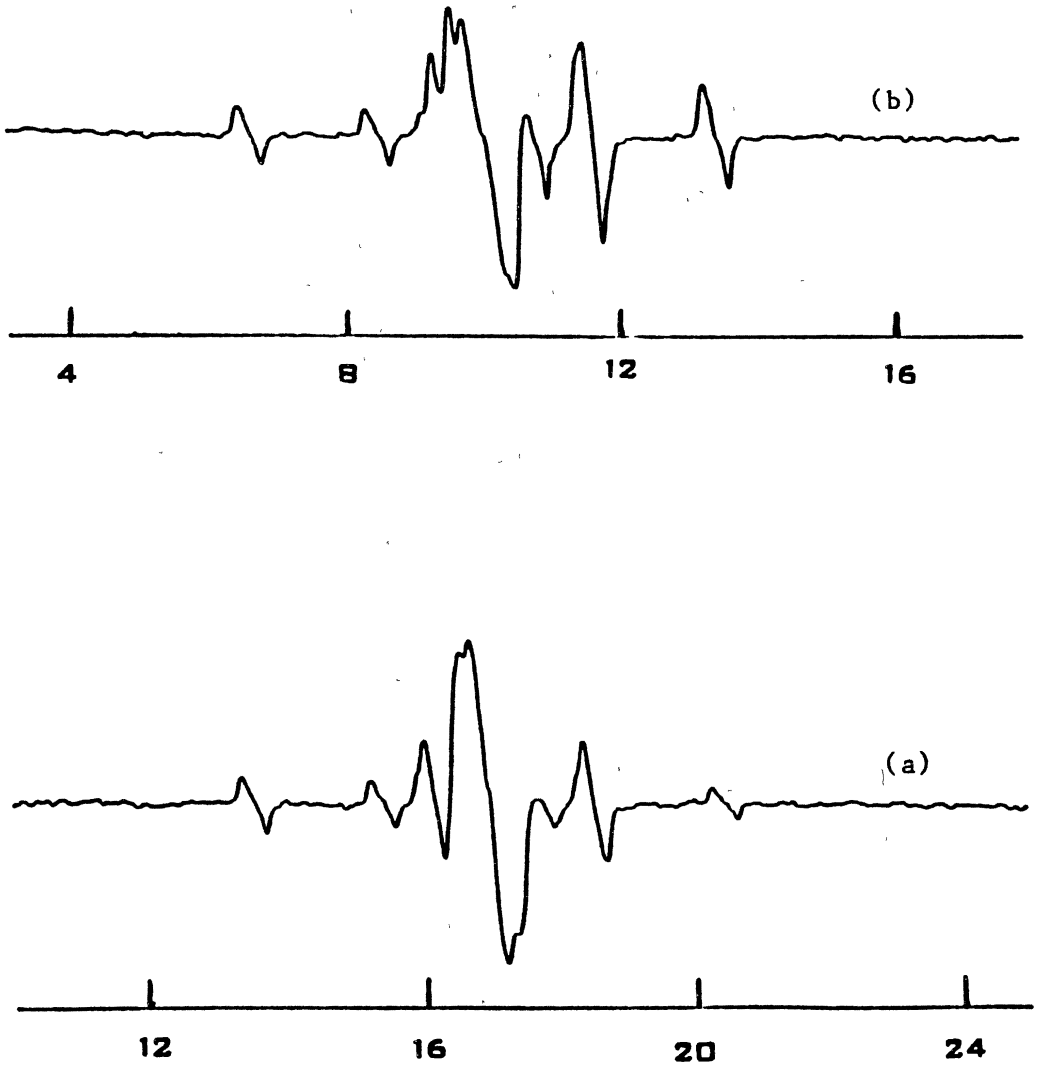

Figure 12. ENDOR Spectrum While Monitoring the (a) High Field and (b) Low Field 0^{o} EPR Line

TABLE 1

NUCLEI IN $KMgF_3$ STRUCTURE POTENTIALLY CONTRIBUTING TO HYPERFINE

Isotope	Natural Abundance (%)	Spin	ENDOR freq. at 3.5 kG (MHz)
F^{19}	100	$\frac{1}{2}$	14.02721
Mg^{25}	10	$\frac{5}{2}$	0.91291
K^{39}	93.26	$\frac{3}{2}$	0.6963030
K^{40}	0.0117	4	0.86582
K^{41}	6.73	$\frac{3}{2}$	0.3821910

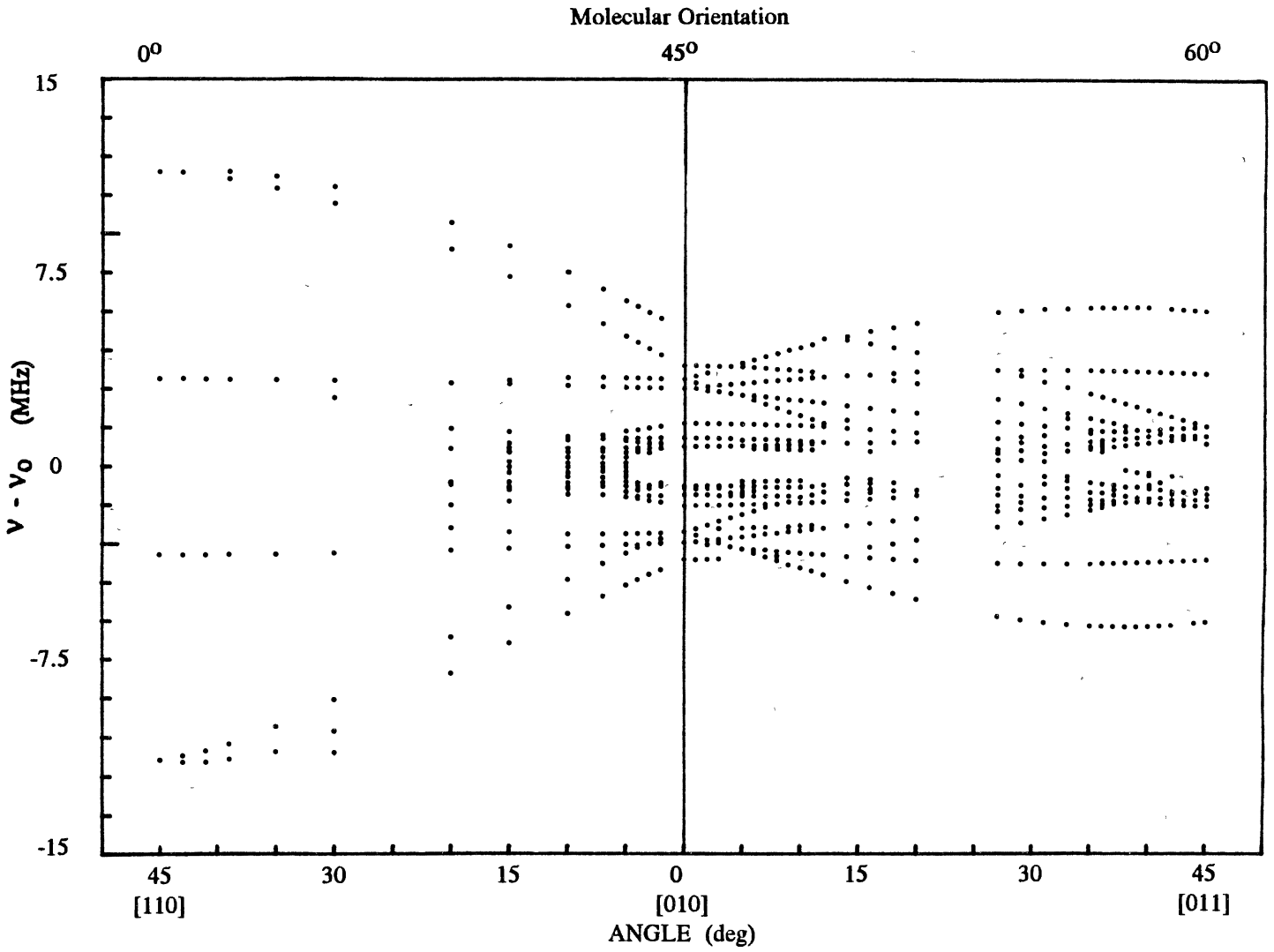

Figure 13. Angular Dependence of ENDOR Lines

Fluorine is a 100% abundant nuclear spin 1/2 so that each of the various neighboring fluorine nuclei should contribute only one pair of lines to the ENDOR spectrum. At this point it is still undetermined as to which of the nuclei contribute which pair of lines to the spectrum. Figure 14 shows the 12 nuclei which make up the first five nearest neighbor fluorine shells. To simplify the figure, potassium nuclei are not shown. In Fig. 14, nuclei which are symmetric about the V_k center are labeled with like letters and nuclei within these groups are denoted by numbers. For some arbitrary orientation of the magnetic field, each of the 12 fluorine nuclei contribute a pair of lines to the spectrum to account for a total of 24 lines. Along the high-symmetry directions many of the nuclei become equivalent with each other with respect to the magnetic field and the [F_2^-] molecule.

The A nuclei lie in a mirror plane of the V_k center and one of their principal axes should lie perpendicular to this plane which is the z axes in Fig. 14. The principal axis corresponding to the largest principal value for the A nuclei should lie nearly along the diagonal [110] direction of Fig. 14 that is to say, in the direction of the V_k center. This is expected to contribute the largest hyperfine interaction of any of the fluorine nuclei due to the p-orbital nature of the V_k center which extends beyond the two nuclei making up the molecule toward the A nuclei. This interaction should be largest when H is along the molecular axis, i.e., the 0^o orientation H $\parallel$ [110] EPR line. Due to the bent bond nature of the V_k center, it is expected that the principal axis of the A nuclei which corresponds to this largest principal value should deviate from the [110] direction just as is the case for the principal axis of the two nuclei comprising the molecule. However, the degree of this deviation should be less than that of the two molecular fluorines, that is to say less than 7^o deviation from [110]. The magnitude of

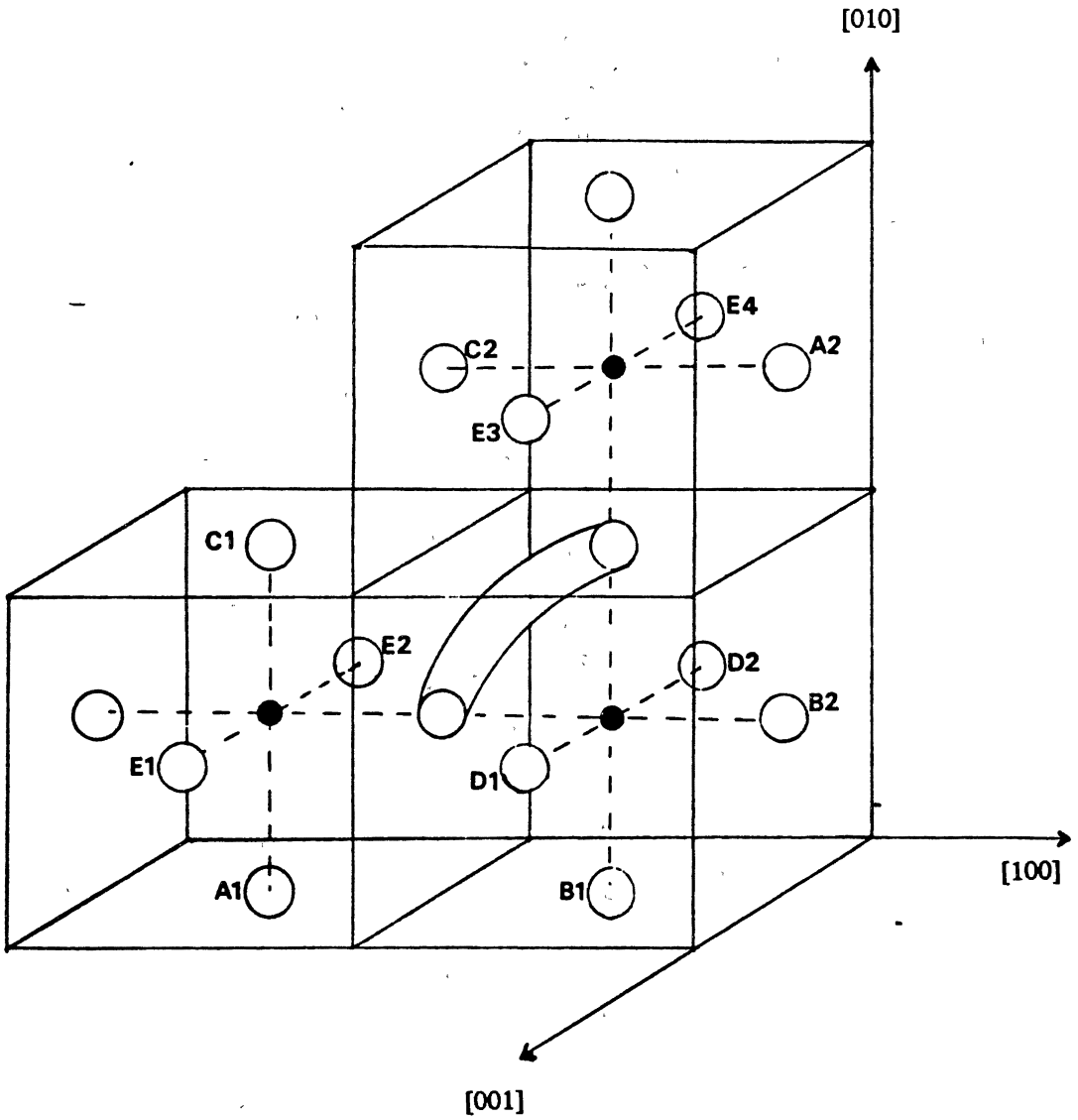

Figure 14. First Five Nearest Neighbor Fluorine Shells

this largest principal value can be estimated from the EPR spectrum. Figure 15 shows an expanded view of the high field 0° EPR line with H ∥ [110]. Along this direction the two A nuclei are equivalent and the EPR line shows the 1:2:1 splitting characteristic of the hyperfine interaction of two equivalent I = 1/2 nuclei. The splitting between the center line and the outer lines is approximately 8 G. Using the following relation along with the approximation $(g/g_e) = 1$, the largest principal value of the A nuclei can be estimated to be about 22 MHz.

$$A(\text{MHz}) = 2.80247\ (g/g_e)\ A(\text{gauss}) \qquad \text{(II.4)}$$

Since the A nuclei are equivalent when H is along the molecular axis, the two nuclei should contribute only 1 pair of lines to the ENDOR spectrum while monitoring the 0° EPR line with H ∥ [110]. As H is rotated away from [110], the two A nuclei become nonequivalent and the single pair of ENDOR lines should split into two pairs. The A nuclei should remain nondegenerate for all other orientations in the 0-45 and 45-60 rotations of Fig. 13.

It is relatively easy to identify in Fig. 13 a set of ENDOR lines which satisfy the above prescribed criteria: a single pair of lines with 22 MHz splitting along the 0° orientation which splits into two pairs when rotated away from this orientation. These ENDOR lines are then singled out and identified as belonging to the A nuclei.

The two D nuclei of Fig. 14 are located close to the center of the molecular ion and should also contribute appreciably to the hyperfine interaction. They also lie in a mirror plane of the molecule and therefore must have one axis perpendicular to this plane, that is to say one axis along the [110] direction. This axis is not expected to correspond to the largest

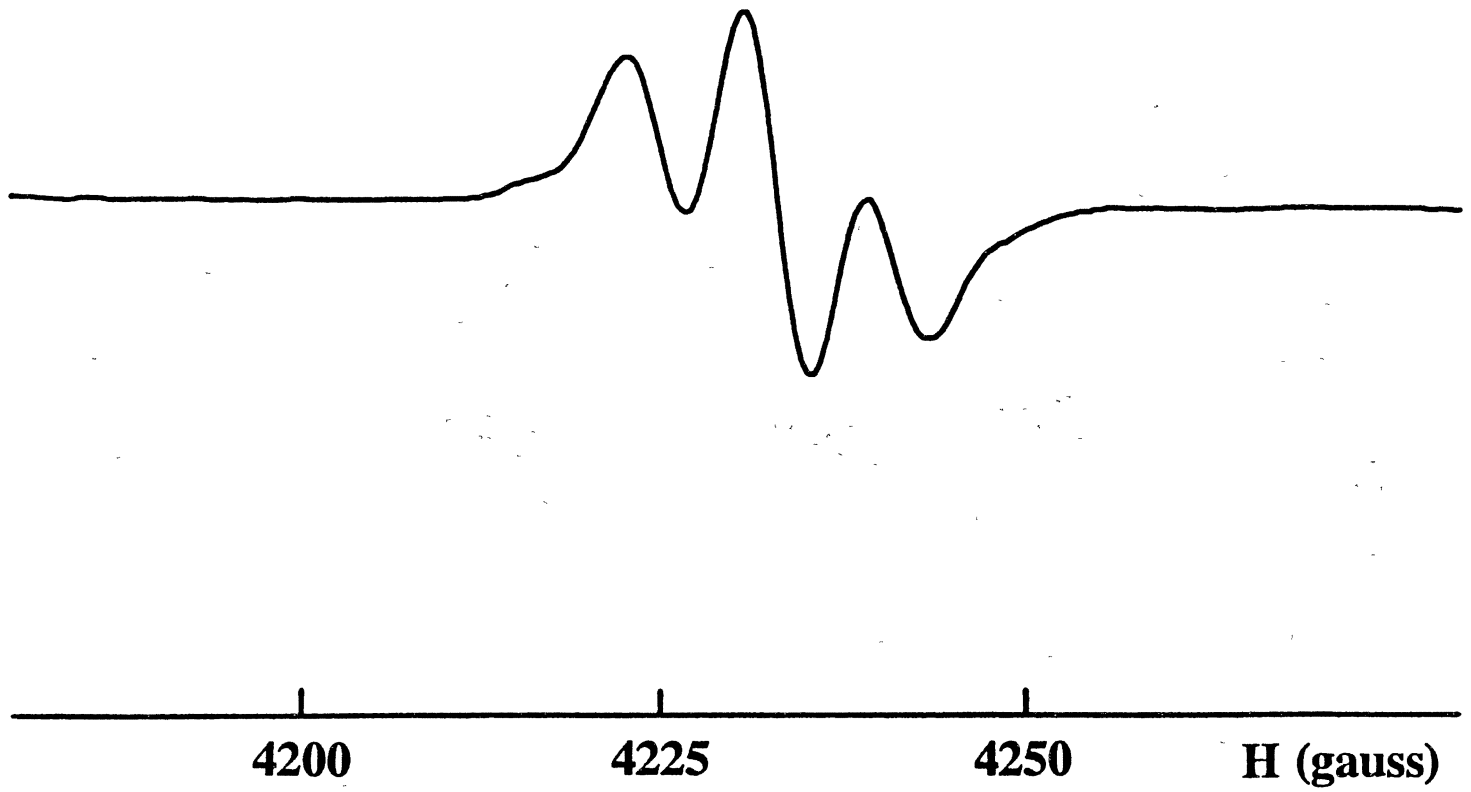

Figure 15. High Field 0^{o} EPR Line When H || [110]

principal value of the D nuclei since it would not be directed toward the molecule but parallel to it. The D nuclei which lie symmetrically above and below the plane of the molecule (the x-y plane of Fig. 14) will be equivalent for all magnetic fields in this plane and nonequivalent when the magnetic field is rotated out of this plane. Thus, in Fig. 13 there should be a single pair of lines in the 0-45 rotation which splits into two pairs as the magnetic field is rotated into the 45-60 plane. Such a set of lines can be found and are thus identified as belonging to the D nuclei.

There are four nuclei in the E set. All four E nuclei are equivalent when H is parallel to the molecular axis. The E1 and E2 nuclei lie symmetrically above and below the x-y plane and are therefore equivalent for all magnetic field orientations in the x-y plane and nonequivalent when the magnetic field is rotated out of this plane. The E3 and E4 nuclei behave similarly but will be nonequivalent to the E1 and E2 nuclei for all magnetic field orientations in the x-y plane except H || [110]. Thus, there should be a single pair of ENDOR lines for the 0^{o} orientation H || [110] which split into two pairs during the 0-45 rotation. Each of these two pairs should again split making four pairs in the 45-60 rotation. A set of lines following these symmetries can be partially identified and are thus assigned to the E nuclei. The reason that a full identification cannot be made is that near the middle of the spectrum there are many lines whose linewidth is nearly that of their separation so that distinguishing between lines is difficult.

The B and C nuclei are expected to contribute the smallest hyperfine interaction, but in general should have the same symmetry as the A nuclei. Their small interaction places their ENDOR lines in the center of the spectrum making identification of these nuclei very difficult. Table 2

TABLE 2

NUMBER OF ENDOR PAIRS FROM
FLUORINE NUCLEI

Direction of H	[110]		[010]		[011]
Orientation of $[F_2^-]$ Molecule	0°		45°		60°
Nuclei					
A	1	2	2	2	2
D	1	1	1	2	2
E	1	2	2	4	4
B	1	2	2	2	2
C	1	2	2	2	2

summarizes the degeneracy patterns for the 5 sets of nuclei expected to contribute the largest hyperfine interaction.

Having identified the nuclei responsible for various ENDOR lines, the principal values and orientations of the principal axes of the various nuclei must be determined. This is accomplished by fitting the data to the spin-Hamiltonian numerically using a computer.

To determine the principal values and principal axes of the A_3 tensor, the angular dependence data was fit to the spin-Hamiltonian

$$\mathcal{H} = \beta\vec{H}\cdot\overleftrightarrow{g}\cdot\vec{S} + \vec{I}_1\cdot\overleftrightarrow{A}_1\cdot\vec{S} + \vec{I}_2\cdot\overleftrightarrow{A}_2\cdot\vec{S} + \vec{I}_3\cdot\overleftrightarrow{A}_3\cdot\vec{S} - g_N\beta_N\vec{H}\cdot(\vec{I}_1 + \vec{I}_2 + \vec{I}_3)\,. \qquad \text{(II.5)}$$

When the direct products are expanded, (II.5) becomes

$$\begin{aligned}\mathcal{H} = {} & \beta\left(H_{x_g}g_{x_g}S_{x_g} + H_{y_g}g_{y_g}S_{y_g} + H_{z_g}g_{z_g}S_{z_g}\right) \\ & + I^1_{x_1}A^1_{x_1}S^1_{x_1} + I^1_{y_1}A^1_{y_1}S^1_{y_1} + I^1_{z_1}A^1_{z_1}S^1_{z_1} \\ & + I^2_{x_2}A^2_{x_2}S^2_{x_2} + I^2_{y_2}A^2_{y_2}S^2_{y_2} + I^2_{z_2}A^2_{z_2}S^2_{z_2} \\ & + I^3_{x_3}A^3_{x_3}S^3_{x_3} + I^3_{y_3}A^3_{y_3}S^3_{y_3} + I^3_{z_3}A^3_{z_3}S^3_{z_3} \\ & - g_N\beta_N H_z\left(I^1_z + I^2_z + I^3_z\right)\end{aligned} \qquad \text{(II.6)}$$

where (x_g, y_g, z_g) is the coordinate system where the g tensor is diagonalized and similarly (x_1, y_1, z_1), (x_2, y_2, z_2) and (x_3, y_3, z_3) are the coordinate systems where the A_1, A_2 and A_3 tensors are diagonalized, respectively. The (x, y, z) coordinate system is reserved for the magnetic field system. Then (II.6) can then be rewitten in the condensed form

$$\mathcal{H} = \beta \sum_{i=1}^{3} H_{i_g} g_{i_g} S_{i_g} + \sum_{n=1}^{3} \sum_{i=1}^{3} I_{i_n}^{n} A_{i_n}^{n} S_{i_n} - g_N \beta_N H_z \sum_{n=1}^{3} I_z^n \qquad \text{(II.7)}$$

where n denotes the nuclei and i_n denotes the i^{th} coordinate of the n^{th} nuclei coordinate system.

The transformation matrix [TG] is defined as transforming a vector written in the g coordinate system to the crystal system. Then an arbitrary vector $\vec{V}$ is transformed as

$$\begin{vmatrix} V_{x_g} \\ V_{y_g} \\ V_{z_g} \end{vmatrix} = [TG] \begin{vmatrix} V_{x_c} \\ V_{y_c} \\ V_{z_c} \end{vmatrix} \qquad \text{(II.8)}$$

Likewise, if [R] transforms from the crystal coordinates to the magnetic field coordinates such that

$$\begin{vmatrix} V_{x_c} \\ V_{y_c} \\ V_{z_c} \end{vmatrix} = [R] \begin{vmatrix} V_x \\ V_y \\ V_z \end{vmatrix} \qquad \text{(II.9)}$$

then

$$\begin{vmatrix} V_{x_g} \\ V_{y_g} \\ V_{z_g} \end{vmatrix} = [TRG] \begin{vmatrix} V_x \\ V_y \\ V_z \end{vmatrix} \qquad \text{where } [TRG] = [TG]\,[R]\ . \qquad \text{(II.10)}$$

In a similar fashion [T1], [T2], and [T3] are defined such that

$$\begin{vmatrix} V_{x_n} \\ V_{y_n} \\ V_{z_n} \end{vmatrix} = [TRn] \begin{vmatrix} V_x \\ V_y \\ V_z \end{vmatrix} \qquad \text{where } [TRn] = [Tn]\ [R] \quad \text{and } n = 1 \text{ or } 2 \text{ or } 3\ . \tag{II.11}$$

Any individual element of a vector can then be written in terms of its magnetic field coordinates as

$$V_{i_n} = \sum_{k=1}^{3} TRn(i,k)\ V_k \ . \tag{II.12}$$

Using (II.12), all of the elements in (II.7) can be written in the magnetic field coordinate system so that the spin-Hamiltonian can now be written

$$\begin{aligned} \mathcal{H} = \beta \sum_{i=1}^{3} \sum_{k=1}^{3} TRG(i,k)\ H_k\ g_{ik} \sum_{p=1}^{3} TRG(i,p)\ S_p \\ + \sum_{n=1}^{3} \sum_{i=1}^{3} \sum_{q=1}^{3} TRn(i,q)\ I_q^n\ A_{i_n}^n \sum_{t=1}^{3} TRn(i,t)\ S_t \\ - g_N \beta_N H_z \sum_{n=1}^{3} I_z^n \end{aligned} \tag{II.13}$$

Defining the magnetic field as the z direction so that $H_x = H_y = 0$ and $H_z = H$, then by regrouping terms, (II.13) is simplified further to the form

$$\mathcal{H} = \beta H \sum_{=1}^{3} QG_p S_p + \sum_{n=1}^{3} \sum_{q=1}^{3} \sum_{t=1}^{3} Qn_{q,t} I_q^n S_t - g_N \beta_N H_z \sum_{n=1}^{3} I_z^n \qquad \text{(II.14)}$$

where

$$QG_p = \sum_{i=1}^{3} g_{i_g} TRG(i,3)\ TRG(i,p) \qquad \text{(II.15)}$$

and

$$Qn_{q,t} = \sum_{i=1}^{3} A_{i_n}^n\ TRn(i,q)\ TRn(i,t) \qquad \text{(II.16)}$$

Using the relations

$$S_1 = S_x = \frac{1}{2}(S_+ + S_-) \qquad S_2 = S_y = \frac{i}{2}(S_+ - S_-)$$
$$I_1 = 1_x = \frac{1}{2}(I_+ + I_-) \qquad I_2 = I_y = \frac{i}{2}(I_+ - I_-) \qquad \text{(II.17)}$$

(II.14) can be written in terms of raising and lowering operators.

$$
\begin{aligned}
\mathcal{H} = {} & \beta H\left[\frac{1}{2}QG_1 - \frac{i}{2}QG_2\right] S_+ \\
& + \beta H\left[\frac{1}{2}QG_1 + \frac{i}{2}QG_2\right] S_- \\
& + \beta H\left[QG_3 \qquad\right] S_z \\
& - g_N\beta_N H \sum_{n=1}^{3} I_z^n \\
& + \sum_{n=1}^{3} \left[\frac{1}{4}(Qn_{1,1} - Qn_{2,2}) - \frac{i}{2}Qn_{1,2}\right] I_+^n S_+ \\
& \quad + \left[\frac{1}{4}(Qn_{1,1} + Qn_{2,2}) \qquad\right] I_-^n S_+ \\
& \quad + \left[\frac{1}{4}(Qn_{1,1} - Qn_{2,2}) + \frac{i}{2}Qn_{1,2}\right] I_-^n S_- \\
& \quad + \left[\frac{1}{2}Qn_{1,3} \qquad - \frac{i}{2}Qn_{2,3}\right] I_+^n S_z \\
& \quad + \left[\frac{1}{2}Qn_{1,3} \qquad + \frac{i}{2}Qn_{2,3}\right] I_-^n S_z \\
& \quad + \left[\frac{1}{2}Qn_{1,3} \qquad - \frac{i}{2}Qn_{2,3}\right] I_z^n S_+ \\
& \quad + \left[\frac{1}{2}Qn_{1,3} \qquad + \frac{i}{2}Qn_{2,3}\right] I_z^n S_- \\
& \quad + \left[Qn_{3,3} \qquad\qquad\right] I_z^n S_z
\end{aligned}
\tag{II.18}
$$

TABLE 3

LOWER HALF OF THE SPIN HAMILTONIAN MATRIX

	^ + + + + −	^ | + + + −	^ + | + + −	^ | | + + −	^ + + | | −	^ | + | + −	^ + | + | −	^ | | | | −	^ + + + | | −	^ | + + | | −	^ + | + | | −	^ | | | | | −	^ + + + + | −	^ | + + + | −	^ + | + + | −	^ | | + + | −	^ + + | | | −	^ | | | | | −
<++++|	(1,1)															
<+++-|	(2,1)	(2,2)														
<++-+|	(3,1)		(3,3)													
<++--|		(4,2)	(4,3)	(4,4)												
<+-++|	(5,1)				(5,5)											
<+-+-|		(6,2)			(6,5)	(6,6)										
<+--+|			(7,3)		(7,5)		(7,7)									
<+---|				(8,4)		(8,6)	(8,7)	(8,8)								
<-+++|	(9,1)		(9,3)		(9,5)				(9,9)							
<-++-|		(10,2)		(10,4)		(10,6)			(10,9)	(10,10)						
<-+-+|	(11,1)		(11,3)				(11,7)		(11,9)		(11,11)					
<-+--|		(12,2)		(12,4)				(12,8)		(12,10)	(12,11)	(12,12)				
<--++|	(13,1)				(13,5)		(13,7)		(13,9)				(13,13)			
<--+-|		(14,2)				(14,6)		(14,8)		(14,10)			(14,13)	(14,14)		
<---+|			(15,3)		(15,5)		(15,7)				(15,11)		(15,13)		(15,15)	
<----|				(16,4)		(16,6)		(16,8)				(16,12)		(16,14)	(16,15)	(16,16)

The system contains four spins (one hole and three nuclei) each of spin 1/2. The basis set then consists of sixteen eigenvectors written as $| m_s, m_{I_1}, m_{I_2}, m_{I_3} >$. The matrix form of the Hamiltonian will be a 16x16 hermitian matrix and is thus specified by it lower half shown in Table 3. The matrix element H(9,1) for example corresponds to the element $< - + + + | H | + + + + >$. The only non-zero terms in the Hamiltonian, (II.18), are those whose operators are S_-, $I^1{}_z S_-$, $I^2{}_z S_-$ and $I^3{}_z S_-$. The above matrix element is then defined to be

$$\mathcal{H}(9,1)=(1/2)QG_1 + (i/2)QG_2 + (1/4)Q1_{1,3} + (i/4)Q1_{2,3} + (1/4)Q2_{1,3} + i/4)Q2_{2,3} + (1/4)Q3_{1,3} + (i/4)Q3_{2,3} \qquad \text{(II.19)}$$

The other non-zero lower half matrix elements are:

$$\mathcal{H}(1,1) = (1/2)QG_3 + (1/4)(Q1_{3,3} + Q2_{3,3} + Q3_{3,3}) - (3/2)\, g_N\beta_N H$$
$$\mathcal{H}(2,2) = (1/2)QG_3 + (1/4)(Q1_{3,3} + Q2_{3,3} - Q3_{3,3}) - (1/2)\, g_N\beta_N H$$
$$\mathcal{H}(3,3) = (1/2)QG_3 + (1/4)(Q1_{3,3} - Q2_{3,3} + Q3_{3,3}) - (1/2)\, g_N\beta_N H$$
$$\mathcal{H}(4,4) = (1/2)QG_3 + (1/4)(Q1_{3,3} - Q2_{3,3} - Q3_{3,3}) + (1/2)\, g_N\beta_N H$$
$$\mathcal{H}(5,5) = (1/2)QG_3 - (1/4)(Q1_{3,3} + Q2_{3,3} + Q3_{3,3}) - (1/2)\, g_N\beta_N H$$
$$\mathcal{H}(6,6) = (1/2)QG_3 - (1/4)(Q1_{3,3} + Q2_{3,3} - Q3_{3,3}) + (1/2)\, g_N\beta_N H$$
$$\mathcal{H}(7,7) = (1/2)QG_3 - (1/4)(Q1_{3,3} - Q2_{3,3} + Q3_{3,3}) + (1/2)\, g_N\beta_N H$$
$$\mathcal{H}(8,8) = (1/2)QG_3 - (1/4)(Q1_{3,3} - Q2_{3,3} - Q3_{3,3}) + (3/2)\, g_N\beta_N H$$
$$\mathcal{H}(9,9) = -(1/2)QG_3 - (1/4)(Q1_{3,3} - Q2_{3,3} - Q3_{3,3}) - (3/2)\, g_N\beta_N H$$
$$\mathcal{H}(10,10) = -(1/2)QG_3 - (1/4)(Q1_{3,3} - Q2_{3,3} + Q3_{3,3}) - (1/2)\, g_N\beta_N H$$
$$\mathcal{H}(11,11) = -(1/2)QG_3 - (1/4)(Q1_{3,3} + Q2_{3,3} - Q3_{3,3}) - (1/2)\, g_N\beta_N H$$
$$\mathcal{H}(12,12) = -(1/2)QG_3 - (1/4)(Q1_{3,3} + Q2_{3,3} + Q3_{3,3}) + (1/2)\, g_N\beta_N H$$
$$\mathcal{H}(13,13) = -(1/2)QG_3 + (1/4)(Q1_{3,3} - Q2_{3,3} - Q3_{3,3}) - (1/2)\, g_N\beta_N H$$
$$\mathcal{H}(14,14) = -(1/2)QG_3 + (1/4)(Q1_{3,3} - Q2_{3,3} + Q3_{3,3}) + (1/2)\, g_N\beta_N H$$
$$\mathcal{H}(15,15) = -(1/2)QG_3 + (1/4)(Q1_{3,3} + Q2_{3,3} - Q3_{3,3}) + (1/2)\, g_N\beta_N H$$
$$\mathcal{H}(16,16) = -(1/2)QG_3 + (1/4)(Q1_{3,3} + Q2_{3,3} + Q3_{3,3}) + (3/2)\, g_N\beta_N H$$

$$\mathcal{H}(9,1) = (1/2)QG_1 + (1/4)(Q1_{1,3} + Q2_{1,3} + Q3_{1,3}) + (i/2)QG_1 + (i/4)(Q1_{1,3} + Q2_{1,3} + Q3_{1,3})$$

$$\mathcal{H}(10,2) = (1/2)QG_1 + (1/4)(Q1_{1,3} + Q2_{1,3} - Q3_{1,3}) + (i/2)QG_1 + (i/4)(Q1_{1,3} + Q2_{1,3} - Q3_{1,3})$$

$$\mathcal{H}(11,3) = (1/2)QG_1 + (1/4)(Q1_{1,3} - Q2_{1,3} + Q3_{1,3}) + (i/2)QG_1 + (i/4)(Q1_{1,3} - Q2_{1,3} + Q3_{1,3})$$

$$\mathcal{H}(12,4) = (1/2)QG_1 + (1/4)(Q1_{1,3} - Q2_{1,3} - Q3_{1,3}) + (i/2)QG_1 + (i/4)(Q1_{1,3} - Q2_{1,3} - Q3_{1,3})$$

$$\mathcal{H}(13,5) = (1/2)QG_1 - (1/4)(Q1_{1,3} + Q2_{1,3} + Q3_{1,3}) + (i/2)QG_1 - (i/4)(Q1_{1,3} + Q2_{1,3} + Q3_{1,3})$$

$$\mathcal{H}(14,6) = (1/2)QG_1 - (1/4)(Q1_{1,3} + Q2_{1,3} - Q3_{1,3}) + (i/2)QG_1 - (i/4)(Q1_{1,3} + Q2_{1,3} - Q3_{1,3})$$

$$\mathcal{H}(15,7) = (1/2)QG_1 - (1/4)(Q1_{1,3} - Q2_{1,3} + Q3_{1,3}) + (i/2)QG_1 - (i/4)(Q1_{1,3} - Q2_{1,3} + Q3_{1,3})$$

$$\mathcal{H}(16,8) = (1/2)QG_1 - (1/4)(Q1_{1,3} - Q2_{1,3} - Q3_{1,3}) + (i/2)QG_1 - (i/4)(Q1_{1,3} - Q2_{1,3} - Q3_{1,3})$$

$$\mathcal{H}(2,1) = (1/4)Q3_{1,3} + (i/4)Q3_{2,3}$$

$$\mathcal{H}(4,3) = (1/4)Q3_{1,3} + (i/4)Q3_{2,3}$$

$$\mathcal{H}(6,5) = (1/4)Q3_{1,3} + (i/4)Q3a$$

$$\mathcal{H}(8,7) = (1/4)Q3_{1,3} + (i/4)Q3_{2,3}$$

$$\mathcal{H}(10,9) = (-1/4)Q3_{1,3} + (-i/4)Q3_{2,3}$$

$$\mathcal{H}(12,11) = (-1/4)Q3_{1,3} + (-i/4)Q3_{2,3}$$

$$\mathcal{H}(14,13) = (-1/4)Q3_{1,3} + (-i/4)Q3_{2,3}$$

$$\mathcal{H}(16,15) = (-1/4)Q3_{1,3} + (-i/4)Q3_{2,3}$$

$$\mathcal{H}(3,1) = (1/4)Q2_{1,3} + (i/4)Q2_{2,3}$$

$$\mathcal{H}(4,2) = (1/4)Q2_{1,3} + (i/4)Q2_{2,3}$$

$$\mathcal{H}(7,5) = (1/4)Q2_{1,3} + (i/4)Q2_{2,3}$$

$$\mathcal{H}(8,6) = (1/4)Q2_{1,3} + (i/4)Q2_{2,3}$$

$$\mathcal{H}(11,9) = (-1/4)Q2_{1,3} + (-i/4)Q2_{2,3}$$

$$\mathcal{H}(12,10) = (-1/4)Q2_{1,3} + (-i/4)Q2_{2,3}$$

$$\mathcal{H}(15,13) = (-1/4)Q2_{1,3} + (-i/4)Q2_{2,3}$$

$$\mathcal{H}(16,14) = (-1/4)Q2_{1,3} + (-i/4)Q2_{2,3}$$

$$\mathcal{H}(5,1) = (1/4)Q1_{1,3} + (i/4)Q1_{2,3}$$

$$\mathcal{H}(6,2) = (1/4)Q1_{1,3} + (i/4)Q1_{2,3}$$

$$\mathcal{H}(7,3) = (1/4)Q1_{1,3} + (i/4)Q1_{2,3}$$

$$\mathcal{H}(8,4) = (1/4)Q1_{1,3} + (i/4)Q1_{2,3}$$

$\mathcal{H}(13,9) = (-1/4)Q1_{1,3} + (-i/4)Q1_{2,3}$

$\mathcal{H}(14,10) = (-1/4)Q1_{1,3} + (-i/4)Q1_{2,3}$

$\mathcal{H}(15,11) = (-1/4)Q1_{1,3} + (-i/4)Q1_{2,3}$

$\mathcal{H}(16,12) = (-1/4)Q1_{1,3} + (-i/4)Q1_{2,3}$

$\mathcal{H}(9,5) = (1/4)(Q1_{1,1} + Q1_{2,2})$

$\mathcal{H}(10,6) = (1/4)(Q1_{1,1} + Q1_{2,2})$

$\mathcal{H}(11,7) = (1/4)(Q1_{1,1} + Q1_{2,2})$

$\mathcal{H}(12,8) = (1/4)(Q1_{1,1} + Q1_{2,2})$

$\mathcal{H}(13,1) = (1/4)(Q1_{1,1} - Q1_{2,2}) + (i/2)Q1_{1,2}$

$\mathcal{H}(14,2) = (1/4)(Q1_{1,1} - Q1_{2,2}) + (i/2)Q1_{1,2}$

$\mathcal{H}(15,3) = (1/4)(Q1_{1,1} - Q1_{2,2}) + (i/2)Q1_{1,2}$

$\mathcal{H}(16,4) = (1/4)(Q1_{1,1} - Q1_{2,2}) + (i/2)Q1_{1,2}$

$\mathcal{H}(9,3) = (1/4)(Q2_{1,1} + Q2_{2,2})$

$\mathcal{H}(10,4) = (1/4)(Q2_{1,1} + Q2_{2,2})$

$\mathcal{H}(13,7) = (1/4)(Q2_{1,1} + Q2_{2,2})$

$\mathcal{H}(14,8) = (1/4)(Q2_{1,1} + Q2_{2,2})$

$\mathcal{H}(11,1) = (1/4)(Q2_{1,1} - Q2_{2,2}) + (i/2)Q2_{1,2}$

$\mathcal{H}(12,2) = (1/4)(Q2_{1,1} - Q2_{2,2}) + (i/2)Q2_{1,2}$

$\mathcal{H}(15,5) = (1/4)(Q2_{1,1} - Q2_{2,2}) + (i/2)Q2_{1,2}$

$\mathcal{H}(16,6) = (1/4)(Q2_{1,1} - Q2_{2,2}) + (i/2)Q2_{1,2}$

$\mathcal{H}(9,3) = (1/4)(Q3_{1,1} + Q3_{2,2})$

$\mathcal{H}(10,4) = (1/4)(Q3_{1,1} + Q3_{2,2})$

$\mathcal{H}(13,7) = (1/4)(Q3_{1,1} + Q3_{2,2})$

$\mathcal{H}(14,8) = (1/4)(Q3_{1,1} + Q3_{2,2})$

$\mathcal{H}(11,1) = (1/4)(Q3_{1,1} - Q3_{2,2}) + (i/2)Q3_{1,2}$

$\mathcal{H}(12,2) = (1/4)(Q3_{1,1} - Q3_{2,2}) + (i/2)Q3_{1,2}$

$\mathcal{H}(15,5) = (1/4)(Q3_{1,1} - Q3_{2,2}) + (i/2)Q3_{1,2}$

$\mathcal{H}(16,6) = (1/4)(Q3_{1,1} - Q3_{2,2}) + (i/2)Q3_{1,2}$

The Hamiltonian matrix elements defined above were incorporated in a computer program to calculate the hyperfine principal values and principal axes. A flow chart of the fitting program is given Fig. 16. The actual program which ran on an Hewlett Packard model 300 computer is given in the Appendix. The principal values and principal axes were determined for

each set of nuclei separately. The data points corresponding to a specific set of nuclei, selected as described earlier, were entered as nuclear transition frequency, and magnetic field. These data points were then compared with those generated from the spin-Hamiltonian. The principal values and principal axes used in the spin-Hamiltonian were systematically change to minimize the difference between the Hamiltonian generated data points and the measured data points. The principal values and principal axes as determined from the above described progam are given in Table 4 where ϕ and θ are the polar and azimuthual angles respectively, along with those for the molecular fluorines as determined from EPR by Hall. Figures 17, 18 and 19 show the experimentally measured data points (represented by the *) and the computer-predicted line positions (represented by lines) for the A, D, and E nuclei described earlier. Figues 20, 21 and 22 show the principal axes orientations given in Table 4.

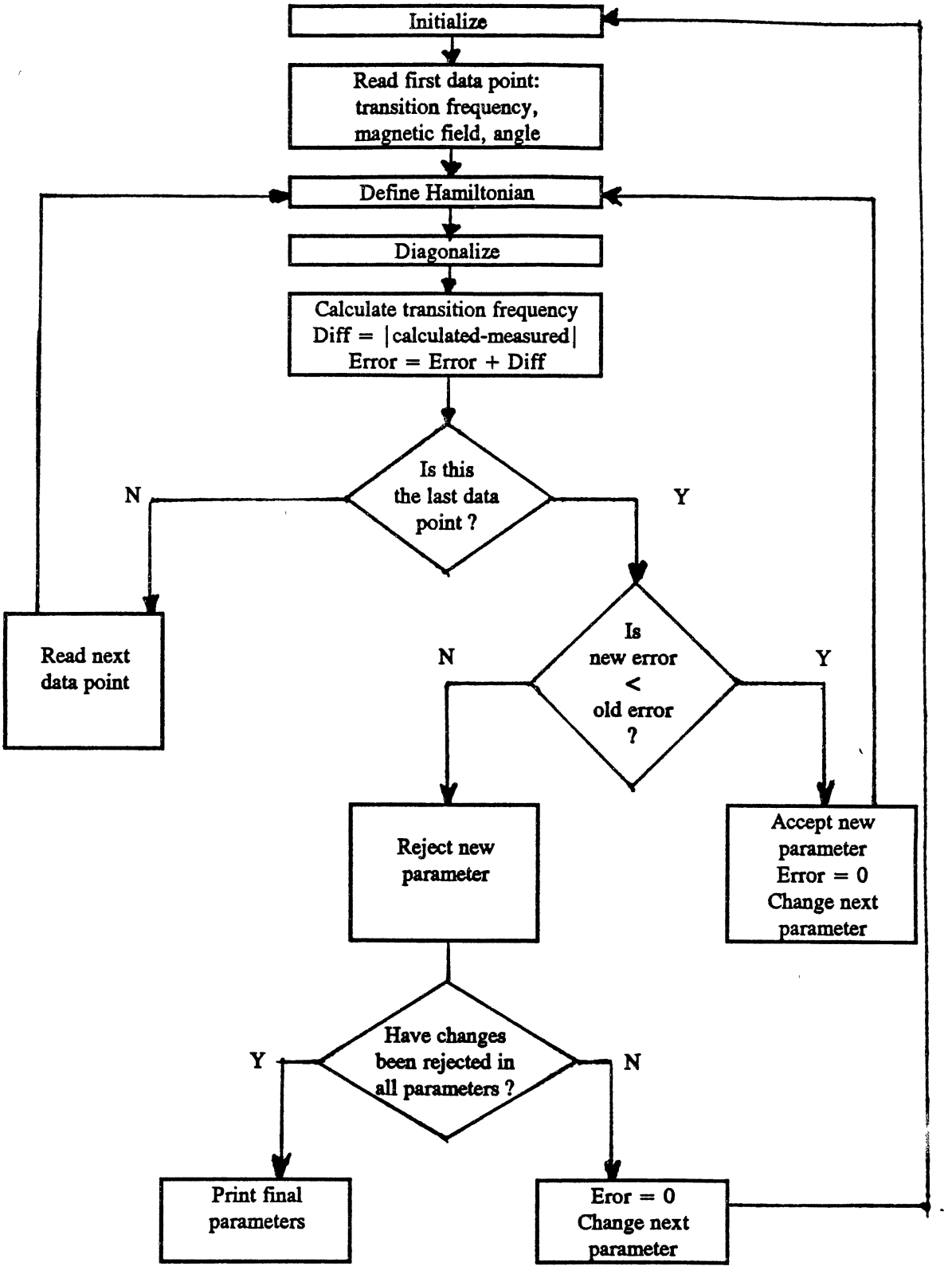

Figure 16. Flow Chart of Fitting Program

TABLE 4

PRINCIPAL VALUES AND
PRINCIPAL AXES
ORIENTATION

Principal Values		Orientation ϕ,θ	
g_x	2.024	90 , 135	
g_y	2.018	0 , 0	Determined
g_z	2.0024	90 , 45	by
$^{M}A_x$	160	90 , 128	Hall
$^{M}A_y$	160	0 , 0	
$^{M}A_z$	2479	90 , 38	
$^{A}A_x$	-1.8	90 , 138.3	
$^{A}A_y$	-1.6	0 , 0	
$^{A}A_z$	22.7	90 , 48.3	Determined
$^{D}Z_x$	8.2	132.3 , 135	by
$^{D}A_y$	3.0	42.3 , 135	Current
$^{D}A_z$	6.8	90 , 45	Investigation
$^{E}A_x$	-2.7	123.4 , 53.8	
$^{E}A_y$	-2.0	68 4 , -22.5	
$^{E}A_z$	12.9	138.9 , -85.6	

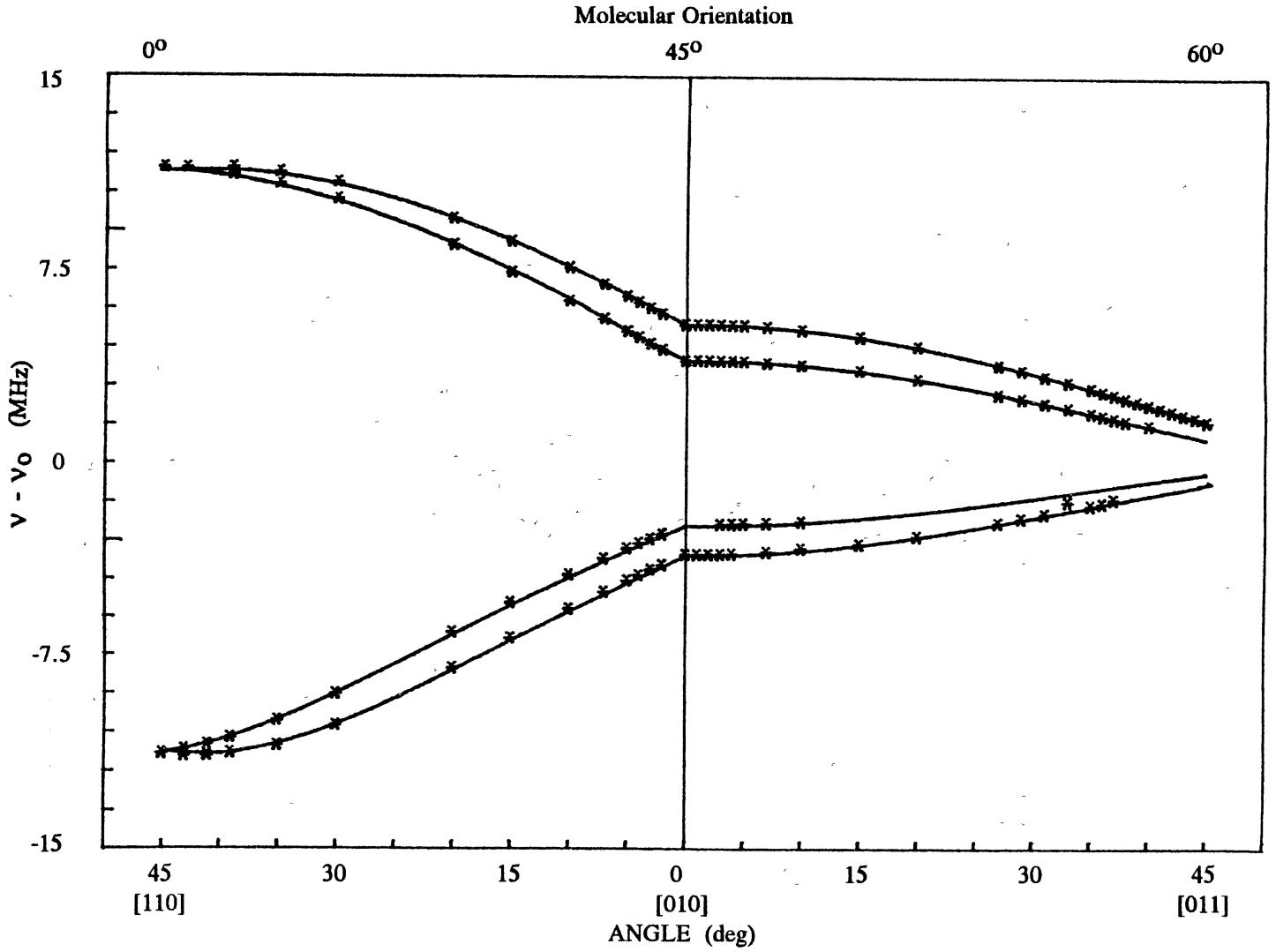

Figure 17. A ENDOR Line Positions

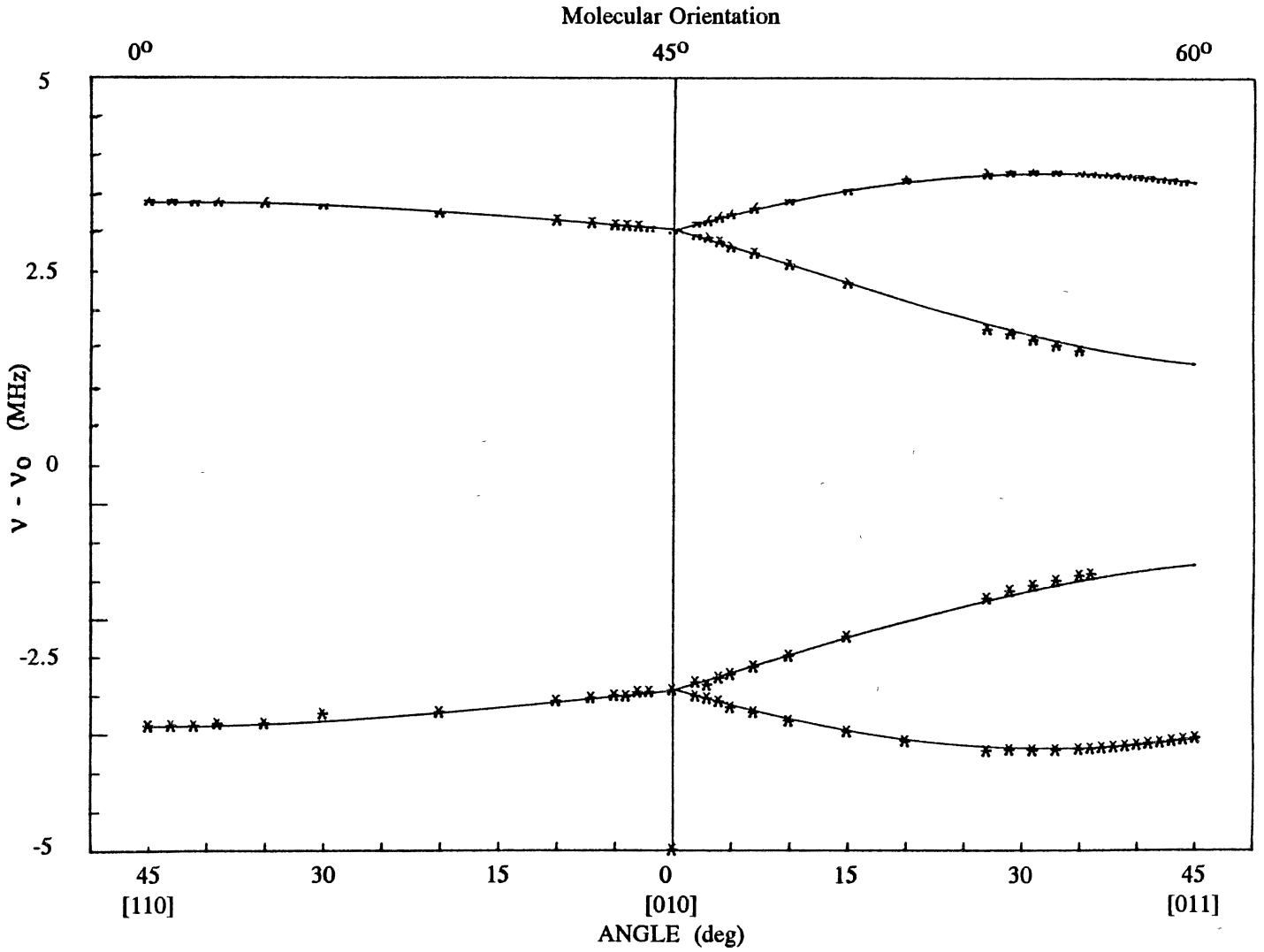

Figure 18. D ENDOR Line Positions

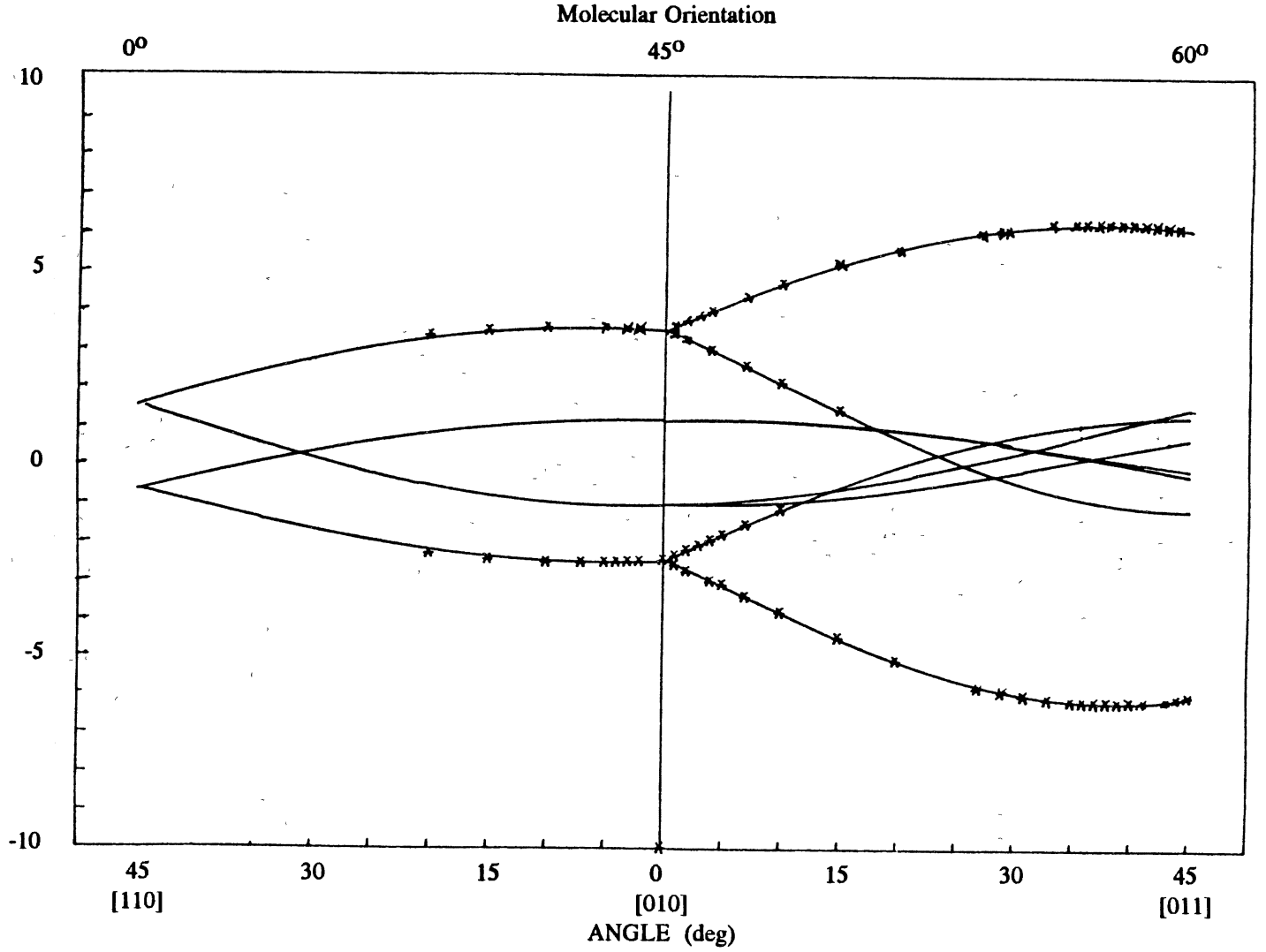

Figure 19. E ENDOR Line Positions

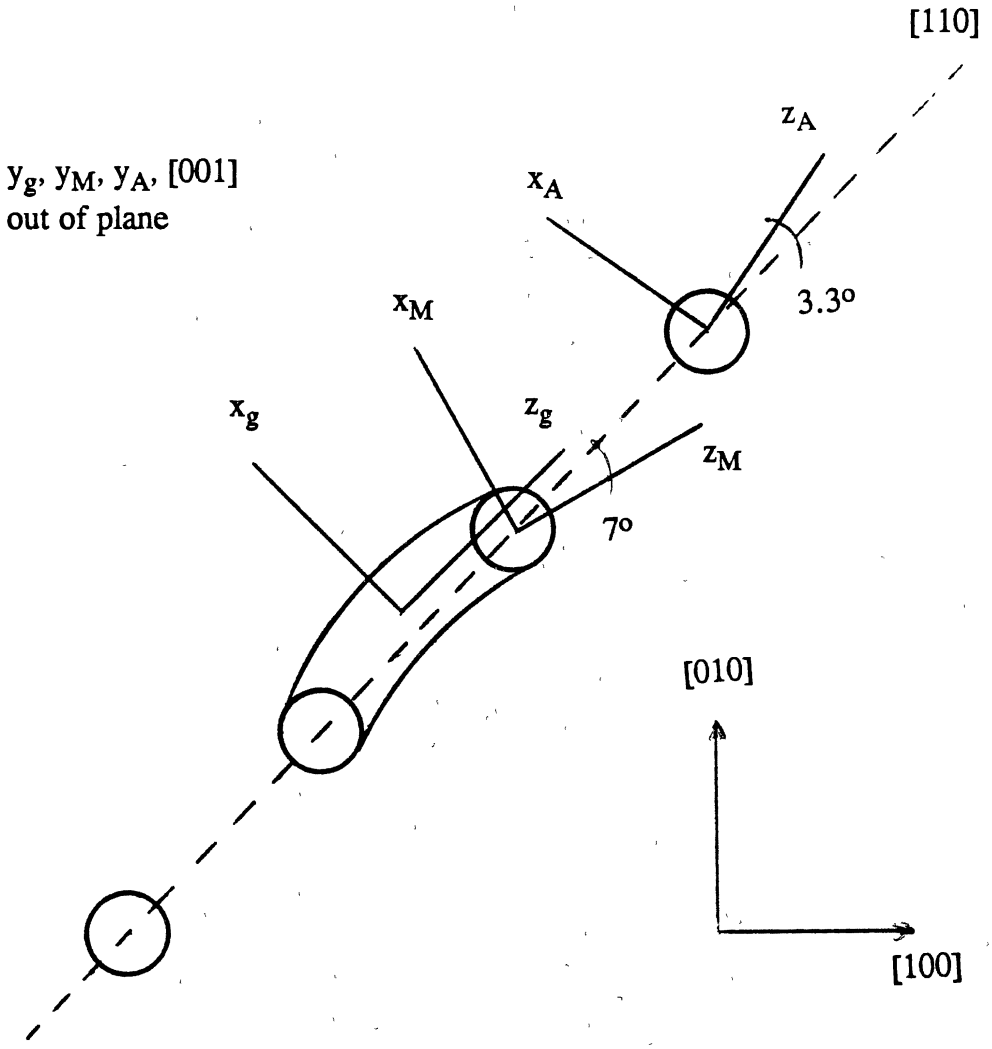

Figure 20. Configuration of Principal Axes of Molecule and A Nucleus

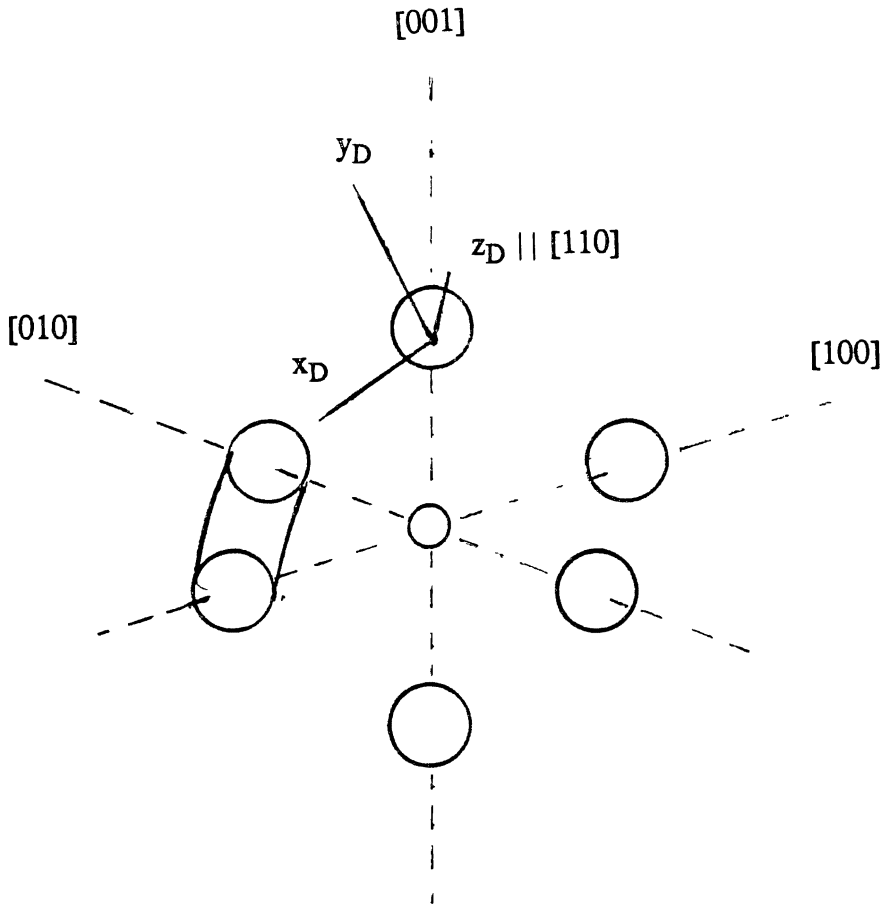

Figure 21. Configuration of Principal Axes of D Nucleus

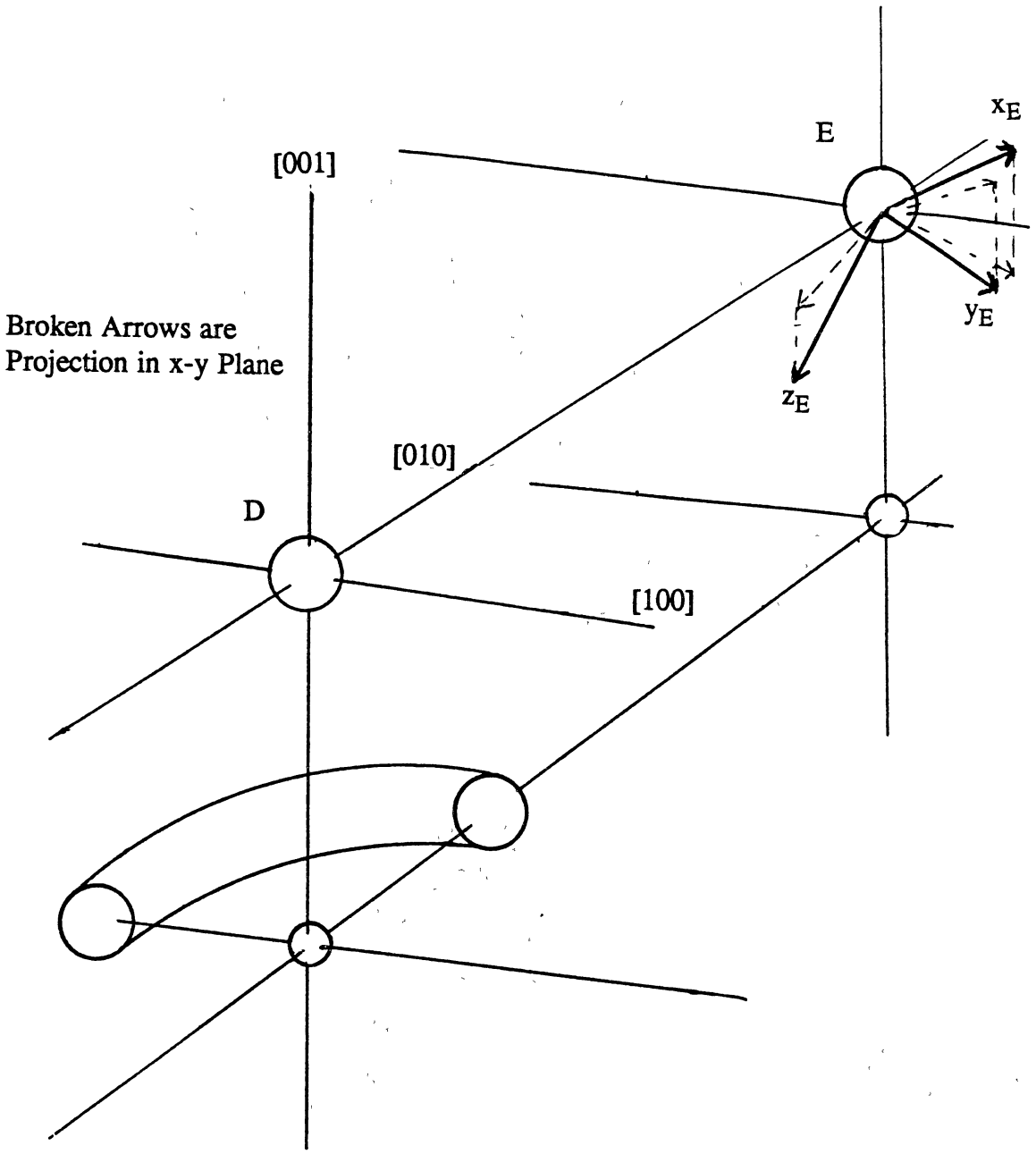

Figure 22. Configuration of Principal Axes of D Nucleus

CHAPTER III

POINT DEFECTS IN KTP

Introduction

Potassium titanyl phosphate ($KTiOPO_4$ or KTP) is a material with application in nonlinear optics and electro-optics.[16,17] It is commonly employed in second-harmonic generation (frequency doubling) of 1.06 μm Nd:YAG laser radiation producing 0.53 μm output.[17,18] KTP has also been shown to permit type-2 phase-matched second harmonic generation and sum-frequency generation down to 0.4950 μm and 0.4589-μm respectively.[19] KTP has been used to produce a Mach-Zehnder electro-optic waveguide capable of modulating light up to 12 GHz.[20]

The rather complicated crystal structure of KTP (Fig. 23)[21] was studied by Tordjman et al. who determined the point group to be mm and the space group to be $Pn2_1a$. The lattice constants are a = 12.814 Å, b = 6.404 Å and c = 10.616 Å. The phosphate octehedra account for 8 of the 10 independent oxygens found in the unit cell. The other two oxygens are bonded to only potassium and, titanium ions and in each case, these two oxygens have one short bond to Ti (bold lines in Fig. 23). The structure is characterized by chains of PO_4 - TiO_6 - PO_4 - TiO_6 - in both the a and b directions. In the a-c plane these chains are separated by TiO_6 octehedra which in turn form a chain of TiO_6 octehedra that zigzag along the c axis. Alternating long and

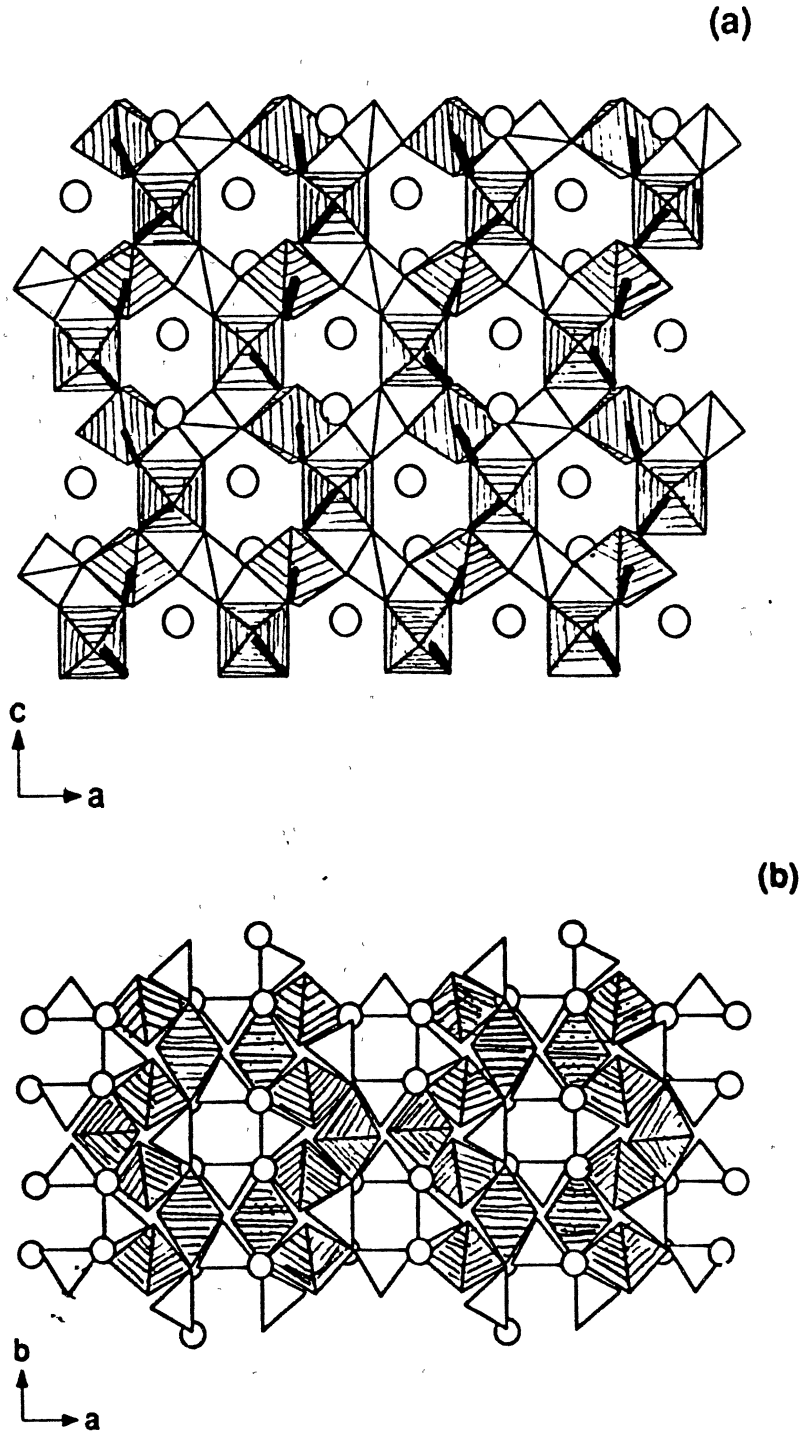

Figure 23. Projection of KTP Structure in (a) a-c Plane and (b) a-b Plane

short Ti-O bonds occur along these chains which result in a net z-directed polarization. This polarization arising from alternating long and short bonds is the major factor giving rise to the large nonlinear-optic and electrooptic coefficients of KTP. Channels exists along the c-axis through which K^+ ions can diffuse with a diffusion coefficient several orders of magnitude greater than in the x-y plane.

Both hydrothermal and flux techniques have been successfully used in the growth of fairly large KTP single crystals.[23-29] The hydrothermal process for KTP requires growing crystals in a high-pressure, high-temperature autoclave operating at 550° to 600° C and at 25,000 psi for approximately 6 weeks. Equipment restrictions due to the high-temperatures and high pressures limits crystal size to approximately 20 mm x 20 mm x 60 mm. The flux technique which is carried out at atmospheric pressure is not hampered by the need for sophisticated high pressure equipment. Flux techniques vary depending on the specific flux used and crystals have been grown from 700°C to 1000°C with growth times ranging from 10 days to 2 months. Typical crystal dimensions from flux growth are 60 mm x 55 mm x 30 mm.

While the nonlinear optic and electro-optic coefficients of KTP grown by the two different techniques are similar, differences exist in dielectric and optical damage properties. KTP crystals are subject to optical damage; one form of which is the production of gray tracks when high power, high repetition rate laser pulses are doubled.[30] Reports of the optical damage threshold for frequency doubling of 1.06 μm light range from 150 to 5000 MW cm^{-2}. Indications to date suggest that the damage threshold for hydrothermally grown KTP is somewhat higher than that for flux grown material.

If a crystal used for nonlinear interaction has even a small amount of absorption, the efficiency of the nonlinear interaction is greatly decreased. The absorption of laser radiation occurs throughout the volume of the crystal through which the beam passes. This causes heating in this illuminated region. Cooling however occurs by conducting heat to the surface of the crystal which then produces thermal gradients. Since the refractive index depends on the temperature, gradients and variations in the refractive index will also be generated. These variations will result in nonideal phasematching in the volume of nonlinear interaction causing degradation in the efficiency of such interactions. The gray tracks characteristic of optical damage in KTP absorb both the fundamental and second harmonic thus rapidly degrading doubling efficiency. Continued operation after the formation of the gray coloration may quickly lead to catastrophic failure.

While the growth of KTP crystals for frequency doublers has been commercialized and are readily available, many aspects of the growth are not well understood. In addition to the variations in optical damage threshold other inconsistencies exist between crystals grown by the two different methods as well as inconsistencies between crystals grown under apparently identical conditions. KTP is generally transparent from 0.35 mm to 4.5 mm, however, some crystals have a slight yellow coloration after growth even though the process followed seems to be the same as those which appear clear. Absorption coefficients may vary by as much as an order of magnitude at some wavelengths. Nonuniformities also exist within a single crystal.

It is the purpose of the current studies herein to show the potential of magnetic resonance as a spectroscopic technique to be used in the evaluation of KTP crystals as well as the identification and characterization of defects. To date there have been only a few EPR studies of KTP. Iron has been studied

in Fe-doped crystals[31,32] and Ti^{3+} spectra have been identified in electric field treated samples.[33] Both of those studies were conducted on flux grown material.

Experimental Procedure

All of the KTP samples used in this investigation were hydrothermally grown and supplied by Litton/Airtron. These samples were actual commercial products prepared to function as frequency doubling devices used to double 1.06 μm Nd:YAG radiation. Sample dimensions were 3 x 3 x 5 mm. The c-axis lies perpendicular to one of the sample faces and perpendicular to the long dimension of the crystal. The a and b axes however, were rotated out of the face by 22° corresponding to the phase-matching angle. Figure 24 shows the orientation of the sample faces with the crystallographic axes

EPR spectra were taken at 20 K on a Bruker ER-300 spectrometer operating at 9.44 GHz with 100-kHz field modulation. All EPR spectra given herein were taken with the magnetic field along the c-direction. Optical absorption spectra were taken at 80 K by mounting the sample in a liquid nitrogen Dewar. An aluminum window for irradiating was perpendicular to the optical faces and quartz glass windows were mounted to allow unimpeded optical access. The liquid nitrogen Dewar was placed in the sample chamber of a Perkin Elmer 330 uv-visible-NIR spectrophotometer. EPR and optical absorption spectra were taken in the as received condition as well as after irradiation and reduction.

Electron irradiations were carried out at 77 K using 1.5 Mev electrons from a Van de Graaff accelerator operating at 10 μA. Radiations for EPR were

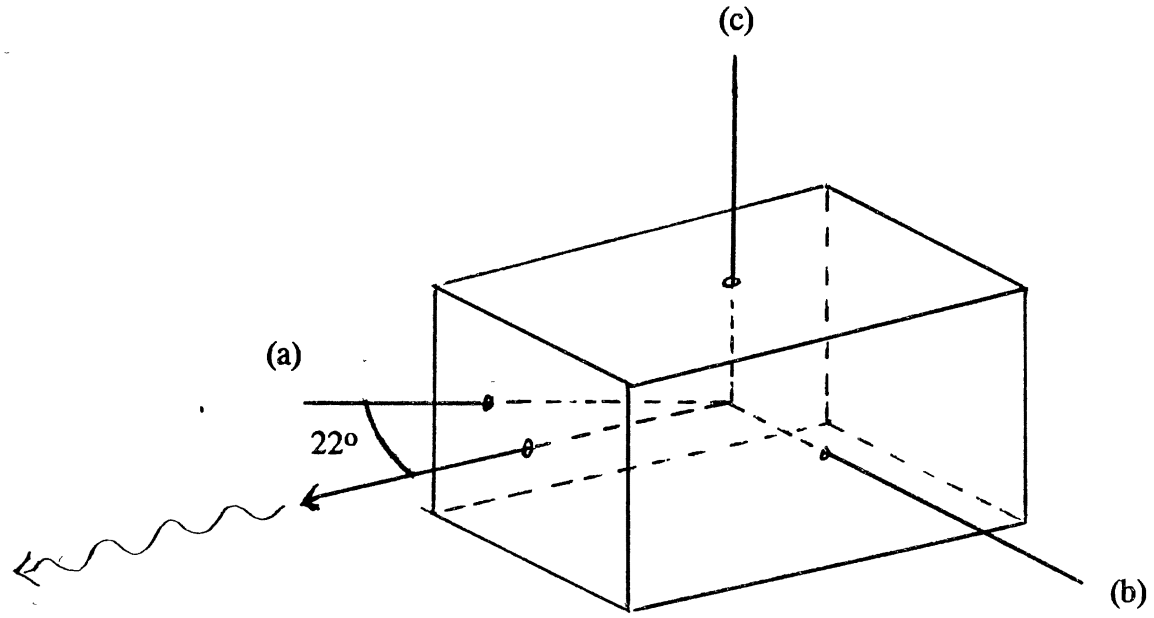

Figure 24. Frequency Doublers Used as Samples

conducted in the same manner as described for $KMgF_3$ in the previous chapter, the samples were irradiated while submerged in liquid nitrogen then quickly transferred to the Oxford Instruments ESR900 continuous flow liquid helium cryostat in the EPR cavity. Radiations for optical absorption were conducted by placing the aluminum window of the liquid nitrogen Dewar directly in the path of the electron beam and the sample turned so that the beam was incident on the optical face. After irradiating, the sample was rotated 90^{o} inside the Dewar so that the optical face would be parallel to the quartz windows and then the Dewar placed in the spectrophotometer.

Pulsed anneals were conducted on both the EPR and optical absorption spectra induced by radiation. For EPR, the pulsed anneals were carried out inside the cryostat and cavity thus eliminating the need and errors of realignment. The cryostat temperature was warmed to the annealing temperature and held for five minutes then cooled back to 20 K and the EPR spectrum recorded. The process was repeated in 20 K steps up to 300 K. In a similar fashion, a pulsed anneal of the optical absorption was conducted without removing the sample and Dewar from the spectrophotometer to eliminate descrepencies due to sample placement. The sample was annealed in the same 20 K steps as for the EPR anneal, cooling back to 80 K after each 5 minute anneal and recording the optical absorption spectra.

Reductions were carried out by placing the samples inside of a stainless steel tube. The tube was placed through an oven so that the sample lay at the center of the oven. The tube was then evacuated with a roughing pump and flushed with argon several times after which the tube was slightly over pressurized with argon. EPR spectra were again taken at 20 K following reduction.

Experimental Results

Of the three device-type samples provided, two were clear to the eye and one showed some yellow coloration in the as-received condition. The yellow coloration being (as described above) an intermittent unexplained inconsistency of growth. All three of the samples showed Fe^{3+} spectra in the as received condition. However there were marked differences in the Fe3+ signal intensity (Fig. 25). However, the Fe^{3+} does not correlate with the yellow coloration as the yellowish sample and one of the clear samples show high concentrations of iron while the other clear sample shows significantly smaller iron signals.

By visual inspection, electron irradiation at 77 K produces a reddish coloration which is not stable when gently warmed to room temperature. It is interesting to note that in an attempt to visually observe thermoluminescence, one of the samples was rapidly warmed to room temperature. While no thermoluminescence was visible the sample showed violent sparking which cracked the crystal. Although the red coloration was no longer present the sample appeared blue-gray. Blue-gray coloration is reported to be a result of optical damage (gray tracking) from high intensity laser radiation. Optical absorption spectra taken at 80 K before and after irradiation are shown in Fig. 26.

Figure 27 shows the EPR spectra before (lower) and after (upper) irradiation. The Fe^{3+} lines decrease in intensity by approximately a factor of four after irradiation. The irradiation also produces three new sets of lines.The first set consists of three lines as shown in Fig. 28. This set of lines is characterized by two lines equally spaced about the third at a magnetic field of 2600 G to 2900 G. The ratio of the lines is 1:4:1 which leads to the

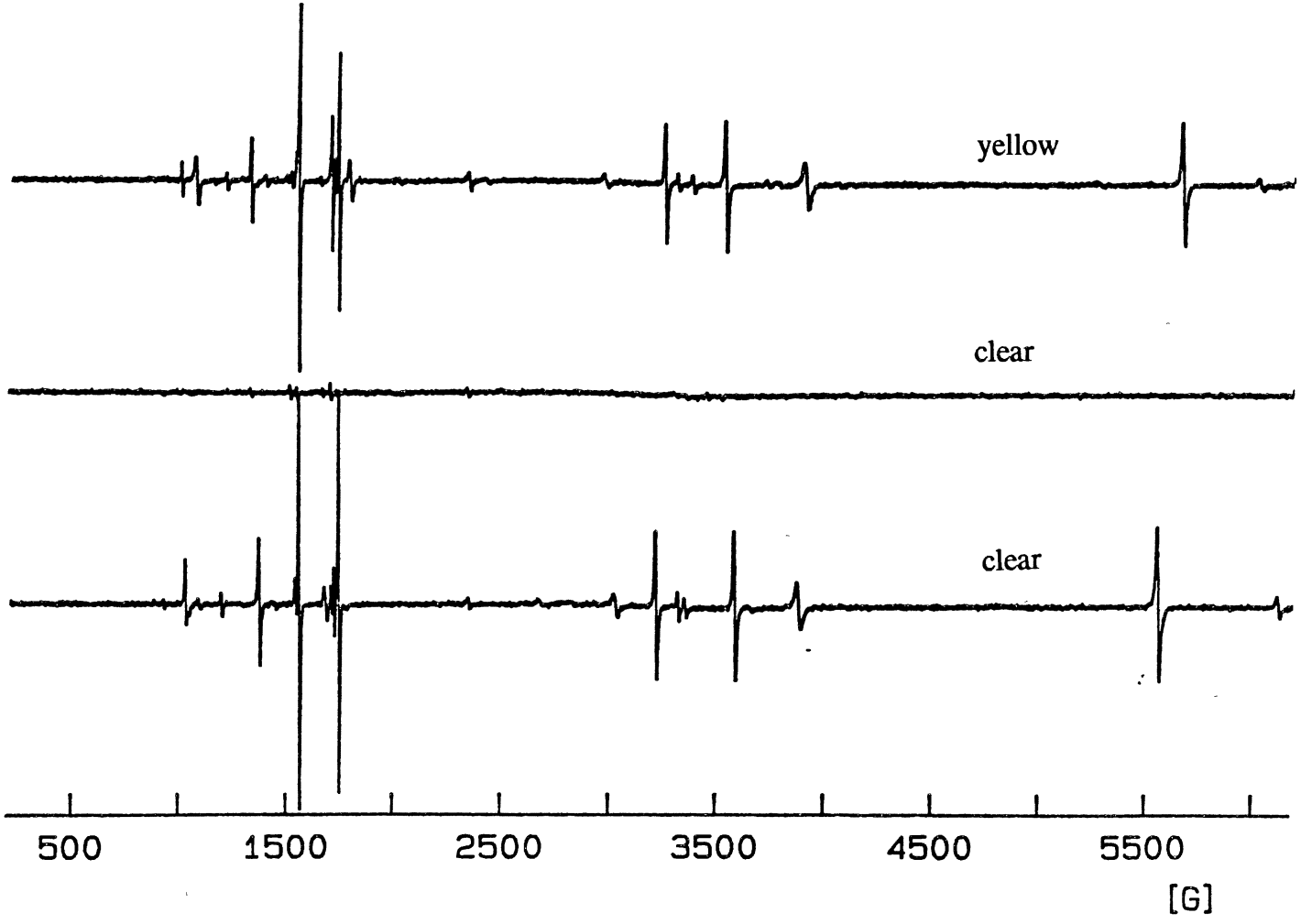

Figure 25. EPR of As Received KTP

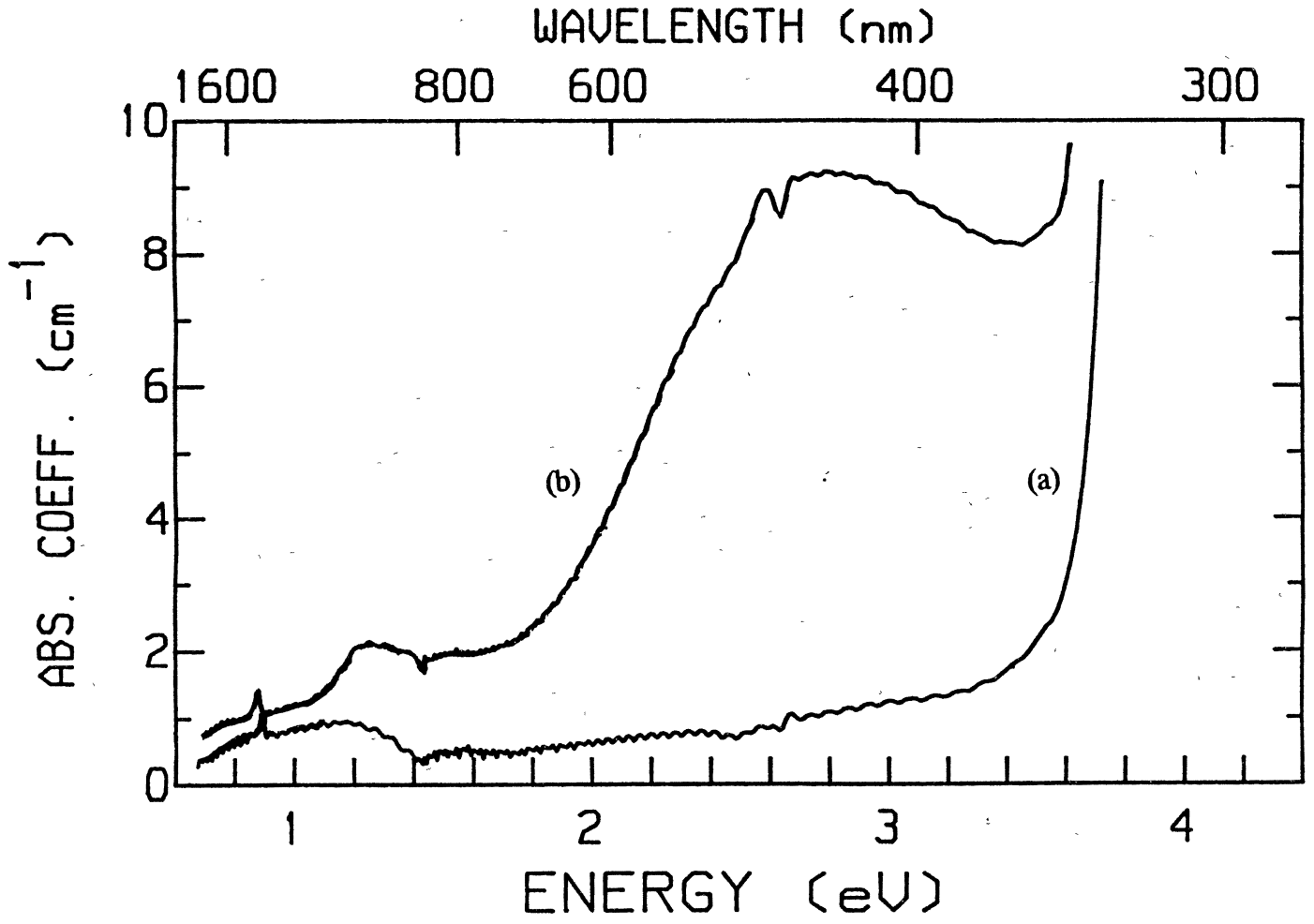

Figure 26. Optical Absorption Spectra (a) Before and (b) After Irradiation

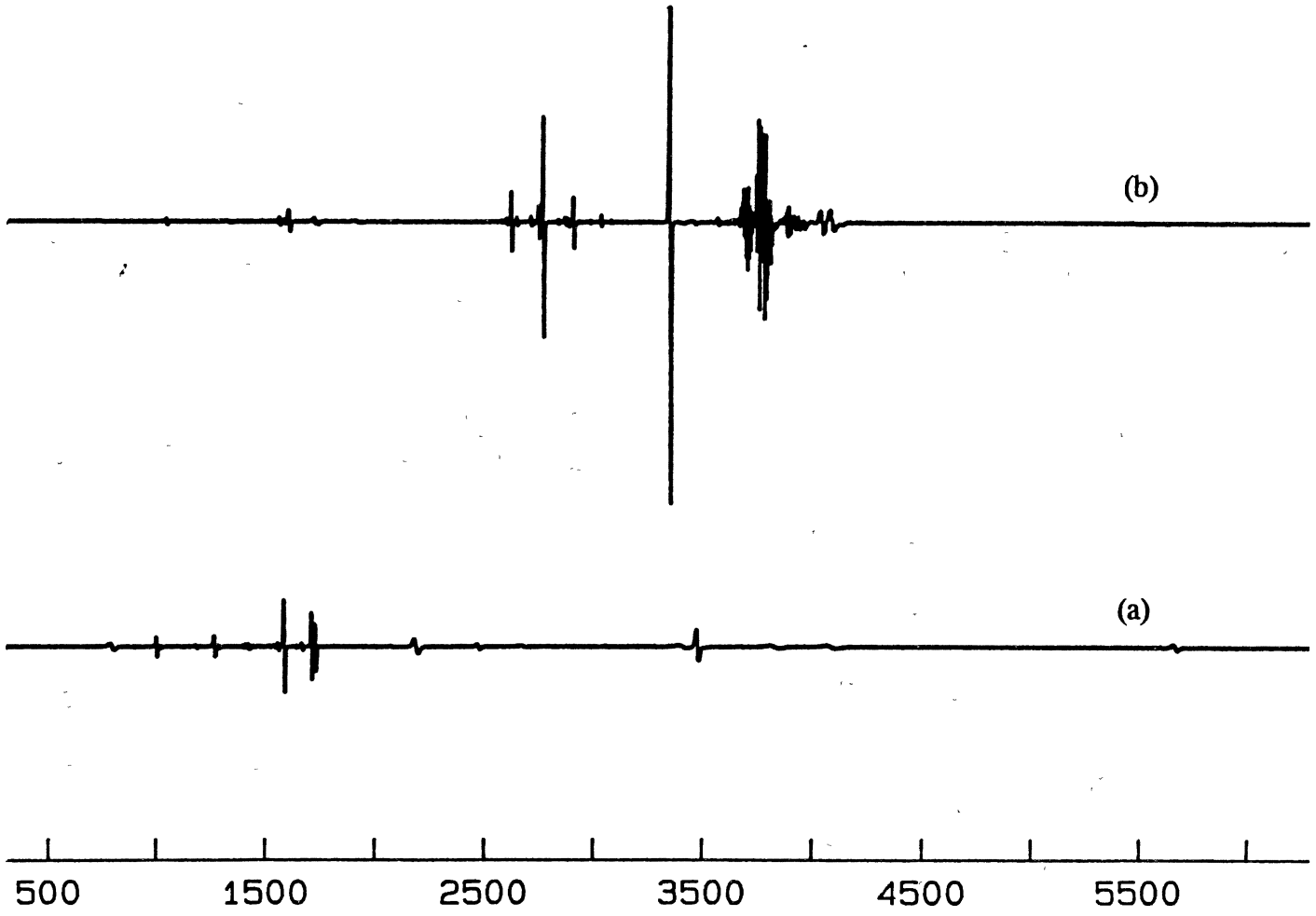

Figure 27. EPR Spectra (a) Before and (b) After Irradiation

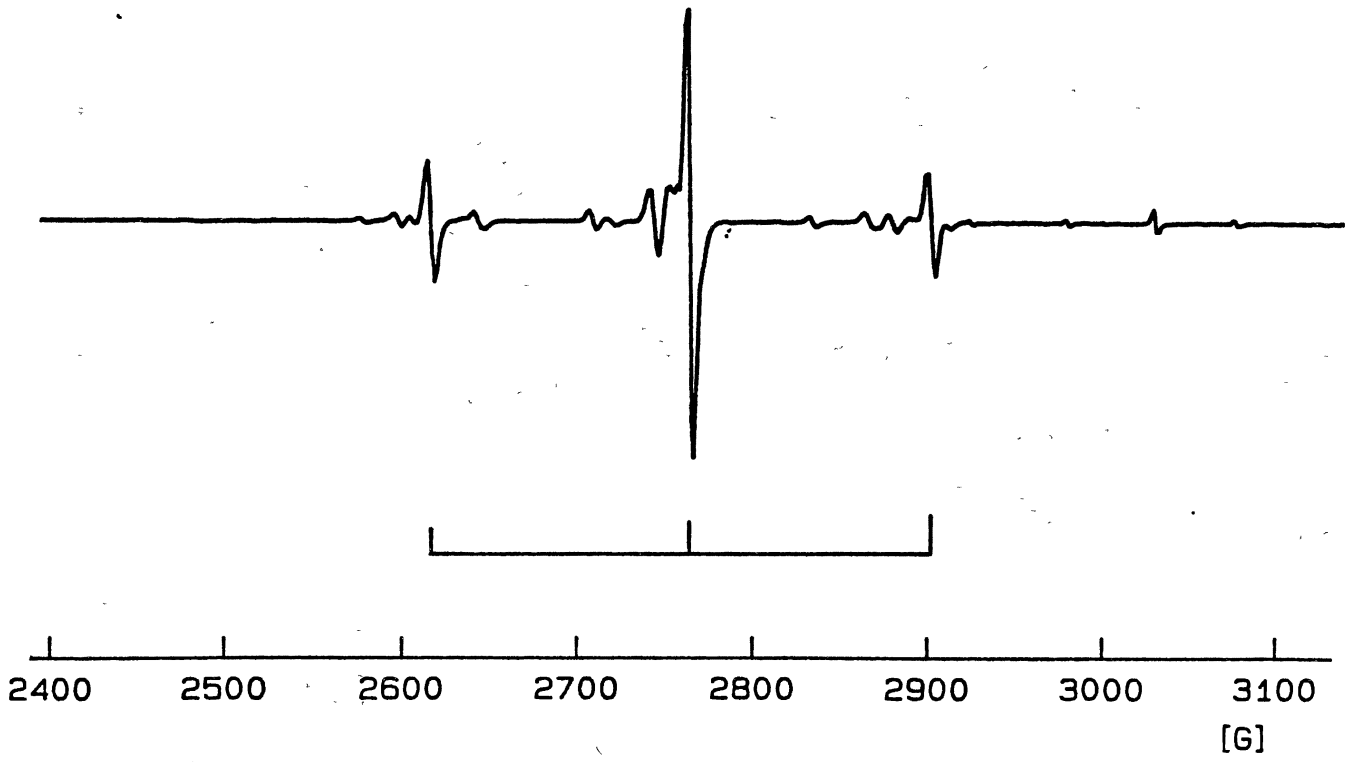

Figure 28. Pt^{3+} EPR Spectrum Produced by Irradiation

identification of the lines as being due to platinum. The 1:4:1 equally spaced lines would suggest trapping centers one third of which have hyperfine interaction due to spin I = 1/2 and two thirds which show no hyperfine interaction. Candidates for such a spectrum must therefore have an isotope with nuclear spin I=1/2 that is nearly 33.3 % abundant and no other paramagnetic isotope. The only nuclei satisfying such criteria is platinum with ^{195}Pt having I = 1/2 being the only magnetic isotope and occurring in a natural abundance of 33.8 %. In addition, the most stable oxidation state of platinum is 4+ with ionic radii of 0.64 Å. Similarly, titanium in KTP is in a 4+ state with an ionic radius of 0.68 Å. Thus the spectrum is unambiguously identified as platinum, which most likely subtitles for titanium in the KTP structure. The identification of a strong platinum signal is somewhat surprising since the autoclave used in the hydrothermal growth process of these crystals is not platinum but gold. It was later determined that platinum crucibles were used in the preparation of nutrients used in the growth process and is a likely source of the platinum impurity.

The higher temperatures of the flux growth process require platinum crucibles and it is likely that growth at higher temperatures in platinum crucibles would lead to higher concentrations of platinum impurities incorporated in the flux grown material. Flux grown samples were not available at the time of this report but immediate future plans include testing of flux material to compare platinum concentrations with that of the hydrothermally grown samples.

The next line in the spectra shown Fig. 29 is a single line at approximately 3350 G corresponding to g = 2 and which shows very little angular dependence. Such a signal is typical of a trapped hole (h^+) and is

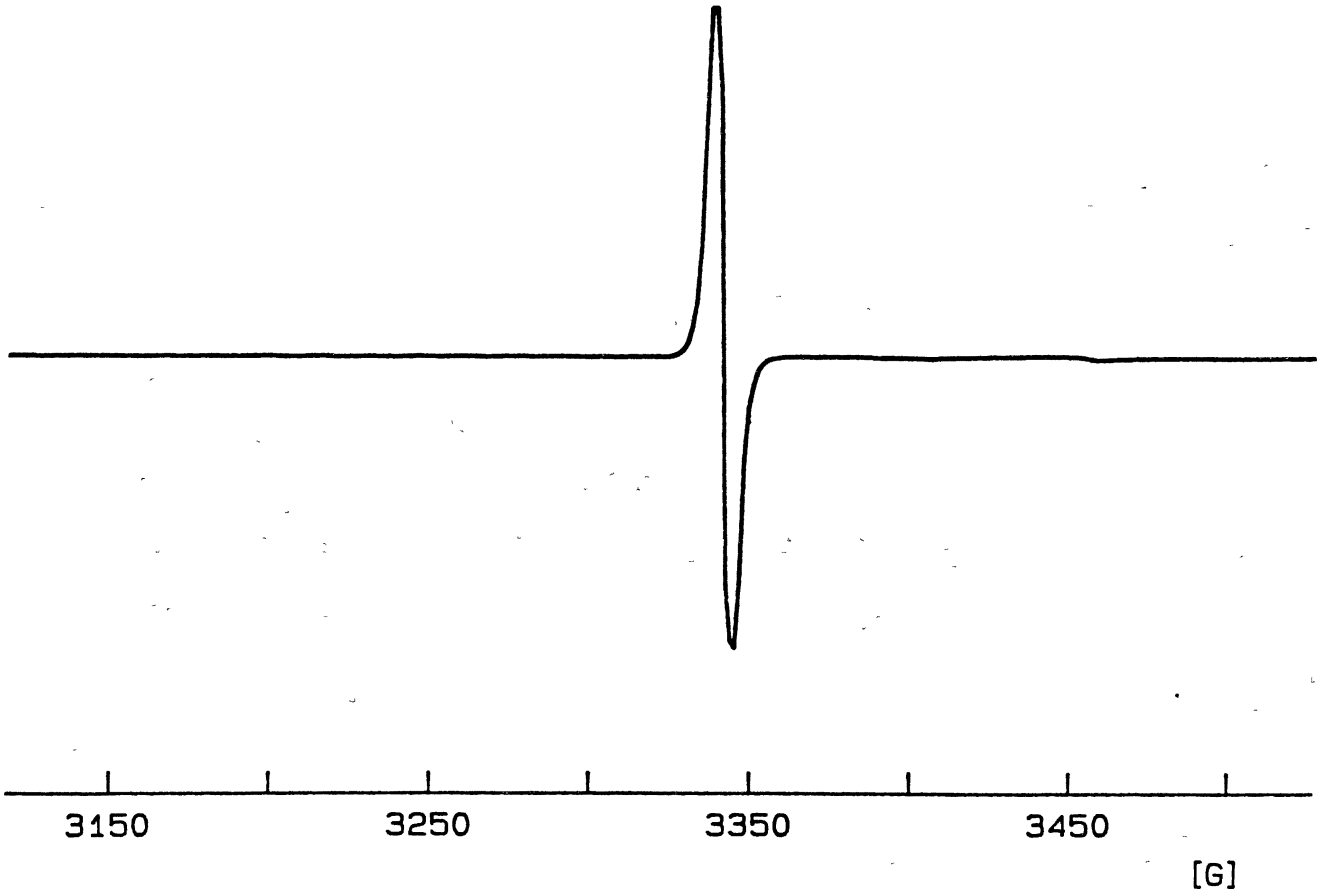

Figure 29. h^+ EPR Spectrum Produced by Irradiation

identified as being such. The third set of lines is similar (although not identical) to spectra reported earlier as tentatively identified as Ti^{3+} in Fig. 30.

A rough production study of these signals was carried out which showed that the decrease in the Fe^{3+} and appearance and increase in the new signals saturate with two to three minutes of irradiation. This would indicate that these radiation induced signals are due to ionization effects and not dislocation.

The results of the pulsed anneal are shown in Fig. 31. The h^{+}, Pt^{3+}, and Ti^{3+} EPR signals decay in the range 120 K to 160 K. In this same temperature range the Fe^{3+} signal recovers and two new platinum signals at slightly higher field appear and are labeled Pt_B and Pt_C in Fig. 32 thus leaving the platinum signal of Fig. 28 which appears upon irradiation as Pt_A.

The first attempt at reduction was a 750° C. anneal in argon for one hour. No apparent damage was caused. The sample was then heated to 850° C for three hours after which the sample was completely black (no transmission of visible light). The EPR spectrum taken at 20 K following the 850° reduction is shown in Fig. 33. Fe^{3+} signals are still present but not observed on the scale of the figure. None of the other EPR signals present after irradiation are present after reduction except the Ti^{3+} around 3800 G were observed. Figure 34 shows an expanded view of the Ti^{3+} signal. By comparison with the Ti^{3+} signal induced by radiation shown in Fig. 30, it can be seen that the two signals are not identical. The origin of these difference are not determined yet.

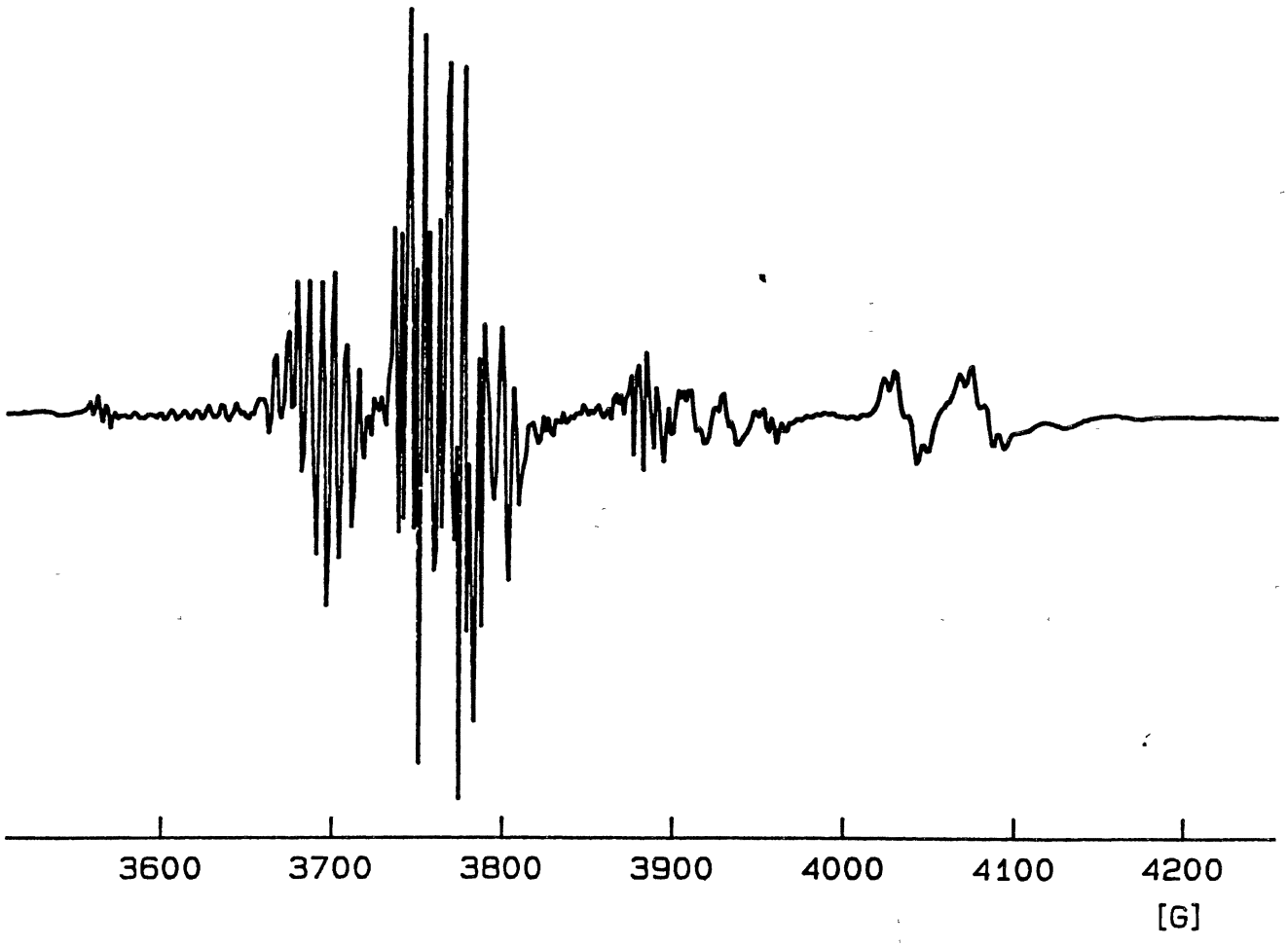

Figure 30. Ti^{3+} EPR Spectrum Produced by Irradiation

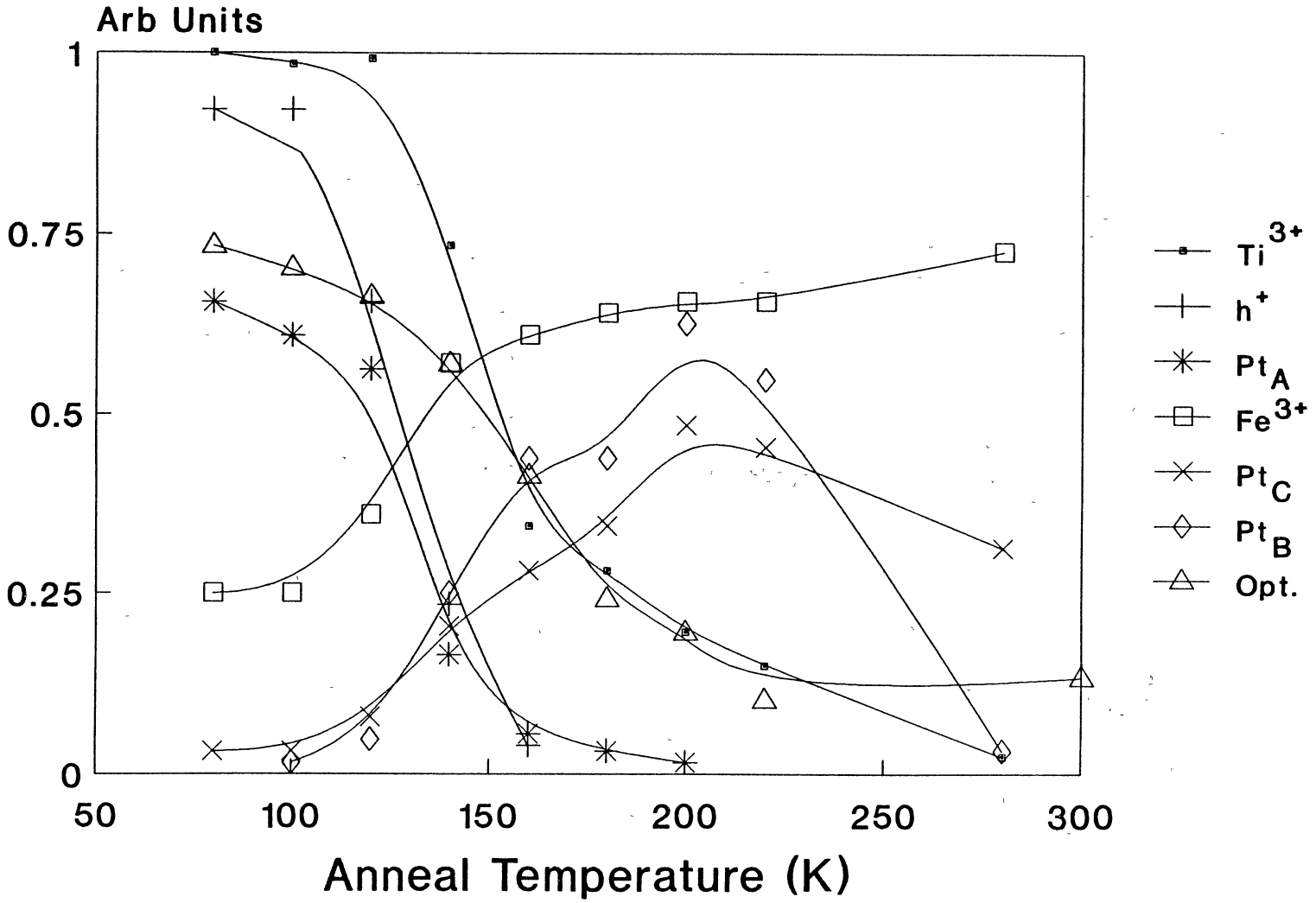

Figure 31. Pulsed Anneal of EPR and Optical Spectra

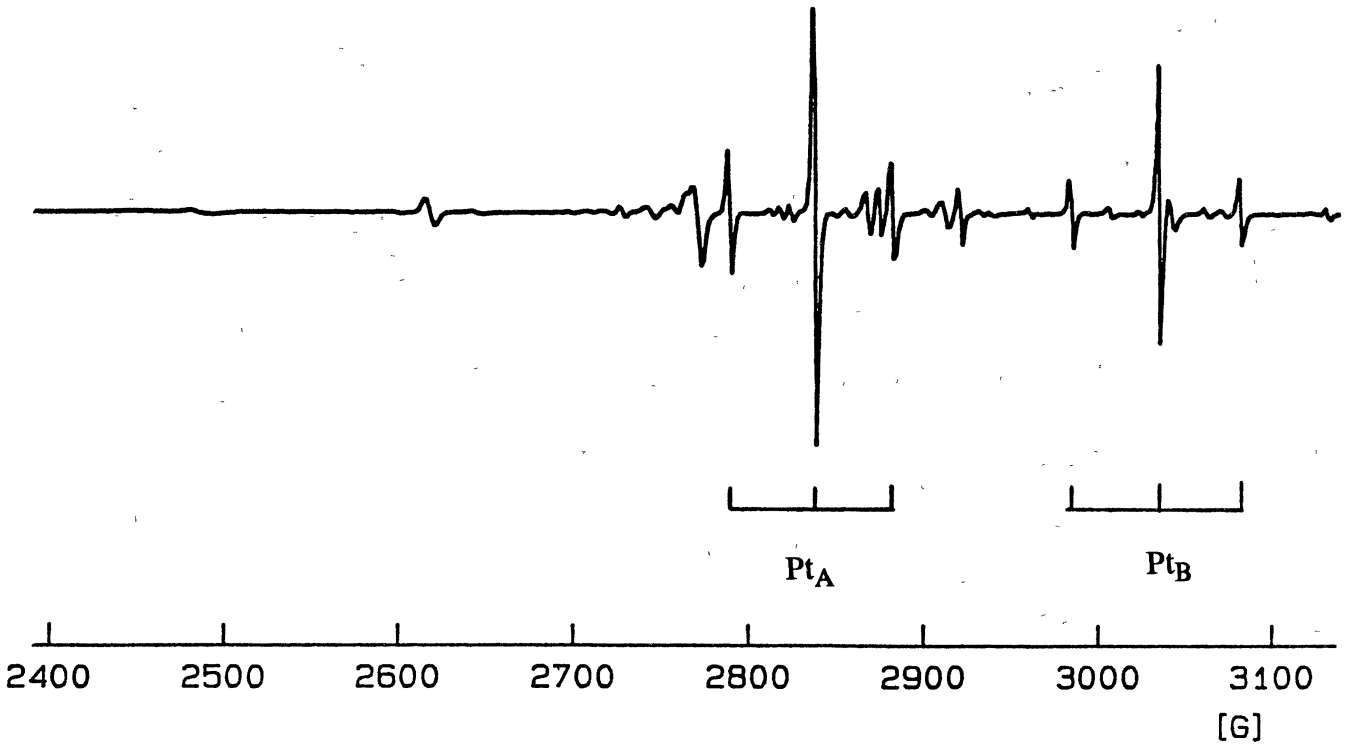

Figure 32. Pt^{3+} Spectra Which Grow in During Anneal

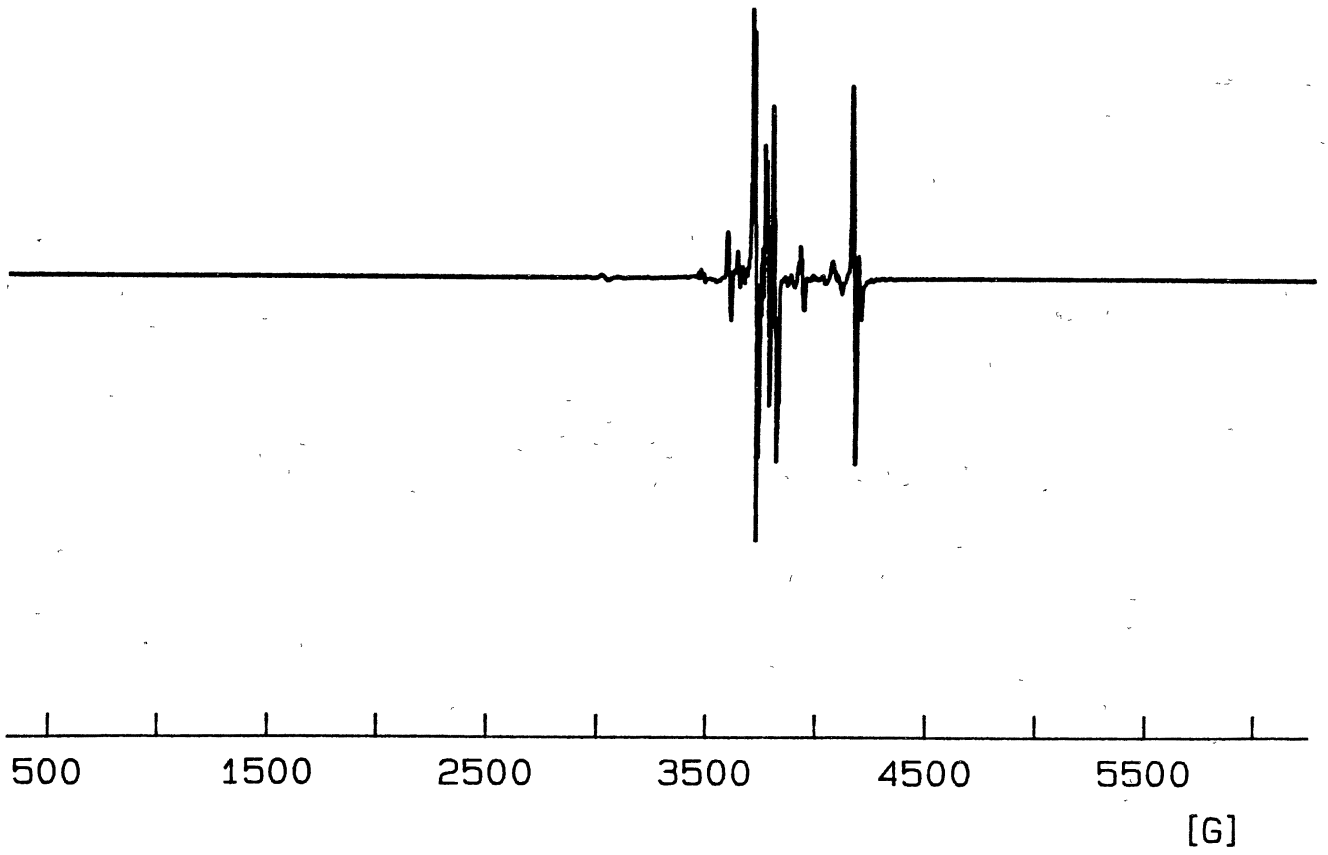

Figure 33. EPR Spectrum After Reduction

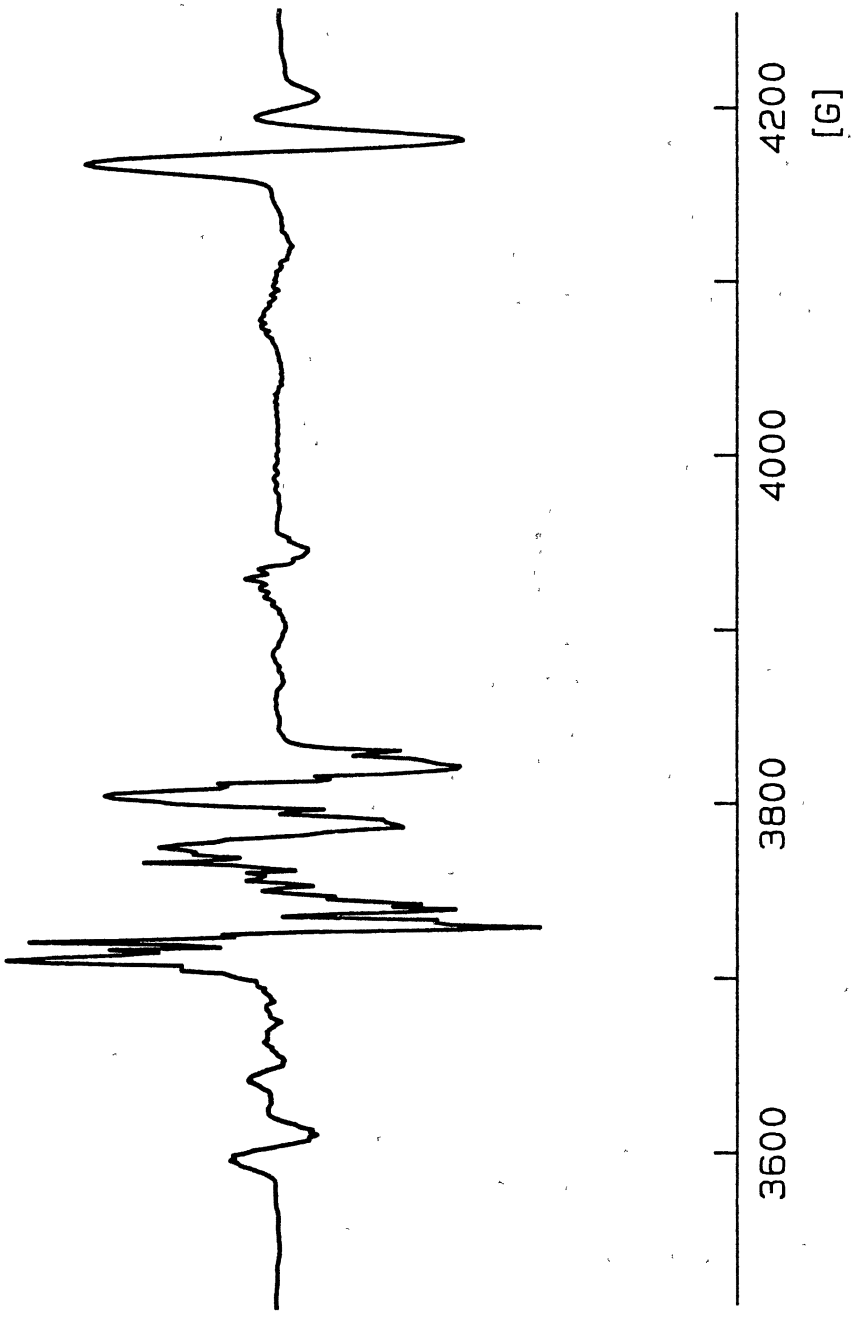

Figure 34. Ti^{3+} EPR Signal After Reduction

CHAPTER IV

CONCLUSION

Electron paramagnetic resonance and electron nuclear double resonance have been and continue to be widly used in the study of defects in solids. Although EPR and ENDOR are not new techniques they continue to offer valuable insight into the nature and origin of many macroscopic phenomena.

Two different levels of magnetic resonace investigations have been presented in this dissertation. Chapter II describes the study of the self-trapped hole, V_k center, in $KMgF_3$. The V_k center and variations therof (perturbed V_k centers) have been the subject of investigation in many materials including $KMgF_3$. These magnetic resonance studies have spaned nearly four decades and yet many questions are yet unresolved. This dissertation has answered one of these lingering questions.

ENDOR has been employed to determine the origin, strength and structure of the hyperfine interaction of neighboring nuclei. The unresolved and partially resolved hyperfine interaction is evident in the EPR spectra. The origin and nature of these interactions have been the source of speculation since they were first reported in the mid 1960's. ENDOR data contained herein absolutely identifies the source of the unresolved hyperfine to be neighboring fluorine nuclei. In addition, the hyperfine tensors of the three most strongly interacting nuclei have been determine. This was achieved by: (1) Monitoring the ENDOR line positions as a function

of magnetic field orientation. (2) Identifing the specific nucleus responsible for a given set of lines from the crystal symmetry and line degeneracies. (3) Writing a computer program to fit the data to a spin-Hamiltonian.

Although $KMgF_3$ is not a commercially significant material, this work should provide a foundation for ENDOR studies of other fluoride materials such as YLF and LiCaF. EPR studies of a V_k center in YLF have already been reported. This ENDOR study in $KMgF_3$ has proven to be a formidable task and it is be expected that ENDOR studies of the much more complicated YLF strucure should be even more difficult.

The second study presented was an EPR investigation of point defects in KTP. KTP is a remakable material with many applications. It is currently manufactured and sold at a fairly high price. Even though it is commercially viable product, many of its properties are not well understood. There appears to be rather significant inconsistencies in the properties of material grown not only by different techniques but also material grown prepared in apparently the same way. Even samples cut from different regions of the same growth show differences. The most significant of these differences is the laser damage threshold.

This dissertation shows how EPR can rapidly identify the general nature of some point defects and relate them to macroscopic properties. Platinum has been identifed as a common, previously unexpected impurity in KTP. Iron has been previously identifed in KTP and speculated by some to be the source of intermittent yellow crystals. The data herein shows that iron is not likely to be a major contributor to the yellow coloration.

These EPR investigations in KTP (in contrast to $KMgF_3$) are the early stages of magnetic resonance studies. These results show magnetic resonance to be a promising tool in the identification of defects in KTP.

REFERENCES

(1) Abragam, A. and B. Bleany, "Electron Paramagnetic Resonance of Transition Ions," Clarendon Press, Oxford, (1970).

(2) Kanzig, W., Phys. Rev. Letters, 4, 117 (1960).

(3) Kanzig, W., J. Phys. Chem. Solids, 17, 80 (1960).

(4) Bass, I. L., and R. L. Mieher, Phys. Rev., 175, 421 (1968).

(5) Kappers, L. A., and L. E. Halliburton, J. Phys. C: Solid State Phys., 7, 589 (1974).

(6) Lewis, J. T., J. L. Kolopus, E. Sonder, and M. M. Abraham, Phys. Rev. B, 7, 810 (1973).

(7) Castner, T. G. and W. Kanzig, J. Phys. Chem. Solids, 3, 178 (1957).

(8) Kabler, M. N., "Hole Centers in Halide Lattices." Point Defects in Solids, Volume I, General and Ionic Crystals. J. H. Crawford and L. M. Slifikin, eds. New York: Plenum Press.

(9) Schoemaker, D., Phys. Rev. B, 7, 786 (1973).

(10) Hall, T. P. P., Brit. J. Appl. Phys., 17, 1011 (1986).

(11) Kevan, L. and L. Kispert, "Electron Spin Double Resonance Spectroscopy," New York. John Wiley and Sons.

(12) Kanzig, W., Phys. Rev., 99, 1890 (1955).

(13) Hersh, H. N., Phys. Rev., 148, 928 (1966).

(14) Rhoads, J., "Radiation Damage In $KMgF_3$," Ph.D. Dissertation, Oklahoma State University (1974).

(15) "Oxford Instruments ESR900 Continuous Flow Cryostat, Operating Manual".

(16) Bierlein, J. D. and C. B. Arweiler, Appl. Phys. Lett., 49, 917 (1986).

(17) Zumsteg, F. C., J. D. Bierlien, and T. E. Gier, J. Appl. Phys., 47, 4980 (1976).

(18) Bierlein, J. D. and T. D. Gier, U. S. Patent 3949323 (April 6, 1976).

(19) Kato, K., IEE J. Quan. Elec., Qe-24 no. 1, (1988).

(20) Laubacher . Proc. Soc. Photo-Opt Intrum. Eng. 993, 80 (1988).

(21) Bierlein, J. D., J. Opt. Soc. Amer. B, 6, (1989).

(22) Tordjman, I., R. Masse, and J. C. Guitel, Z. Kristallogr, 139, 103 (1974).

(23) Gashurov, G. and R. F. Belt, "Growth of KTP", Tuanble Solid State Lasers for Remote Sensing, Springer Verlag, New York, (1985).

(24) Laudise, R. A., R. J. Cava, and Caporasso, J. Crystal Growth, 74, 275 (1986).

(25) Cai and Yang, J. Cryst. Growth, 79, 974 (1986).

(26) Shen, D. Z. and C. E. Huang, Prog. Crystal Growth Characterization, 11, 269 (1985).

(27) Jacco, J. C., G. M. Loiacono, M. Jaso, G. Mizell, and B. Greenberg, J. Crystal Growth, 70, 484 (1984).

(28) Liui, Y. G., B. Xu, J. R. Han, X. Y. Liu, and M. H. Jiang, Chin. J. Lasers, 13, 438 (1986).

(29) Ballman, A. A., H. Brown, D. H. Olson, and C. E. Ric, J. Crystal Growth, 75, 390 (1986).

APPENDIX

SPIN HAMILTONIAN FITTING PROGRAM

```
10    OPTION BASE 1
20    DEG
30    DIM Ar(16,16),A1(16,16),Trg(3,3),Tr1(3,3),Tr2(3,3),Tr3(3,3)
40    DIM Tg(3,3),T1(3,3),T2(3,3),T3(3,3),R(3,3),G(3),Tt3(3,3)
50    DIM Rr(3,3),R3(3,3),R1(3,3),R2(3,3)
60    DIM D(16),E(16),E2(16),Tau(2,16)
70    DIM A(3,3),Tr(0:3,3,3),D(0:3,3,3)
80    DIM P(6),Para(6)
90    DIM Dat(150,8),Delta(6)
100   DIM Rxz(3,3),Ryy(3,3),Rxzy(3,3),Rn(3,3)
110   DIM Rch0(3,3),Rch6(3,3),Iden(3,3)
120   REM****************************** CONSTANTS ********************************
130   REM
140   MASS STORAGE IS ":,700,1"
150   INPUT "FILE NAME",Fid$
160   ASSIGN @Fid TO Fid$
170   FOR I=1 TO 150
180       FOR J=1 TO 8
190           ENTER @Fid;Dat(I,J)
200           IF Dat(I,1)=1000 THEN GOTO 230
210       NEXT J
220   NEXT I
230   ASSIGN @Fid TO *
240   REM ***************************************************************************
250   REM ***************************************************************************
260   Delta(1)=.1
270   Delta(2)=.1
280   Delta(3)=.1
290   Delta(4)=.1
300   Delta(5)=.1
310   Delta(6)=.1
320   Jj=5
330   Idat=1
340   Icount=0
350   N=16
360   Nm=16
370   Error=1000
380   B=9.2741/6.6262
390   Bn=.005051/6.6262
400   Gn=5.2577
410   Gnb1=Gn*Bn/2
420   Gnb2=Gn*Bn/2
430   Gnb3=Gn*Bn/2
440   Rxz(1,3)=1
450   Rxz(2,2)=1
460   Rxz(3,1)=1
470   Ryy(1,1)=1
480   Ryy(2,2)=-1
490   Ryy(3,3)=1
500   Rxzy(3,1)=1
510   Rxzy(2,2)=-1
520   Rxzy(1,3)=1
530   Iden(1,1)=1
540   Iden(2,2)=1
550   Iden(3,3)=1
560   REM ***************************************************************************
570   Phig=45
580   G(1)=2.024
590   G(2)=2.018
600   G(3)=2.0024
610   Tg(1,1)=COS(Phig)
620   Tg(1,3)=SIN(Phig)
630   Tg(2,2)=1
640   Tg(3,1)=-SIN(Phig)
```

```
650   Tg(3,3)=COS(Phig)
660   REM ************************************************************************
670   Ph12=52
680   A(1,1)=160
690   A(1,2)=160
700   A(1,3)=2479
710   A(2,1)=160
720   A(2,2)=160
730   A(2,3)=2479
740   T2(1,1)=COS(Ph12)
750   T2(1,3)=SIN(Ph12)
760   T2(2,2)=1
770   T2(3,1)=-SIN(Ph12)
780   T2(3,3)=COS(Ph12)
790   MAT T1= T2*Rxz
800   REM************************* INPUT ***************************************
810   PRINT "FOR NUCLEI A ENTER 1"
820   PRINT "FOR NUCLEI B ENTER 2"
830   PRINT "FOR NUCLEI C ENTER 3"
840   PRINT "FOR NUCLEI D ENTER 4"
850   PRINT "FOR NUCLEI E ENTER 5"
860   INPUT "NUCLEI",Nuc
870   ON Nuc GOTO 890,990,1090,1190,1290
880   REM ************************************************************************
890   Npam=4
900   Para(1)=-1.6
910   Para(2)=-1.8
920   Para(3)=22.7
930   Para(4)=48.3
940   Para(5)=0
950   Para(6)=0
960   GOTO 1380
970   REM ************************************************************************
980   REM ************************************************************************
990   Npam=4
1000  Para(1)=35
1010  Para(2)=19
1020  Para(3)=-28
1030  Para(4)=1
1040  Para(5)=9
1050  Para(6)=7
1060  GOTO 1380
1070  REM ************************************************************************
1080  REM ************************************************************************
1090  Npam=4
1100  Para(1)=35
1110  Para(2)=19
1120  Para(3)=-28
1130  Para(4)=1
1140  Para(5)=9
1150  Para(6)=7
1160  GOTO 1380
1170  REM ************************************************************************
1180  REM ************************************************************************
1190  Npam=3
1200  Para(1)=8.2
1210  Para(2)=3
1220  Para(3)=42.3
1230  Para(4)=6.8
1240  Para(5)=45
1250  Para(6)=0
1260  GOTO 1380
1270  REM ************************************************************************
1280  REM ************************************************************************
1290  Npam=6
1300  Para(1)=-2.7
```

```
1310  Para(2)=-2.0
1320  Para(3)=12.9
1330  Para(4)=139.0
1340  Para(5)=4.5
1350  Para(6)=-57.0
1360  GOTO 1380
1370  REM ************************************************************************
1380  P(1)=Para(1)
1390  P(2)=Para(2)
1400  P(3)=Para(3)
1410  P(4)=Para(4)
1420  P(5)=Para(5)
1430  P(6)=Para(6)
1440  REM ************************************************************************
1450  FOR I=1 TO 3
1460  FOR J=1 TO 3
1470  T3(I,J)=0
1480  Tt3(I,J)=0
1490  NEXT J
1500  A(3,I)=0
1510  NEXT I
1520  A(3,1)=P(1)
1530  A(3,2)=P(2)
1540  A(3,3)=P(3)
1550  Theta=P(4)
1560  Pph1=P(5)
1570  Ps1=P(6)
1580  Tt3(1,1)=COS(Ps1)*COS(Pph1)-COS(Ps1)*SIN(Pph1)*SIN(Theta)
1590  Tt3(1,2)=COS(Ps1)*SIN(Pph1)+COS(Theta)*COS(Pph1)*SIN(Ps1)
1600  Tt3(1,3)=SIN(Ps1)*SIN(Theta)
1610  Tt3(2,1)=-SIN(Ps1)*COS(Pph1)-COS(Theta)*SIN(Pph1)*COS(Ps1)
1620  Tt3(2,2)=-SIN(Ps1)*SIN(Pph1)+COS(Theta)*COS(Pph1)*COS(Ps1)
1630  Tt3(2,3)=COS(Ps1)*SIN(Theta)
1640  Tt3(3,1)=SIN(Theta)*SIN(Pph1)
1650  Tt3(3,2)=-SIN(Theta)*COS(Pph1)
1660  Tt3(3,3)=COS(Theta)
1670  REM ************************************************************************
1680  REM ***************************** DATA *************************************
1690  IF Dat(Idat,1)=1000 THEN GOTO 4130
1700  Nucn=Dat(Idat,1)
1710  kplan=Dat(Idat,2)
1720  Ph1=Dat(Idat,3)
1730  H=Dat(Idat,4)
1740  Freqm=Dat(Idat,5)
1750  Freqml=Dat(Idat,6)
1760  IF Nuc=1 AND Nucn=1 THEN MAT Rn= Rxz
1770  IF Nuc=1 AND Nucn=2 THEN MAT Rn= Iden
1780  IF Nuc=4 AND Nucn=1 THEN MAT Rn= Iden
1790  IF Nuc=4 AND Nucn=2 THEN MAT Rn= Ryy
1800  IF Nuc=5 AND Nucn=2 THEN MAT Rn= Iden
1810  IF Nuc=5 AND Nucn=1 THEN MAT Rn= Ryy
1820  IF Nuc=5 AND Nucn=3 THEN MAT Rn= Rxz
1830  IF Nuc=5 AND Nucn=4 THEN MAT Rn= Rxzy
1840  MAT T3= Tt3*Rn
1850  GOTO 1920
1860  FOR I=1 TO 3
1870  FOR J=1 TO 3
1880  PRINT Tt3(I,J),T3(I,J)
1890  NEXT J
1900  NEXT I
1910  REM ************************************************************************
1920  FOR I=1 TO 3
1930  FOR J=1 TO 3
1940  Rch0(I,J)=0
1950  Rch6(I,J)=0
1960  R1(I,J)=0
```

```
1970  NEXT J
1980  NEXT I
1990  REM ********************************************************************************
2000  IF Kplan=1 THEN Phi=-Phi
2010  Rch0(1,1)=COS(Phi)
2020  Rch0(1,3)=SIN(Phi)
2030  Rch0(2,2)=1
2040  Rch0(3,1)=-SIN(Phi)
2050  Rch0(3,3)=COS(Phi)
2060  Rch6(1,1)=1
2070  Rch6(2,2)=COS(Phi)
2080  Rch6(2,3)=-SIN(Phi)
2090  Rch6(3,2)=SIN(Phi)
2100  Rch6(3,3)=COS(Phi)
2110  REM ********************************************************************************
2120  IF Kplan=2 THEN
2130      MAT Rr= Rch0
2140  END IF
2150  IF Kplan=1 THEN
2160      MAT Rr= Rch0
2170      Phi=-Phi
2180  END IF
2190  IF Kplan=3 THEN
2200      MAT Rr= Rch6
2210      Phi=-Phi
2220  END IF
2230  REM
2240  REM*********************************************************************************
2250  REM
2260  MAT Trg= Tg*Rr
2270  MAT Tr1= T1*Rr
2280  MAT Tr2= T2*Rr
2290  MAT Tr3= T3*Rr
2300  FOR I=1 TO 3
2310      FOR J=1 TO 3
2320          Tr(0,I,J)=Trg(I,J)
2330          Tr(1,I,J)=Tr1(I,J)
2340          Tr(2,I,J)=Tr2(I,J)
2350          Tr(3,I,J)=Tr3(I,J)
2360      NEXT J
2370  NEXT I
2380  FOR I=0 TO 3
2390      FOR J=1 TO 3
2400          FOR K=1 TO 3
2410              Q(I,J,K)=0
2420          NEXT K
2430      NEXT J
2440  NEXT I
2450  FOR L=1 TO 3
2460      FOR K=1 TO 3
2470          Q(0,3,L)=Q(0,3,L)+B*H*Tr(0,K,3)*Tr(0,K,L)*G(K)
2480          Q(0,L,3)=Q(0,3,L)
2490      NEXT K
2500  NEXT L
2510  FOR I=1 TO 3
2520      FOR L=1 TO 3
2530          FOR J=1 TO 3
2540              FOR K=1 TO 3
2550                  Q(I,L,J)=Q(I,L,J)+A(I,K)*Tr(I,K,L)*Tr(I,K,J)
2560              NEXT K
2570          NEXT J
2580      NEXT L
2590  NEXT I
2600  REM ********************************************************************************
2610   FOR I=1 TO 16
2620   FOR J=1 TO 16
```

```
2630    Ar(I,J)=0
2640    Ai(I,J)=0
2650    NEXT J
2660    NEXT I
2670    Ar(1,1)=Q(0,3,3)/2+(+Q(1,3,3)+Q(2,3,3)+Q(3,3,3))/4-(+Gnb1+Gnb2+Gnb3)*H
2680    Ar(2,2)=Q(0,3,3)/2+(+Q(1,3,3)+Q(2,3,3)-Q(3,3,3))/4-(+Gnb1+Gnb2-Gnb3)*H
2690    Ar(3,3)=Q(0,3,3)/2+(+Q(1,3,3)-Q(2,3,3)+Q(3,3,3))/4-(+Gnb1-Gnb2+Gnb3)*H
2700    Ar(4,4)=Q(0,3,3)/2+(+Q(1,3,3)-Q(2,3,3)-Q(3,3,3))/4-(+Gnb1-Gnb2-Gnb3)*H
2710    Ar(5,5)=Q(0,3,3)/2+(-Q(1,3,3)+Q(2,3,3)+Q(3,3,3))/4-(-Gnb1+Gnb2+Gnb3)*H
2720    Ar(6,6)=Q(0,3,3)/2+(-Q(1,3,3)+Q(2,3,3)-Q(3,3,3))/4-(-Gnb1+Gnb2-Gnb3)*H
2730    Ar(7,7)=Q(0,3,3)/2+(-Q(1,3,3)-Q(2,3,3)+Q(3,3,3))/4-(-Gnb1-Gnb2+Gnb3)*H
2740    Ar(8,8)=Q(0,3,3)/2+(-Q(1,3,3)-Q(2,3,3)-Q(3,3,3))/4-(-Gnb1-Gnb2-Gnb3)*H
2750    Ar(9,9)=-Q(0,3,3)/2+(-Q(1,3,3)-Q(2,3,3)-Q(3,3,3))/4-(+Gnb1+Gnb2+Gnb3)*H
2760    Ar(10,10)=-Q(0,3,3)/2+(-Q(1,3,3)-Q(2,3,3)+Q(3,3,3))/4-(+Gnb1+Gnb2-Gnb3)*H
2770    Ar(11,11)=-Q(0,3,3)/2+(-Q(1,3,3)+Q(2,3,3)-Q(3,3,3))/4-(+Gnb1-Gnb2+Gnb3)*H
2780    Ar(12,12)=-Q(0,3,3)/2+(-Q(1,3,3)+Q(2,3,3)+Q(3,3,3))/4-(+Gnb1-Gnb2-Gnb3)*H
2790    Ar(13,13)=-Q(0,3,3)/2+(+Q(1,3,3)-Q(2,3,3)-Q(3,3,3))/4-(-Gnb1+Gnb2+Gnb3)*H
2800    Ar(14,14)=-Q(0,3,3)/2+(+Q(1,3,3)-Q(2,3,3)+Q(3,3,3))/4-(-Gnb1+Gnb2-Gnb3)*H
2810    Ar(15,15)=-Q(0,3,3)/2+(+Q(1,3,3)+Q(2,3,3)-Q(3,3,3))/4-(-Gnb1-Gnb2+Gnb3)*H
2820    Ar(16,16)=-Q(0,3,3)/2+(+Q(1,3,3)+Q(2,3,3)+Q(3,3,3))/4-(-Gnb1-Gnb2-Gnb3)*H
2830    Ar(9,1)=+Q(0,3,1)/2+Q(1,1,3)/4+Q(2,1,3)/4+Q(3,1,3)/4
2840    Ar(10,2)=+Q(0,3,1)/2+Q(1,1,3)/4+Q(2,1,3)/4-Q(3,1,3)/4
2850    Ar(11,3)=+Q(0,3,1)/2+Q(1,1,3)/4-Q(2,1,3)/4+Q(3,1,3)/4
2860    Ar(12,4)=+Q(0,3,1)/2+Q(1,1,3)/4-Q(2,1,3)/4-Q(3,1,3)/4
2870    Ar(13,5)=+Q(0,3,1)/2-Q(1,1,3)/4+Q(2,1,3)/4+Q(3,1,3)/4
2880    Ar(14,6)=+Q(0,3,1)/2-Q(1,1,3)/4+Q(2,1,3)/4-Q(3,1,3)/4
2890    Ar(15,7)=+Q(0,3,1)/2-Q(1,1,3)/4-Q(2,1,3)/4+Q(3,1,3)/4
2900    Ar(16,8)=+Q(0,3,1)/2-Q(1,1,3)/4-Q(2,1,3)/4-Q(3,1,3)/4
2910    Ai(9,1)=+Q(0,3,2)/2+Q(1,2,3)/4+Q(2,2,3)/4+Q(3,2,3)/4
2920    Ai(10,2)=+Q(0,3,2)/2+Q(1,2,3)/4+Q(2,2,3)/4-Q(3,2,3)/4
2930    Ai(11,3)=+Q(0,3,2)/2+Q(1,2,3)/4-Q(2,2,3)/4+Q(3,2,3)/4
2940    Ai(12,4)=+Q(0,3,2)/2+Q(1,2,3)/4-Q(2,2,3)/4-Q(3,2,3)/4
2950    Ai(13,5)=+Q(0,3,2)/2-Q(1,2,3)/4+Q(2,2,3)/4+Q(3,2,3)/4
2960    Ai(14,6)=+Q(0,3,2)/2-Q(1,2,3)/4+Q(2,2,3)/4-Q(3,2,3)/4
2970    Ai(15,7)=+Q(0,3,2)/2-Q(1,2,3)/4-Q(2,2,3)/4+Q(3,2,3)/4
2980    Ai(16,8)=+Q(0,3,2)/2-Q(1,2,3)/4-Q(2,2,3)/4-Q(3,2,3)/4
2990    Ar(2,1)=+Q(3,1,3)/4
3000    Ar(4,3)=+Q(3,1,3)/4
3010    Ar(6,5)=+Q(3,1,3)/4
3020    Ar(8,7)=+Q(3,1,3)/4
3030    Ar(10,9)=-Q(3,1,3)/4
3040    Ar(12,11)=-Q(3,1,3)/4
3050    Ar(14,13)=-Q(3,1,3)/4
3060    Ar(16,15)=-Q(3,1,3)/4
3070    Ai(2,1)=+Q(3,2,3)/4
3080    Ai(4,3)=+Q(3,2,3)/4
3090    Ai(6,5)=+Q(3,2,3)/4
3100    Ai(8,7)=+Q(3,2,3)/4
3110    Ai(10,9)=-Q(3,2,3)/4
3120    Ai(12,11)=-Q(3,2,3)/4
3130    Ai(14,13)=-Q(3,2,3)/4
3140    Ai(16,15)=-Q(3,2,3)/4
3150    Ar(3,1)=+Q(2,1,3)/4
3160    Ar(4,2)=+Q(2,1,3)/4
3170    Ar(7,5)=+Q(2,1,3)/4
3180    Ar(8,6)=+Q(2,1,3)/4
3190    Ar(11,9)=-Q(2,1,3)/4
3200    Ar(12,10)=-Q(2,1,3)/4
3210    Ar(15,13)=-Q(2,1,3)/4
3220    Ar(16,14)=-Q(2,1,3)/4
3230    Ai(3,1)=+Q(2,2,3)/4
3240    Ai(4,2)=+Q(2,2,3)/4
3250    Ai(7,5)=+Q(2,2,3)/4
3260    Ai(8,6)=+Q(2,2,3)/4
3270    Ai(11,9)=-Q(2,2,3)/4
3280    Ai(12,10)=-Q(2,2,3)/4
```

```
3290   Ai(15,13)=-Q(2,2,3)/4
3300   Ai(16,14)=-Q(2,2,3)/4
3310   Ar(5,1)=+Q(1,1,3)/4
3320   Ar(6,2)=+Q(1,1,3)/4
3330   Ar(7,3)=+Q(1,1,3)/4
3340   Ar(8,4)=+Q(1,1,3)/4
3350   Ar(13,9)=-Q(1,1,3)/4
3360   Ar(14,10)=-Q(1,1,3)/4
3370   Ar(15,11)=-Q(1,1,3)/4
3380   Ar(16,12)=-Q(1,1,3)/4
3390   Ai(5,1)=+Q(1,2,3)/4
3400   Ai(6,2)=+Q(1,2,3)/4
3410   Ai(7,3)=+Q(1,2,3)/4
3420   Ai(8,4)=+Q(1,2,3)/4
3430   Ai(13,9)=-Q(1,2,3)/4
3440   Ai(14,10)=-Q(1,2,3)/4
3450   Ai(15,11)=-Q(1,2,3)/4
3460   Ai(16,12)=-Q(1,2,3)/4
3470   Ar(9,5)=Q(1,1,1)/4+Q(1,2,2)/4
3480   Ar(10,6)=Q(1,1,1)/4+Q(1,2,2)/4
3490   Ar(11,7)=Q(1,1,1)/4+Q(1,2,2)/4
3500   Ar(12,8)=Q(1,1,1)/4+Q(1,2,2)/4
3510   Ar(13,1)=Q(1,1,1)/4-Q(1,2,2)/4
3520   Ar(14,2)=Q(1,1,1)/4-Q(1,2,2)/4
3530   Ar(15,3)=Q(1,1,1)/4-Q(1,2,2)/4
3540   Ar(16,4)=Q(1,1,1)/4-Q(1,2,2)/4
3550   Ai(13,1)=Q(1,1,2)/2
3560   Ai(14,2)=Q(1,1,2)/2
3570   Ai(15,3)=Q(1,1,2)/2
3580   Ai(16,4)=Q(1,1,2)/2
3590   Ar(9,3)=Q(2,1,1)/4+Q(2,2,2)/4
3600   Ar(10,4)=Q(2,1,1)/4+Q(2,2,2)/4
3610   Ar(13,7)=Q(2,1,1)/4+Q(2,2,2)/4
3620   Ar(14,8)=Q(2,1,1)/4+Q(2,2,2)/4
3630   Ar(11,1)=Q(2,1,1)/4-Q(2,2,2)/4
3640   Ar(12,2)=Q(2,1,1)/4-Q(2,2,2)/4
3650   Ar(15,5)=Q(2,1,1)/4-Q(2,2,2)/4
3660   Ar(16,6)=Q(2,1,1)/4-Q(2,2,2)/4
3670   Ai(11,1)=Q(2,1,2)/2
3680   Ai(12,2)=Q(2,1,2)/2
3690   Ai(15,5)=Q(2,1,2)/2
3700   Ai(16,6)=Q(2,1,2)/2
3710   Ar(9,2)=Q(3,1,1)/4+Q(3,2,2)/4
3720   Ar(11,4)=Q(3,1,1)/4+Q(3,2,2)/4
3730   Ar(13,6)=Q(3,1,1)/4+Q(3,2,2)/4
3740   Ar(15,8)=Q(3,1,1)/4+Q(3,2,2)/4
3750   Ar(10,1)=Q(3,1,1)/4-Q(3,2,2)/4
3760   Ar(12,3)=Q(3,1,1)/4-Q(3,2,2)/4
3770   Ar(14,5)=Q(3,1,1)/4-Q(3,2,2)/4
3780   Ar(16,7)=Q(3,1,1)/4-Q(3,2,2)/4
3790   Ai(10,1)=Q(3,1,2)/2
3800   Ai(12,3)=Q(3,1,2)/2
3810   Ai(14,5)=Q(3,1,2)/2
3820   Ai(16,7)=Q(3,1,2)/2
3830  GOSUB 4690
3840  GOSUB 5550
3850  Freqc=D(10)-D(9)
3860  Ffreq=14.02721/3500*H
3870  Freq1=D(8)-D(7)
3880  IF Freqm=1000 THEN
3890      Erc=0
3900  ELSE
3910      Erc=ABS(Freqc-Freqm)
3920      Icount=Icount+1
3930  END IF
3940  IF Freqm1=1000 THEN
```

```
3950        Erl=0
3960    ELSE
3970        Erl=ABS(Freql-Freqml)
3980        Icount=Icount+1
3990    END IF
4000    Eror=Eror+Erc+Erl
4010    Dat(Idat,7)=Freqc
4020    Dat(Idat,8)=Freql
4030    Idat=Idat+1
4040    REM *** TO PRINT EACH DATA PT. REM NEXT LINE************
4050    GOTO Skip1
4060    PRINT " "
4070    PRINT Dat(Idat-1,1),Dat(Idat-1,2),Dat(Idat-1,3),Dat(Idat-1,4)
4080    PRINT USING "K";"FREQM = ",Freqm,"      FREQC = ",Freqc,"    ERC = ",Erc
4090    PRINT USING "K";"FREQML = ",Freqml,"    FREQL = ",Freql,"    ERL = ",Erl
4100 Skip1:  REM ************************************************************
4110    GOTO 1690
4120    REM ***************************************************************************
4130    REM ***** TO OUTPUT DATA REM NEXT LINE ********************************
4140    GOTO Skip2
4150    INPUT "OUTPUT FILE NAME",Fid$
4160    CREATE BDAT Fid$,2000,8
4170    ASSIGN @Fid TO Fid$
4180    FOR I=1 TO 150
4190        OUTPUT @Fid;Dat(I,1)
4200        IF Dat(I,1)=1000 THEN GOTO 4290
4210        OUTPUT @Fid;Dat(I,2)
4220        OUTPUT @Fid;Dat(I,3)
4230        OUTPUT @Fid;Dat(I,4)
4240        OUTPUT @Fid;Dat(I,5)
4250        OUTPUT @Fid;Dat(I,6)
4260        OUTPUT @Fid;Dat(I,7)
4270        OUTPUT @Fid;Dat(I,8)
4280    NEXT I
4290    ASSIGN @Fid TO *
4300    STOP
4310 Skip2:  REM ************************************************************
4320    IF Eror<Error THEN
4330        Para(Jj)=P(Jj)
4340        Error=Eror
4350        Eror=0
4360        BEEP
4370        PRINT Para(*),Error,Icount
4380        IF Jj=Npam THEN Jj=0
4390        Jj=Jj+1
4400        Idat=1
4410        Icount=0
4420        Iflag=0
4430        P(Jj)=Para(Jj)-Delta(Jj)
4440        GOTO 1450
4450    ELSE
4460        IF Iflag=1 THEN
4470            Eror=0
4480            P(Jj)=Para(Jj)
4490            BEEP
4500            PRINT Para(*),Error,Icount
4510            IF Jj=Npam THEN Jj=0
4520            Jj=Jj+1
4530            Idat=1
4540            Icount=0
4550            Iflag=0
4560            P(Jj)=Para(Jj)-Delta(Jj)
4570            GOTO 1450
4580        END IF
4590        Eror=0
4600        P(Jj)=Para(Jj)+Delta(Jj)
```

```
4610        Idat=1
4620        Icount=0
4630        Iflag=1
4640        GOTO 1450
4650    END IF
4660    STOP
4670    REM *************** Subroutine 2870 ******************
4680  INTEGER U,V,W,X
4690    Tau(1,N)=1
4700    Tau(2,N)=0
4710    FOR I1=1 TO N
4720    D(I1)=Ar(I1,I1)
4730    NEXT I1
4740    FOR I1=1 TO N
4750    U=N+1-I1
4760    X=U-1
4770    T=0
4780    Sscale=0
4790    IF X<1 THEN 4860
4800    FOR Kcount=1 TO X
4810    Sscale=Sscale+ABS(Ar(U,Kcount))+ABS(A1(U,Kcount))
4820    NEXT Kcount
4830    IF Sscale<>0 THEN 4890
4840    Tau(1,X)=1
4850    Tau(2,X)=0
4860    E(U)=0
4870    E2(U)=0
4880    GOTO 5480
4890    FOR K1=1 TO X
4900    Ar(U,K1)=Ar(U,K1)/Sscale
4910    A1(U,K1)=A1(U,K1)/Sscale
4920    T=T+Ar(U,K1)*Ar(U,K1)+A1(U,K1)*A1(U,K1)
4930    NEXT K1
4940    E2(U)=Sscale*Sscale*T
4950    Y=SQR(T)
4960    E(U)=Sscale*Y
4970    F=ABS(SQR(Ar(U,X)*Ar(U,X)+A1(U,X)*A1(U,X)))
4980    IF F=0 THEN 5070
4990    Tau(1,X)=(A1(U,X)*Tau(2,U)-Ar(U,X)*Tau(1,U))/F
5000    Ps1=(Ar(U,X)*Tau(2,U)+A1(U,X)*Tau(1,U))/F
5010    T=T+F*Y
5020    Y=1+Y/F
5030    Ar(U,X)=Y*Ar(U,X)
5040    A1(U,X)=Y*A1(U,X)
5050    IF X=1 THEN 5430
5060    GOTO 5100
5070    Tau(1,X)=-Tau(1,U)
5080    Ps1=Tau(2,U)
5090    Ar(U,X)=Y
5100    F=0
5110    FOR J=1 TO X
5120    Y=0
5130    G1=0
5140    FOR K2=1 TO J
5150    Y=Y+Ar(J,K2)*Ar(U,K2)+A1(J,K2)*A1(U,K2)
5160    G1=G1-Ar(J,K2)*A1(U,K2)+A1(J,K2)*Ar(U,K2)
5170    NEXT K2
5180    Jp1=J+1
5190    IF X<Jp1 THEN 5240
5200    FOR K3=Jp1 TO X
5210    Y=Y+Ar(K3,J)*Ar(U,K3)-A1(K3,J)*A1(U,K3)
5220    G1=G1-Ar(K3,J)*A1(U,K3)-A1(K3,J)*Ar(U,K3)
5230    NEXT K3
5240    E(J)=Y/T
5250    Tau(2,J)=G1/T
5260    F=F+E(J)*Ar(U,J)-Tau(2,J)*A1(U,J)
```

```
5270  NEXT J
5280  Ha=F/(T+T)
5290  FOR J1=1 TO X
5300  F=Ar(U,J1)
5310  Y=E(J1)-Ha*F
5320  E(J1)=Y
5330  F1=-A1(U,J1)
5340  G1=Tau(2,J1)-Ha*F1
5350  Tau(2,J1)=-G1
5360  FOR K4=1 TO J1
5370  O2O=F1*Tau(2,K4)+G1*A1(U,k4)
5380  Ar(J1,K4)=Ar(J1,K4)-F*E(K4)-Y*Ar(U,K4)+O2O
5390  O21=F1*E(K4)+G1*Ar(U,K4)
5400  A1(J1,K4)=A1(J1,K4)-F*Tau(2,K4)-Y*A1(U,K4)-O21
5410  NEXT K4
5420  NEXT J1
5430  FOR K5=1 TO X
5440  Ar(U,k5)=Sscale*Ar(U,K5)
5450  A1(U,K5)=Sscale*A1(U,k5)
5460  NEXT K5
5470  Tau(2,X)=-Ps1
5480  Ha=D(U)
5490  D(U)=Ar(U,U)
5500  Ar(U,U)=Ha
5510  A1(U,U)=Sscale*SQR(T)
5520  NEXT I1
5530  RETURN
5540  REM *************** Subroutine 3720 ***************
5550  Achep=.00000001
5560  Ierr=0
5570  IF N=1 THEN 6160
5580  FOR Uu=2 TO N
5590  E(Uu-1)=E(Uu)
5600  NEXT Uu
5610  E(N)=0
5620  FOR Xx=1 TO N
5630  V=0
5640  FOR O=Xx TO N
5650  IF O=N THEN 5680
5660  IF ABS(E(O))<=Achep*(ABS(D(O))+ABS(D(O+1))) THEN 5680
5670  NEXT O
5680  Pp=D(Xx)
5690  IF O=Xx THEN 6050
5700  IF V=30 THEN 6150
5710  V=V+1
5720  Gg=(D(Xx+1)-Pp)/(2*E(Xx))
5730  Rs=SQR(Gg*Gg+1)
5740  Gg=D(O)-Pp+E(Xx)/(Gg+SGN(Gg)*Rs)
5750  S=1
5760  C=1
5770  Pp=0
5780  Mm1=O-Xx
5790  FOR I11=1 TO Mm1
5800  Uu=O-I11
5810  Z=S*E(Uu)
5820  Bb=C*E(Uu)
5830  IF ABS(Z)<ABS(Gg) THEN 5900
5840  C=Gg/Z
5850  Rs=SQR(C*C+1)
5860  E(Uu+1)=Z*Rs
5870  S=1/Rs
5880  C=C*S
5890  GOTO 5950
5900  S=Z/Gg
5910  Rs=SQR(S*S+1)
5920  E(Uu+1)=Gg*Rs
```

```
5930  C=1/Rs
5940  S=S*C
5950  Gg=D(Uu+1)-Pp
5960  Rs=(D(Uu)-Gg)*S+2*C*Bb
5970  Pp=S*Rs
5980  D(Uu+1)=Gg+Pp
5990  Gg=C*Rs-Bb
6000  NEXT I1 1
6010  D(Xx)=D(Xx)-Pp
6020  E(Xx)=Gg
6030  E(0)=0
6040  GOTO 5640
6050  IF X1=1 THEN 6110
6060  FOR I1 1=2 TO Xx
6070  Uu=Xx+2-I1 1
6080  IF Pp >=D(Uu-1) THEN 6120
6090  D(Uu)=D(Uu-1)
6100  NEXT I1 1
6110  Uu=1
6120  D(Uu)=Pp
6130  NEXT X1
6140  GOTO 6160
6150  Ierr=X1
6160  RETURN
6170  end
```

VITA

Michael Paul Scripsick

Candidate for the Degree of

Doctor of Philosophy

Thesis: MAGNETIC RESONANCE AND OPTICAL INVESTIGATIONS OF $KMgF_3$ AND $KTiOPO_4$

Major field: Physics

Biographical:

Personal Data: Born in Kiowa, Kansas, August 26, 1963, the son of John B. and Lottie V. Scripsick.

Education: Graduated from Burlington High School, Burlington, Oklahoma, May 1981. Received Bachelor of Science Degree, December, 1985, Oklahoma State University, Stillwater, Oklahoma. Completed requirements for the Degree of Doctor of Philosophy, December, 1990, Oklahoma State University, Stillwater, Oklahoma.